Engineering Sciences

OCT 2 '76

Branch Library

WIND FORCES AND MOMENTS ON MICROWAVE ANTENNAS

by

Michael Poreh

and

Jack E. Cermak

A Report to
ROSE, CHULKOFF AND ROSE
Structural Engineers

Sponsored by

Long Lines Department
AMERICAN TELEPHONE AND TELEGRAPH COMPANY

Fluid Mechanics and Wind Engineering Program
Department of Civil Engineering
Colorado State University
Fort Collins, Colorado 80523

September 1976

U18401 0074475

CER76-77MP-JEC12

TABLE OF CONTENTS

TABLE OF CONTENTS
Continuation

TABLE OF CONTENTS
Continuation

TABLE OF CONTENTS
Continuation

ACKNOWLEDGMENTS

The authors gratefully acknowledge the contributions of all those who assisted in carrying out the several phases of this project.

The structure model was fabricated by personnel of the Engineering Research Center Machine Shop. Mr. James A. Garrison carried out the flow visualization program. Mr. Herbert Brauer, Mr. Hiroo Shiojiri and Ms. Janet Floersch accomplished the data acquisition and reduction.

INTRODUCTION

The purpose of this investigation is to obtain quantitative information that will relate the forces and moments acting on a single microwave antenna or on any of several configurations of two- or four-horn antenna clusters to the speed and direction of the approaching wind. The study provides input for a rational design of the towers that support such microwave antenna arrays.

The flow around a single antenna horn or around a cluster of antennas is very complex and defies exact theoretical analysis. The theory indicates, however, that the drag force D, the lateral force L and the moments M_P and M_R, as defined in Fig. 1, can be expressed in the following universal forms:

$$D = C_D \, A \, \rho \, U^2/2 \tag{1}$$

$$L = C_L \, A \, \rho \, U^2/2 \tag{2}$$

$$M_P = C_{MP} \, A \, L \, \rho \, U^2/2 \tag{3}$$

$$M_R = C_{MR} \, A \, L \, \rho \, U^2/2 \tag{4}$$

In these equations A is a reference area; in the present study, unless otherwise stated, A is chosen to be the area of the antennas and platform projected on a plane normal to the wind direction. The length L is a typical (arbitrary) length; in this study we have chosen as a typical prototype length L = 10 ft. The mean wind speed U is taken approximately at the height of the center of mass of the antenna horn or horns as shown in Fig. 8. The mass density of air near the structure is denoted in the equations by ρ. Denoting by Δp the dynamic pressure, $\rho U^2/2$, as measured by a pitot tube, equations (1), (2), (3) and (4) can also be expressed as follows:

$$D = C_D \; A \; \Delta p \tag{5}$$

$$L = C_L \; A \; \Delta p \tag{6}$$

$$M_P = C_{MP} \; A \; L \; \Delta p \tag{7}$$

$$M_R = C_{MR} \; A \; L \; \Delta p \tag{8}$$

The aerodynamic coefficients C_D, C_L, C_{MP} and C_{MR}, for a specified body and wind orientation, known also as the drag coefficient, the lateral force coefficient and the moment coefficients, respectively, are primarily determined according to theory, by the Reynolds number of the flow which is defined as

$$Re = \frac{UL}{\nu} , \tag{9}$$

where ν is the kinematic viscosity of the air. This theory forms the basis for wind tunnel simulation of aerodynamic phenomena in which the values of these coefficients are determined from measurements of the forces and moments acting on small scale models.

Since the aerodynamic coefficients depend primarily on the Reynolds number, these tests should usually be made so that the Reynolds number of the prototype is equal to that of its model. This condition cannot always be met in existing wind tunnels. Fortunately, however, both theoretical considerations and experimental evidence show that beyond a certain critical Reynolds number, there is no significant change in the value of the aerodynamic coefficients. The value of this critical Reynolds number depends on the geometry of the body and the turbulence level of the air stream.

Therefore, whenever both the prototype Reynolds number and the model Reynolds number exceed the critical value, it is permissible to use the model-derived coefficients as the basis for computation of prototype forces and moments. The regime in which the value of the coefficients remains essentially constant is called the regime of Reynolds Number Independence.

Of course, it is also required that the basic features of the flow field be simulated in the wind-tunnel tests. This requirement is satisfied by testing the models in an approaching flow in which the vertical velocity profile and turbulence characteristics are similar to those of the prototype flow.

The test program for this study was therefore organized as follows:

(a) a survey of the approaching velocity field was performed and recorded;

(b) tests to determine the effect of the Reynolds number were made;

(c) the nature of the flow around specified antenna cluster configurations was studied and recorded using visual techniques; and

(d) measurements of forces and moments in the regime of Reynolds Number Independence were made, and values of the aerodynamic coefficients were determined.

EXPERIMENTAL CONFIGURATION

Wind Tunnel

This study was performed in part in the industrial aerodynamics wind tunnel and in part in the meteorological wind tunnel of the Fluid Dynamics and Diffusion Laboratory at Colorado State University.

The industrial aerodynamics wind tunnel is a closed circuit facility driven by a 75 hp variable pitch propeller. The test section is 6 ft by 6 ft and 62 ft long, fed through a 4 to 1 contraction ratio. The roof is adjustable to maintain a zero pressure gradient along the test section. Mean velocity can be adjusted continuously from 1 to 75 fps. A schematic drawing of this tunnel is shown in Fig. 2.

The meteorological wind tunnel is also a closed circuit type with a 6 ft square test section. Its length is 80 ft. Zero pressure gradient is maintained by means of an adjustable roof. Mean velocity can be varied continuously from 1 to 120 fps. A schematic drawing of this tunnel is shown in Fig. 3.

The model was centrally mounted on the turntables in both tunnels as indicated in the figures.

Spire-type vortex generators and a 4 in.-high two dimensional barrier provided a boundary layer trip at the entrance to the test section. The downwind floor of the test section was smooth. This arrangement was designed to provide a boundary layer thickness of approximately 45 in. at the position of the model and a mean velocity profile similar to that for a rural environment.

Model

To obtain accurate measurements of mean forces and moments on a structure, a model is usually constructed to the largest scale that will not produce serious blockage in the wind tunnel. In this study, a 1:16 scaled model of the upper portion of the support tower, the platform, and the antenna array was constructed to prototype specifications supplied by the sponsors. (See Appendix) The cross section area of the model was at most 5% of the wind-tunnel cross section. A photograph of the model is shown in Fig. 4.

The upper portion of the support tower was modelled in steel so that all significant particulars of the prototype were represented.

The platform was modelled using 1/2 in. high steel bars, in such a way as to permit mounting of the antenna horns in specified configurations. An upper view of the platform is shown in Fig. 5. The prototype platform dimensions were 29 ft x 29 ft. The space in which the antenna horns were installed corresponds to an 8 ft-8 in. x 8 ft-8 in. square in the prototype.

This platform model was not directly attached to the tower model, but was connected to the force balance which in turn was fastened to the tower.

To simulate an effectively solid-surfaced platform, caused in nature by icing of the platform grating, a cardboard overlay covering the top of the model platform was used. The space required by the prototype specifications to accomodate mounting of each antenna horn (7 ft x 7 ft) was left uncovered.

A separate platform model for single antenna horn configurations was constructed of 1/2 x 6 3/4 x 10 3/4 in. steel plate, as shown in Fig. 6.

The pyramidal antenna horn models were fabricated of "Lucite" in the Engineering Research Center shop. The "Gabriel" conical antenna-horn model built to a scale of 1:16 (see Fig. 6) was supplied by the sponsor. Hereafter the pyramidal antenna horns are referred to simply as "antennas." The "Gabriel" conical antenna horn is called the "conical antenna."

The four pyramidal antenna-horn models were attached directly to the model platform to represent accurately the several prototype configurations specified by the sponsors as given in the appendix. Fig. 4 is a photograph of the antennas mounted in "Condition 3."

In addition, tests were run in a configuration involving a two-story antenna array, as shown in Fig. 7. For this case, the lower story configuration was assembled as in "condition 3." The upper platform in this case was modelled of 1/2 in. solid plywood plate with four antenna horns made of styrofoam. These horns were mounted in a 16 ft prototype separation configuration. The plane of the upper platform was parallel to the plane of the lower platform. The vertical separation of platforms in the model corresponded to a prototype separation of 15 ft. The principal axes in the plane of the upper platform were oriented at an angle of 45 degrees with respect to the principal axes in the plane of the lower platform.

To damp the excess vibration of the multiple antenna-platform assembly, two dashpots, shown in Fig. 7, were installed on the model. The cylinders containing viscous fluid were attached to the tower portion of the model. The pistons were attached to the platform-antenna assembly in such a way that they did not discernibly contribute to the forces or moments acting on the platform-antenna assembly.

EXPERIMENTAL TECHNIQUES

Flow Visualization

Visualization of the flow in the vicinity of the model is helpful in understanding and interpreting the mean force and moment measurements. Titanium tetrachloride smoke was released from upstream sources close to the model. Motion and still-picture records of the flow patterns were taken and constitute a part of the final report to the sponsor. Selected photographs appear in Fig. 40- .

Measurements of Flow Characteristics

Velocity and turbulence intensity profiles of the flow under test conditions were made at the locations of the model (turntables) in the two tunnels with the model removed. The integral scale of the longitudinal component of turbulence at the height of the center of mass of the antennas was also determined. Results of these measurements will be discussed later in the report.

The measurements were made with a single hot-wire anemometer. The instrumentation used was a Thermo-Systems constant-temperature anemometer (Model 1050) with a 0.001 in.-diameter platinum film sensing element 0.020 in. long. Output was read from a Hewlett-Packard integrated digital voltmeter (Model 2401C) for mean voltage and a DISA rms meter (Model 55D35) for rms. voltage.

The reference velocity was obtained by using a standard Pitot tube. The dynamic pressure Δp was recorded by a Baratron Pressure Gage in mm of mercury.

Measurements of Forces and Moments

Mean force and moment measurements were made using a strain-gauge instrumented force balance manufactured by Inca Engineering Corporation of San Gabriel, California. This balance can measure all six components of forces and moments, although the sensitivity to forces along the balance axis is too low for the accuracy desired. For this reason the balance was aligned with its axis in a vertical position for measurement of horizontal forces and moments.

PRELIMINARY TESTS

Survey of the Approaching Velocity Field

The flow field at the locations of the model was surveyed. The mean velocity profile in both tunnels exhibit similarity in the sense that variation of the ratio of the local mean velocity in the boundary layer to the mean velocity outside the boundary layer $U(z)/U(\infty)$ is independent of the value of $U(\infty)$ as shown in Fig. 8. The boundary layer thickness was also the same in both tunnels and is estimated to be $\delta = 45$ in. The primary reason for obtaining the same boundary-layer thickness, in spite of the slight difference in the length of the test sections, is that δ was primarily determined by the vortex generaters and trip fence used to augment the thickness of the boundary layer at the entrances to the tunnels.

The height of the tower was such that the top of the platform was located at the height of 34 in. from the floor of the tunnel and the estimated center of pressure of the horn's surface was at 38 in. from the floor, as shown in Fig. 8. As seen from this figure the variation of the approaching velocity across the horns was very small, of the order of a few percent. The reference velocity U in subsequent tests was taken as the velocity at 38 in. from the floor measured upstream from the model.

The distribution of the turbulence intensity in the tunnels is also shown in Fig. 8. At the height of the horns it varied between 4 to 5 percent.

The measured characteristics of the flow field appear to be similar to the average characteristics of the atmospheric boundary layer as discussed by Cermak*. It should be stressed, however, that the existing force and

*Laboratory Simulation of the Atmospheric Boundary Layer. AIAA Journal, Vol. 9, No. 9, Sept. 1971. pp 1746-1754.

moment measurements are average values and do not contain the gust loading. Thus, it is recommended that the peak forces and moments for gust loading be obtained by using Equations (1) - (4) with U replaced by the estimated gust velocity.

Drag of Platform

Preliminary tests were conducted to determine the drag of the four-horn platform (Fig. 5) and to find the possible effect of platform inclination due to wind forces in the tests. It should be noted that during the tests the platform and horns were connected to the elastic balance. The maximum inclination of the platform during the tests was estimated to be smaller than 1 1/2 degrees. The effect of such an inclination on the drag of the horns is expected to be very small; however, it was not clear whether the relatively large change in the projected area of the inclined platform would increase the drag. The platform's drag was therefore measured at two orientations of its principal axes, 0 and 45 degrees, at 0, 2 and 4 degree inclinations. The data are given in Table 1.

The results clearly show that the effect of 1 1/2 degree inclination of the platform is negligible. The value of the drag coefficient of the uncovered platform at 0 degree orientation was found to be very high $C_D = 5.88$. Usually a value of $C_D = 2$ is expected for a bar oriented normal to the flow and $C_D = 1$ for a solid short plate. In this case, however, the platform is made of several parallel bars. Although the downstream bars do not change the projected area, a considerable aerodynamic force is exerted on them to produce a large value of the drag coefficient. When oriented at 45 degrees, the drag coefficient of the platform goes down to $C_D = 3.7$. Note that the total ratio of the horizontal area of the platform to the projected area is decreased, by 1.4.

No correction was made in the tests for drag increase due to effects of the supporting elements which connected the platform to the balance. It is estimated that the supporting elements increased the drag of the platform by approximately 15%. The effect of these elements on the total drag of the antenna horns and platform is, however, one order of magnitude smaller.

A comparison between the drag of the covered platform and that of the uncovered platform, given in Table 1, clearly shows, as expected, that the drag of the uncovered platform is slightly higher.

The drag of the platform used for the single-horn tests was even smaller but so was the drag on the horns. In this case it was estimated that the wake of the horn reduced the platform's drag by 50 percent. This estimate was made by measuring the drag on the platform with the horn held in its place without touching the platform. The data were corrected accordingly and the drag of single horns as discussed later is the net drag of the horns.

Reynolds-number Effects

Tests were conducted to examine the effect of the Reynolds number on the drag coefficient and to determine the lower bound of the Reynolds Number Independence regime.

The horns were mounted on the platform in "Condition 1" (See Appendix) and the drag was measured for four wind directions at five Reynolds numbers ranging from 1.1×10^5 to 3.2×10^5, which correspond to speeds of 33 and 100 ft/sec. (Note that the Reynolds number was calculated using Equation 9 with $L = 0.625$ ft which correspond to $L = 10$ ft in the prototype.) The corresponding drag coefficients are given in Table 2 and plotted in Fig. 9.

It is clear from the results that beyond Re $\cong$ 2.5 x 10^5 or V = 70 ft/sec no Reynolds number effect is detected. It was therefore decided to continue the tests at a speed of approximately 70 ft/sec (48 mi/hr) where C_D is not a function of the Reynolds number and where the effect of inclination and model vibrations are small.

Similar tests were conducted with a single pyramidal horn and with a single conical horn. The results of these tests are shown in Fig. 10. The scatter here is slightly larger due to the smaller magnitude of the drag. The data do not, however, show a clear Reynolds number dependence. The single horn tests were conducted at a velocity of approximately U = 84 ft/sec. (Note that the velocity in ft/sec equals approximately $54\sqrt{\Delta p}$ where Δp is expressed in mm of mercury. The coefficient 54 depends on the density of the air at the altitude where the velocity is measured.)

FORCES AND MOMENTS ACTING ON ANTENNA CLUSTERS

Program and Conditions of Tests

The forces and moments defined in Fig. 1 have been measured on a single (pyramidal) horn, a conical horn, a two-horn cluster, and various configurations of four-horn clusters. A summary of the testing program is given in Table 3. The exact orientation of the horns, the separation between the horns and the projected areas of the cluster in each configuration and wind orientation are given in the Appendix.

The drag, lateral force and moment coefficients were calculated using Equations (5) to (8). The height of the drag force y_D was calculated using the ratio of the pitching moment to the drag force:

$$y_D = \frac{M_P}{D} \quad . \tag{10}$$

Forces Acting on a Single Pyramidal Horn

The forces, moments and calculated values of the aerodynamic coefficients of a single pyramidal horn are given in Tables 4 and 5.

It should be pointed out again that the absolute magnitudes of the lateral forces and moments recorded in this case were small compared to the full-scale range of the balance. This reduced the accuracy of the single-horn measurements relative to the multiple-horn data. Nevertheless, inspection of the recorded data clearly indicates the lateral forces are usually very small compared to the drag forces. Only at orientations between 20° and 60° was the lateral force coefficient significant, but even in these cases its value was less than 30% of the drag coefficient. The resultant force

$$F = (D^2 + L^2)^{1/2}$$

would therefore be at most 5% larger than the drag force. This finding, as we shall see later, is also typical of the two- and four-horn configurations and it clearly indicates that the significance of the lateral forces is relatively small. The roll moment was also found to be very small and relatively insignificant.

The values of the drag coefficients at different wind orientations are plotted in Fig. 11. The maximum value of the drag coefficient,

$$C_D = 1.31 ,$$

was recorded when the horn was facing the wind, $\theta = 0$. In the range $20^o < \theta \leq 90^o$ the value of the drag coefficient varied between $1.0 < C_D < 1.2$. On the other hand, when the antenna faced the downstream direction, $90 < \theta \leq 180$, the drag coefficient was about 20% lower and varied between $0.8 < C_D < 1.0$.

The removal of the blinders (mark ▲ in Fig. A1 of the appendix) decreased the drag coefficient by approximately 10% in the cases where the angle of incidence between the blinder and the wind was 30 to 90 degrees.

<u>Forces on a Conical Antenna</u>

The data for the single conical "Gabriel" type antenna are given in Table 6. In this case too, the absolute magnitudes and relative significance of the lateral forces and the rolling moments were small. (In one case a ratio of $C_L/D_D = 1/3$ was recorded but in this case the relative magnitude of C_D was also small).

The variation of the drag coefficient is plotted in Fig. 12. A maximum value of

$$C_D = 0.89$$

was obtained when the antenna was facing the wind, $\theta = 0$. In the other orientations the value of the drag coefficient varied between $C_D = 0.51$, when oriented at a right angle to the wind, and $C_D = 0.8$. The relatively low value of C_D in the $\theta = 90^o$ orientation is not surprising as the upper shape of the antenna has a form of a cylinder which has a rather low drag coefficient.

Forces and Moments on a Two-horn Configuration

Although the tests of the two-horn configuration were performed at the end of the program, it is instructive to analyze the results of these tests before those of the four-horn configuration. The data of the tests are given in Table 7 and the variation of the drag coefficient is plotted in Fig. 13.

As seen from this figure the drag coefficient in this configuration varies from a minimum of $C_D = 1.15$ to a maximum of $C_D = 1.65$. Let us first examine the values of the drag coefficients for the range $60^o \leq \theta \leq 120^o$. In this range there is only a slight interaction between the two horns. This claim is also supported by the visual observations of the flow pattern which have been recorded in a motion picture. (Still photographs of the flow pattern in several cases are given in Figs 40- . The quality of these is not very high because of the long time of exposure. They do show, however, the structure of the wake behind the horns and the complex flow pattern due to the interaction between the wake and the back horns). In Figs. 22-39 we have plotted schematic views of the clusters in "Condition 3", as seen by an observer looking down wind. Our case, Condition 3C, is slightly different as the separation between the horns is 16 ft and only horns (1) and (2) are mounted on the platform. Nevertheless the general view of the configuration 3C in the range $60 \leq \theta \leq 120$ is apparent from Figs. 26 to 28. In the case $\theta = 60^o$ we find, for example, that both horns face the wind with their backs. Let us try to estimate the drag of this configuration.

Horn No. 1 is at an angle of 110^o with respect to the wind and horn No. 2 is at an angle of 135^o to the wind. According to Table 1 the drag coefficient of the platform is approximately 4. The corresponding areas of the two horns and the platform are 116, 141 and 25 ft^2. The total projected area is actually only 276 because of some shading. Thus the total drag coefficient should be

$$C_D \sim \frac{0.80 \times 116 + 0.85 \times 141 + 4.0 \times 25}{276} = 1.13 \ .$$

The measured drag coefficient was

$$C_D = 1.21 \ .$$

When the two horns face the wind as in the orientation $\theta = 240^o$ and $\theta = 260^o$ the individual drag coefficients go up as shown in Fig. 11, which causes the total drag to increase to approximately

$$C_D = 1.47 \ .$$

Such calculations are of course not very reliable since they neglect the interaction between the various elements of the cluster. However, they do give a partial explanation for the variation of C_D. They fail completely when the horns are close to each other and when one horn is partially located in the wake of another horn as in the cases $\theta = 0$ and $\theta = 180$. In these cases the projected areas are drastically reduced, however, the force acting on the shaded sections of the back horn are not zero. This increases the drag coefficient considerably. Indeed, one finds for $\theta = 0$ $C_D = 1.65$, and for $\theta = 180^{\circ}$ $C_D = 1.52$.

The case of $\theta = 340^o$ where C_D reaches a minimum is more difficult to explain. One possible explanation is that although the back horn is hardly shaded by the front one, the force on the back horn is reduced due to the wake.

It should be noted that although the drag coefficient is maximum at $\theta = 0$, the largest force on the structure is exerted when $\theta = 260^o$. In this case the projected area has its maximum and the drag coefficient is also high as both horns face the wind.

Let us examine now the variation of the roll moment coefficient denoted in Table 7 by C_{MR}. Its absolute value has maximums at $\theta = 0$ and $\theta = 180$. Indeed in these orientations the two horns are on one side of the platform. The value of C_{MR} for these cases can be estimated using the following approximations:

$$M_R \sim D \cdot \ell \cdot \alpha$$

where ℓ is approximately half the separation (8 ft) and α is the portion of the drag force which acts on the horns. (About 30% of the drag, which acts on the platform, does not create a moment.) Since $D = C_D\ A\ \rho\ U^2/2$ and $M_R = C_{MR}\ A \cdot L\ \rho\ U^2/2$ ($L = 10$ ft), one gets

$$C_{MR} \sim C_D \cdot \ell/L \cdot \alpha = 0.92$$

which is very close to the measured value. Of course such calculations can usually yield only a rough estimate.

Estimates of the pitching moment become more difficult. Obviously the pitching moment should always be positive since the resultant drag force acts at a height y_D above the level of the platform. The measured values of y_D varied from $y_D = 1.6$ to $y_D = 5.6$. The variations in the height of y_D is primarily due to the shift of the center of pressure of the projected area of the cluster. When a horn is facing the wind the center of pressure is high, and when a horn is facing the side ($\theta \sim 90^o$) it goes down. The relative magnitude of the force on the platform has also an effect on the position of y_D. (It should be stressed that when the absolute value of the moments become small as in the 80^o orientation the accuracy of our y_D measurements is decreased.

The magnitude of the lateral forces acting on the two-horn cluster is relatively very small, around 20% of the drag force. This is equivalent to an increase of only 2% in the magnitude of the total force F, defined in Eq. 10.

Forces and Moments on Four-horn Clusters (20 ft. Separation)

We have tested the wind effects on three configurations of four-horn clusters with a 20 ft separation between neighboring horns. We have then tested one four-horn configuration with 16 ft separation and the effect of an upper platform with four horns on the drag of a lower platform.

Tables 8 and 9, as well as figs. 14 to 16, show the data for Condition 1, with a covered and with an uncovered platform. The drag coefficients varied in this condition between 1.0 and 1.63 for the cluster with the covered platform and between 1.1 to 1.67 for the uncovered platform. Since the projected area of the platform in clusters of four horns is relatively small, of the order of 5%, the relative effect of covering the platform was rather small although it is clear that it has in most cases a positive effect and the covering of the platform reduced the drag. It should be stressed, however, that the covering in our model was relatively smooth and has hardly increased the projected area.

In examining the variation of the drag coefficient, one should distinguish between three cases. When the cluster is at 0^{o} and 180^{o} orientation with respect to the wind, the back horns are largely hidden behind the front ones. In these cases the projected area goes considerably down but since some force is exerted on the back horns the drag coefficient goes up to about

$$C_D = 1.7$$

Around $\theta = 45^{o}$, 135^{o}, 225^{o} and 315^{o} only one of the horns is shaded. Indeed, the drag coefficient graph showed a small maximum in the neighborhood of these angles and values around

$$C_D = 1.4$$

were recorded. When the horns on the back are not shaded, the drag coefficient goes down to values around

$$C_D = 1.2 \ .$$

Similar results were obtained for "Condition 2" and "Condition 3". The data for these cases is tabulated and plotted in Tables 10 and 11 and Figs. 17 and 18. The maximum drag coefficient was recorded a $\theta = 0$ for "Condition 2"

$$C_D = 1.9 \ .$$

It is noted that at $\theta = 0$ the shading of the back horns was the largest and the projected area was the smallest. This case does not give, however, the maximum drag, which had been recorded in "Condition 3" at an angle of $\theta = 300^o$ when the projected area was 518.5 ft^2.

Obviously only a very rough estimate of the drag coefficient in such a complex configuration can be made. It was therefore decided to examine the entire set of data in order to look for the general dependence of C_D on the projected area. Figure 19 shows all the data plotted versus the prototype area A.

The figure clearly suggests that both the average and the maximum values of the drag coefficient, for a given value of A, decrease as the value of A decreases, although large variations of ± 20% at each value of the projected area exist. The upper bound of the data is approximately described by the equation

$$C_D = 2.0 \left(\frac{\text{Area (ft}^2)}{250}\right)^{-0.5} \qquad (11)$$

which results in a drag which is proportional to the square root of the area.

It is noted that in this log-log plot a line of constant drag is described by a curve $C_D \propto A^{-1}$ which correspond to a line with a slope 1:1. The line of constant drag which passes through the point which corresponds to $\theta = 300$, Condition 3, is shown in this curve by a dashed line.

Although it is difficult to fully explain why C_D varied considerably at the same projected area, a partial explanation is sometimes possible. Consider the two points in Fig. 19 which correspond to $A \simeq 426$ sq. ft. (Condition 3, $\theta = 80^o$ and 260^o). The two cases are described in Figs. 26 and 30.

It is obvious from Fig. 26 that in the case $\theta = 80^o$ all the four horns are oriented with their back to the wind. We have seen earlier that a lower drag coefficient result for such an orientation. It is not surprising therefore that a value of $C_D = 1.15$ was recorded here compared to a value of $C_D = 1.43$ at $\theta = 260^o$.

The lateral force coefficients for all three conditions, as well as the roll-moment coefficients, were found to be relatively small.

The position of the drag force above the platform for four-horn clusters varied in the range

$$3.0 \text{ ft} < y_D \leq 7.6 \text{ ft} .$$

The largest value recorded was at $\theta = 0$ for the covered platform. In this case the center of pressure of the horn was high and the force on the platform was relatively low.

Analysis of "Condition 3A" and "Condition 3B"

In Condition 3A we have tested the effect of decreasing the separation between neighboring horns to 16 ft. In comparing "Condition 3A" to "Condition 3" it is found that the drag coefficients have in general been decreased by approximately 10%. Taking into consideration the slight difference in the stagnation pressure between the two experiments it can be shown that the maximum drag had also decreased by 10%.

The effect of an upper platform, shown in Fig. 21, has also been to reduce the drag but not uniformly. Unfortunately the data points corresponding to $\theta = 240^{o}$ and 260^{o} were found to be in error and were omitted. It is also noted that the maximum drag appeared at a slightly different angle and its value was 16% smaller.

Both Condition 3A and 3B suggest that a compact arrangement of the horns would reduce the drag of the cluster.

Experimental Error Analysis

One should distinguish between errors in the experimental evaluation of the drag coefficient for the models and possible deviation of drag coefficients for the prototypes from those of the models.

The balance and electronic system are supported by their specification to be accurate within 0.1% of full scale. Our experience is, however, that a 0.4% error is a more realistic value. The full scale of the balance is 50 lbs which gives an error of 0.2 lbs. This would mean a possible error of $\pm$ 2% error in the drag measurements of the four-horn clusters, a $\pm$ 4% in the two-horn clusters and a possible $\pm$ 8% error in the single horn experiments.

The error in the stagnation pressure measurement is estimated to be of the order of $\pm$ 2%. Now, the authors had not noticed before the experimental work was completed that the configuration of the cluster in "Condition 2" is symmetric about one of the axes. Thus, we have measured 12 pairs of data points which should ideally give the same drag coefficients. Denoting the two readings of each pair by a_i and b_i we have calculated the average value $m_i = (a_i + b_i)/2$ and the deviation $d_i = | a_i/m_i - 1.0 |$ for each pair. A maximum deviation of $d_i = 0.04$ was recorded but the average value of d_i was 0.02. This is consistent without previous estimates of the possible error. It is therefore suggested that standard deviation of the errors for the four-horn cluster measurements is approximately 3%.

The errors for the single horn measurements and the lateral forces are of course larger by a factor of 3. Another effect which has been neglected is that of the blockage. It is estimated that the blockage has increased the measured values of the drag coefficient by approximately 2-4%. No correction has however been made for this effect.

Theoretically, the values of the prototype coefficients should be equal to those of the model. However, the standard deviation of the prototype data would probably be much larger than in the model. In particular one should recall that the accuracy of estimating the wind velocity in nature is not very high and that the forces are proportional to the square of the velocity.

One may thus conclude that the experimental errors in this study are relatively small and the values proposed could be used for design of the supporting tower provided an acceptable estimate of the wind velocity and gust level is available.

A NUMERICAL EXAMPLE

Calculate the maximum drag acting on a four-horn antenna configuration in "Condition 3" when the wind speed is 100 mi/hour (146.7 ft/sec). According to Table 11 the maximum drag occurs at $\theta = 300^o$. The projected area at this orientation is A = 518.5 sq. ft. The drag coefficient is $C_D = 1.33$.

Assuming that the tower is located at sea-level the density of the air is assumed to be

$$\rho = 0.127 \quad \text{kgf-sec}^2/\text{m}^4 = 0.00242 \quad \text{slug/ft}^3$$

giving a dynamic pressure

$$\Delta p = \frac{\rho U^2}{2} = 26.03 \qquad \text{lbs/ft}^2 \quad .$$

The total drag according to Eq. 5 would thus be

$$D = C_D \, \Delta p \cdot A = (1.33)\ (26.03)\ (518.5) = 17950 \text{ lbs.}$$

The position of the drag force will be at

$$y_D = 5.3 \text{ ft.}$$

above the platform.

The lateral force and roll moment in this case are practically zero.

SUMMARY

Mean wind forces and moments acting on 1:16 scale models of various microwave antenna cluster configurations were measured in a wind tunnel. Aerodynamic force and moment coefficients for the Reynolds Number Independence Regime were determined.

The drag coefficient of a single pyramidal horn was found to vary in the range

$$0.8 \leq C_D \leq 1.3 \ .$$

Values larger than $C_D = 1.0$ were obtained when the horn was facing the wind $0 \leq \theta \leq 90^\circ$, whereas values of $C_D < 1.0$ were always recorded when the horn was facing the downwind direction, $90^\circ < \theta \leq 180^\circ$.

The drag coefficient of the "Gabriel" conical horn was usually 30% lower than that of the pyramidal horn and varied in the range

$$0.5 < C_D < 0.9 \ .$$

The drag coefficient of the platform used to support four-horn clusters was found to be relatively very large, particularly when the platform was not covered. In one case the large number of steel bars located in the wake increased the drag coefficient of the platform up to

$$C_D = 5.9 \ .$$

The experiments have also indicated that the effect of a vertical wind component would be to further increase the drag of the platform.

The drag coefficient of two- and four-horn configurations which included the platform was found to vary in the range

$$1.0 < C_D < 1.9 \ .$$

The average value of C_D appears to be inversely proportional to the square root of the projected area giving a total drag which increases as the square root of the projected area. Its value for a given projected area is apparently affected by the orientation of the individual horns and was usually high when all four horns were facing the wind. Also note that the maximum drag does not occur at the orientation where C_D is maximum.

A compact cluster configuration, due to a small separation between the horns or a two-story configuration usually reduced the drag coefficients.

The lateral forces acting on the cluster normal to the wind direction were found to be generally small. The vectorially combined force of the drag and lateral force was at most 5% higher than the drag force alone. The roll moment was found to be insignificant in case of four-horn clusters but was large in case of two-horn clusters.

FIGURES

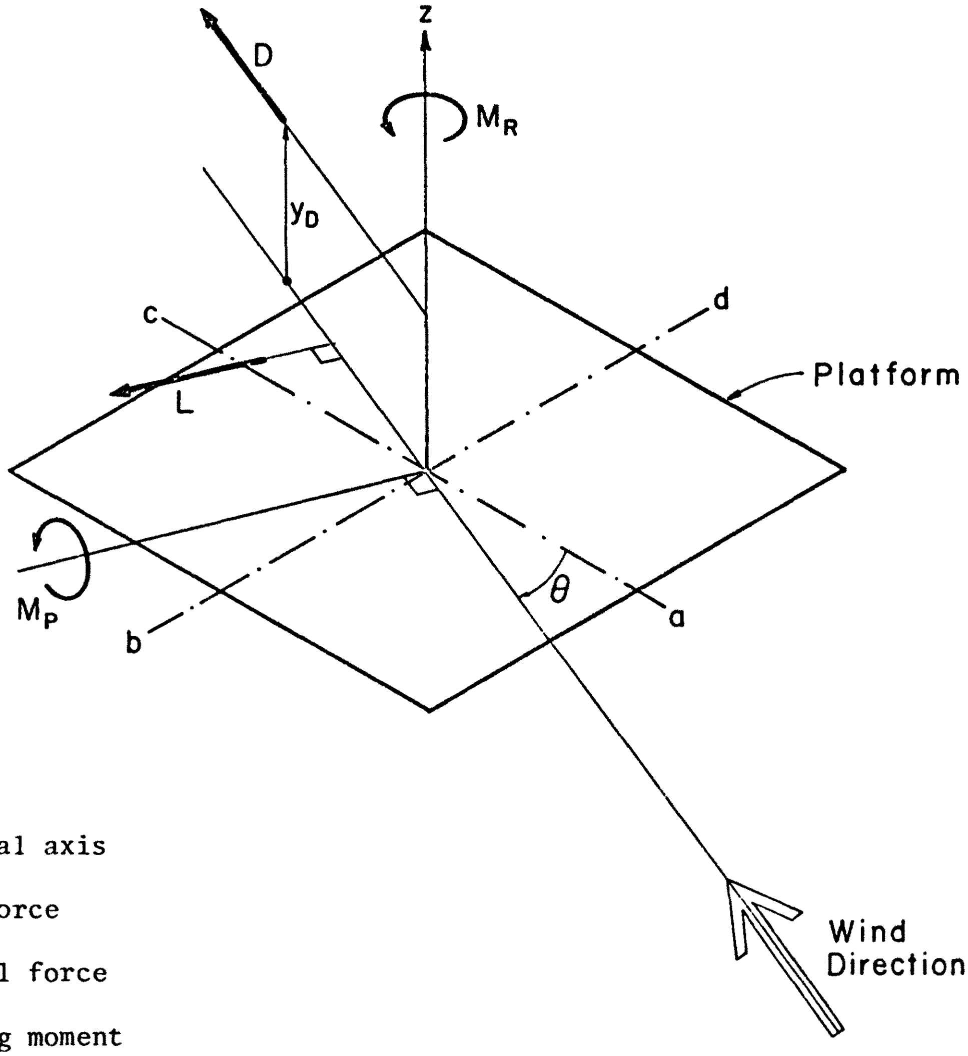

z vertical axis

D drag force

L lateral force

M_R rolling moment

M_P pitching moment

y_D height above platform of drag force ($y_D = M_P/D$)

θ angle defining wind orientation

a-c, b-d principal axes of platform

Fig. 1 Definition of coordinate system, forces and moments

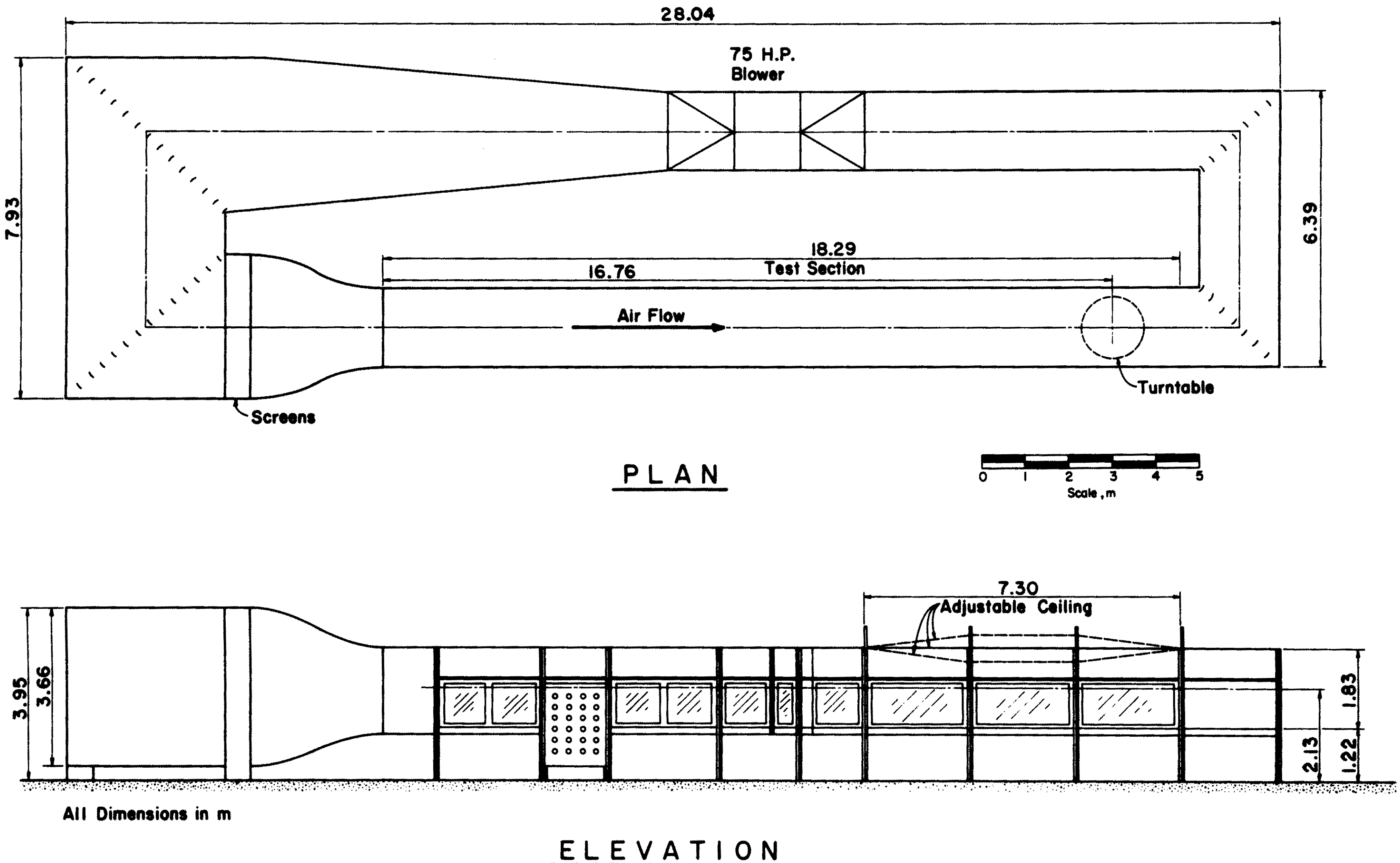

Fig. 2 INDUSTRIAL AERODYNAMICS WIND TUNNEL
FLUID DYNAMICS & DIFFUSION LABORATORY
COLORADO STATE UNIVERSITY

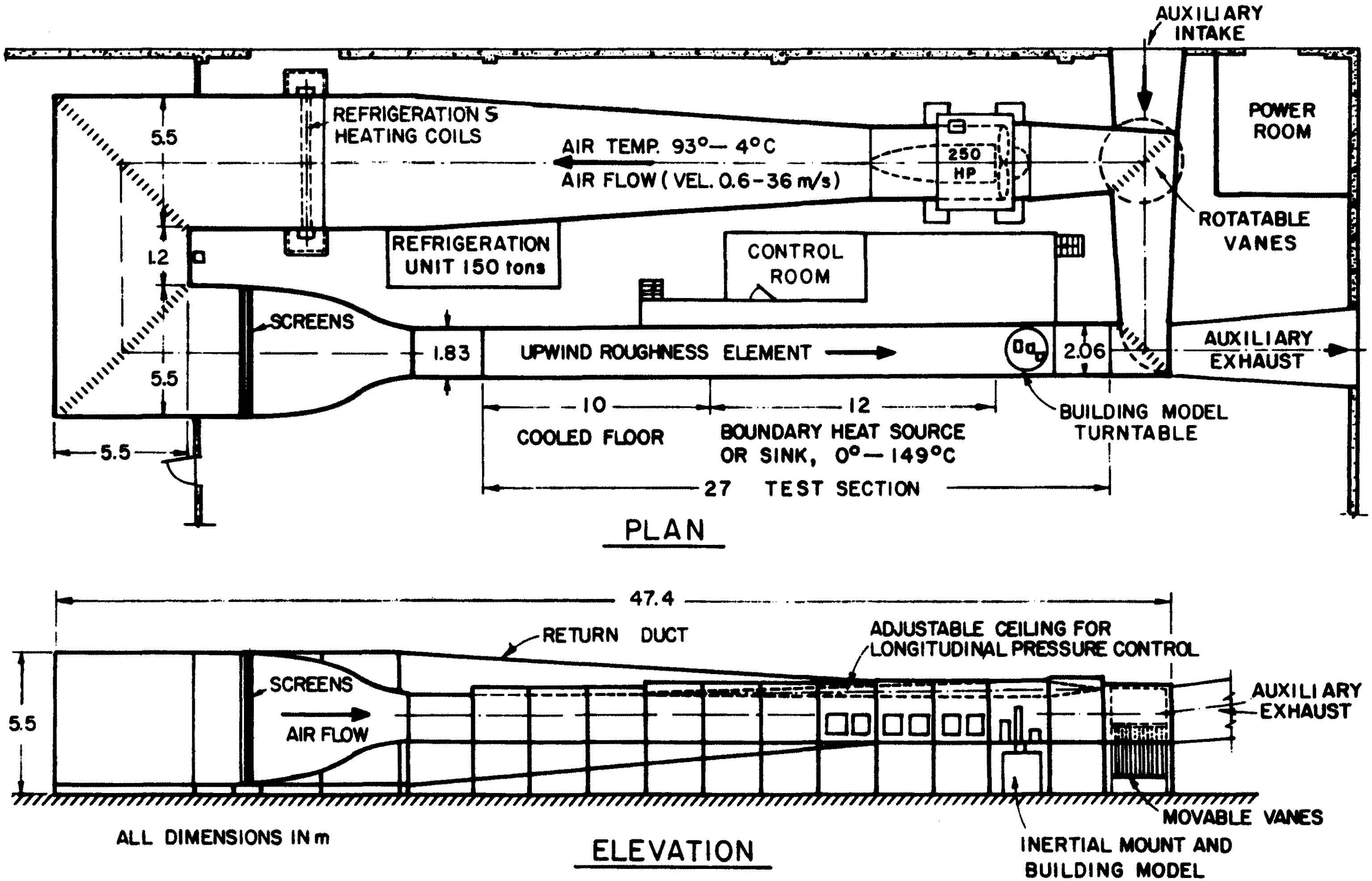

Fig. 3 METEOROLOGICAL WIND TUNNEL (Completed in 1963)
FLUID DYNAMICS & DIFFUSION LABORATORY
COLORADO STATE UNIVERSITY

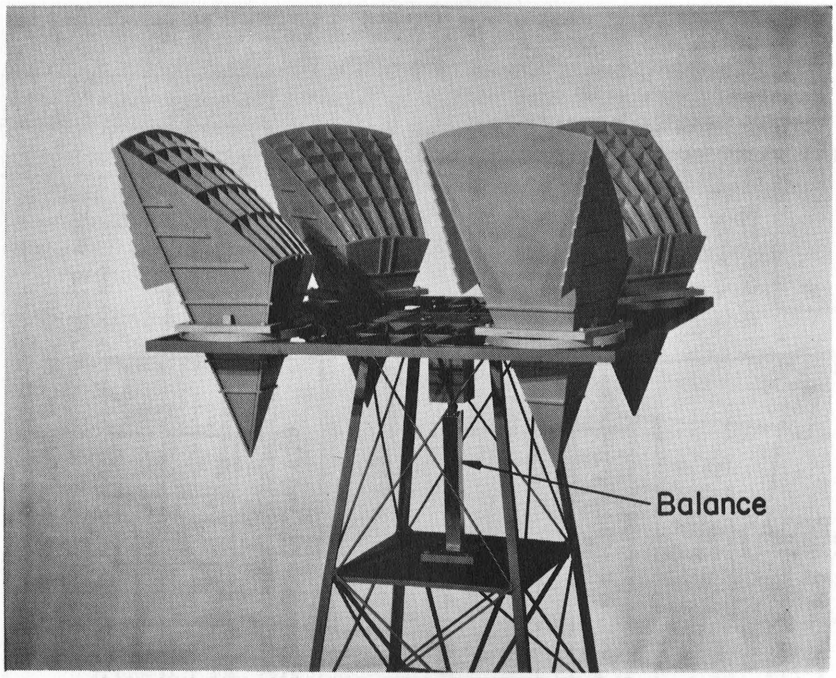

Fig. 4 Photograph of model (Condition 3).

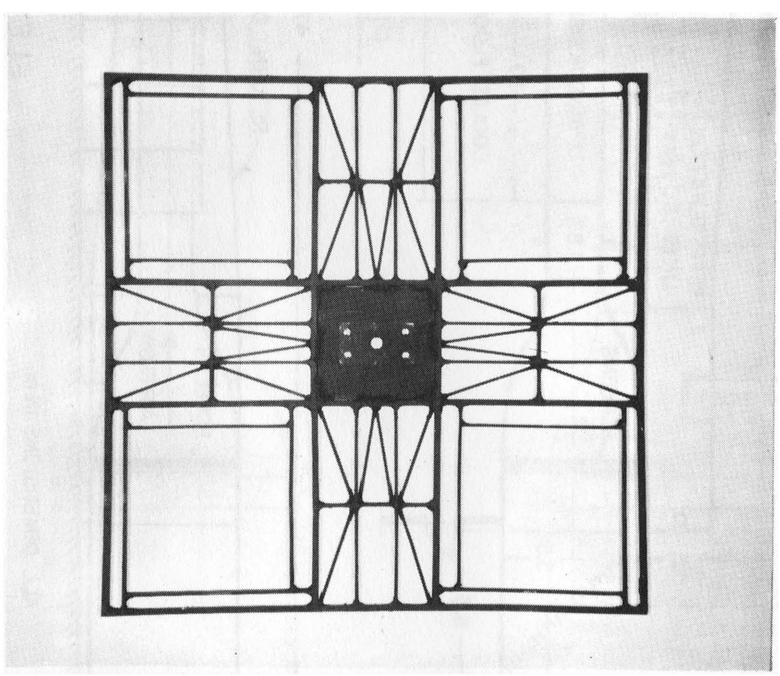

Fig. 5 Photograph of platform.

Fig. 6 "Gabriel" conical antenna horn mounted on a single horn platform

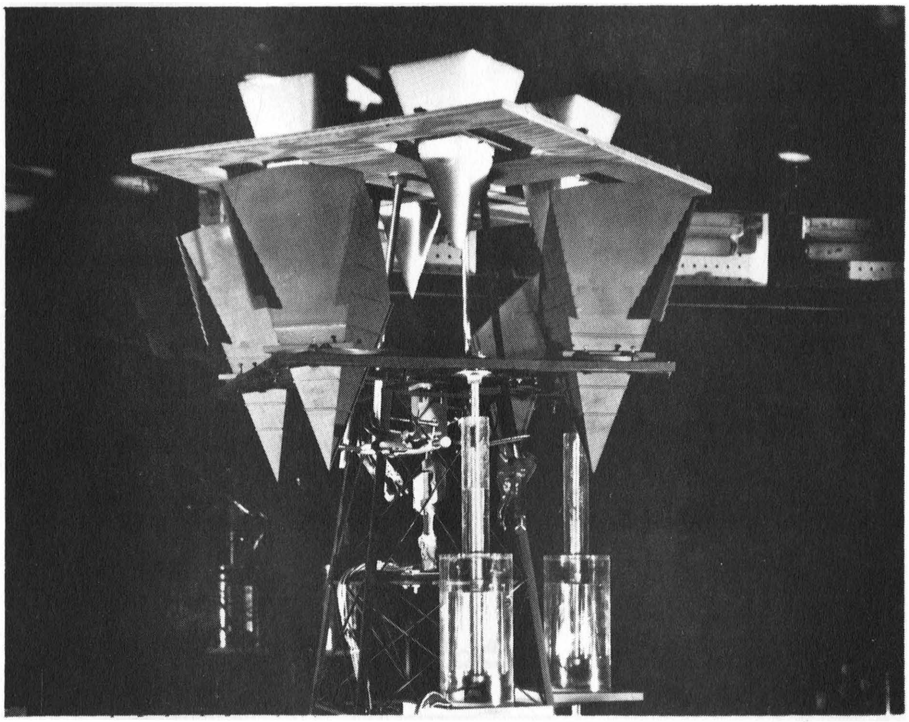

Fig. 7 Photograph of the two story array. (The viscous dash pots are shown in front of the model.)

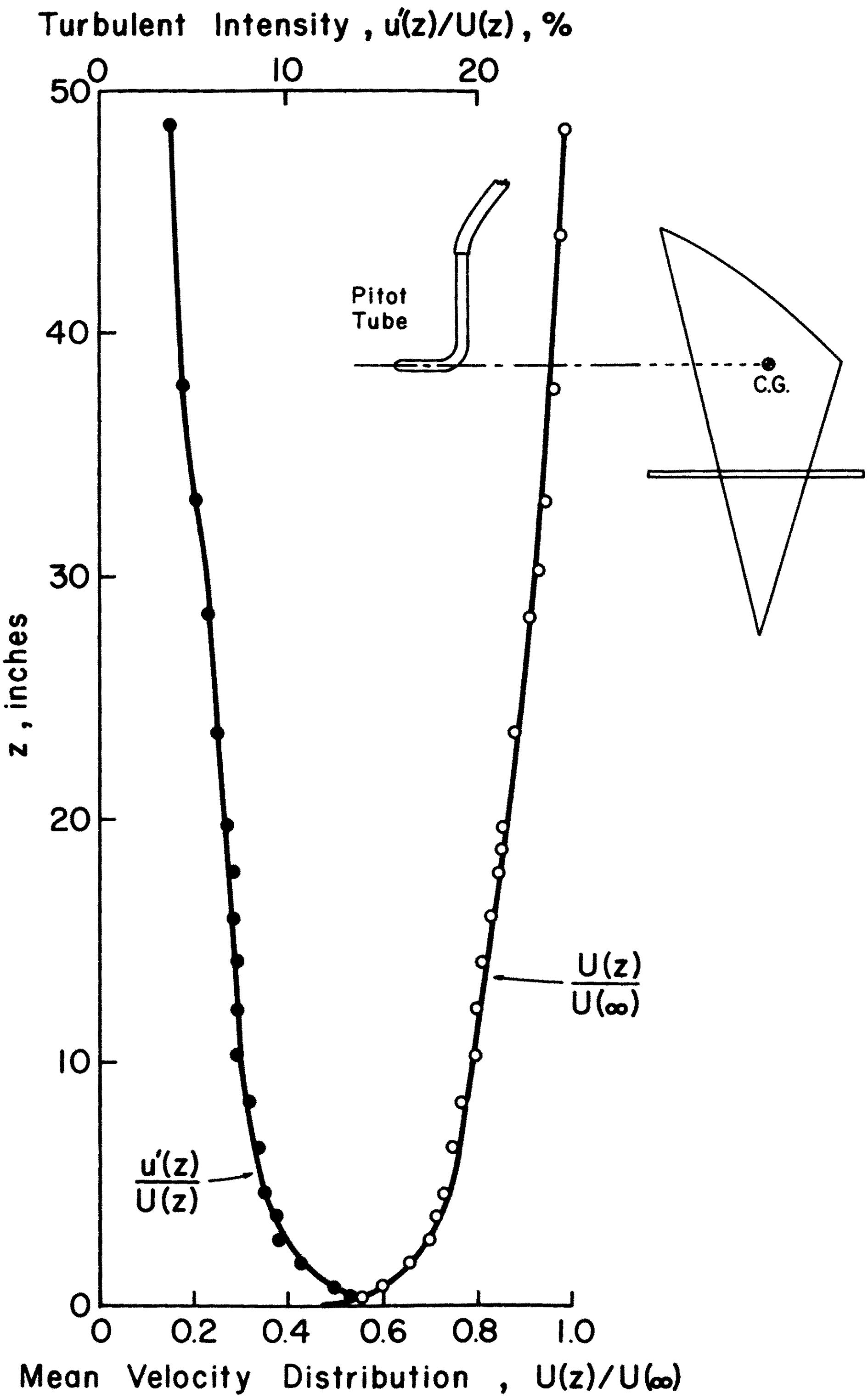

Fig. 8 Mean velocity and turbulent intensity distribution in the industrial and meteorological wind tunnels during tests.

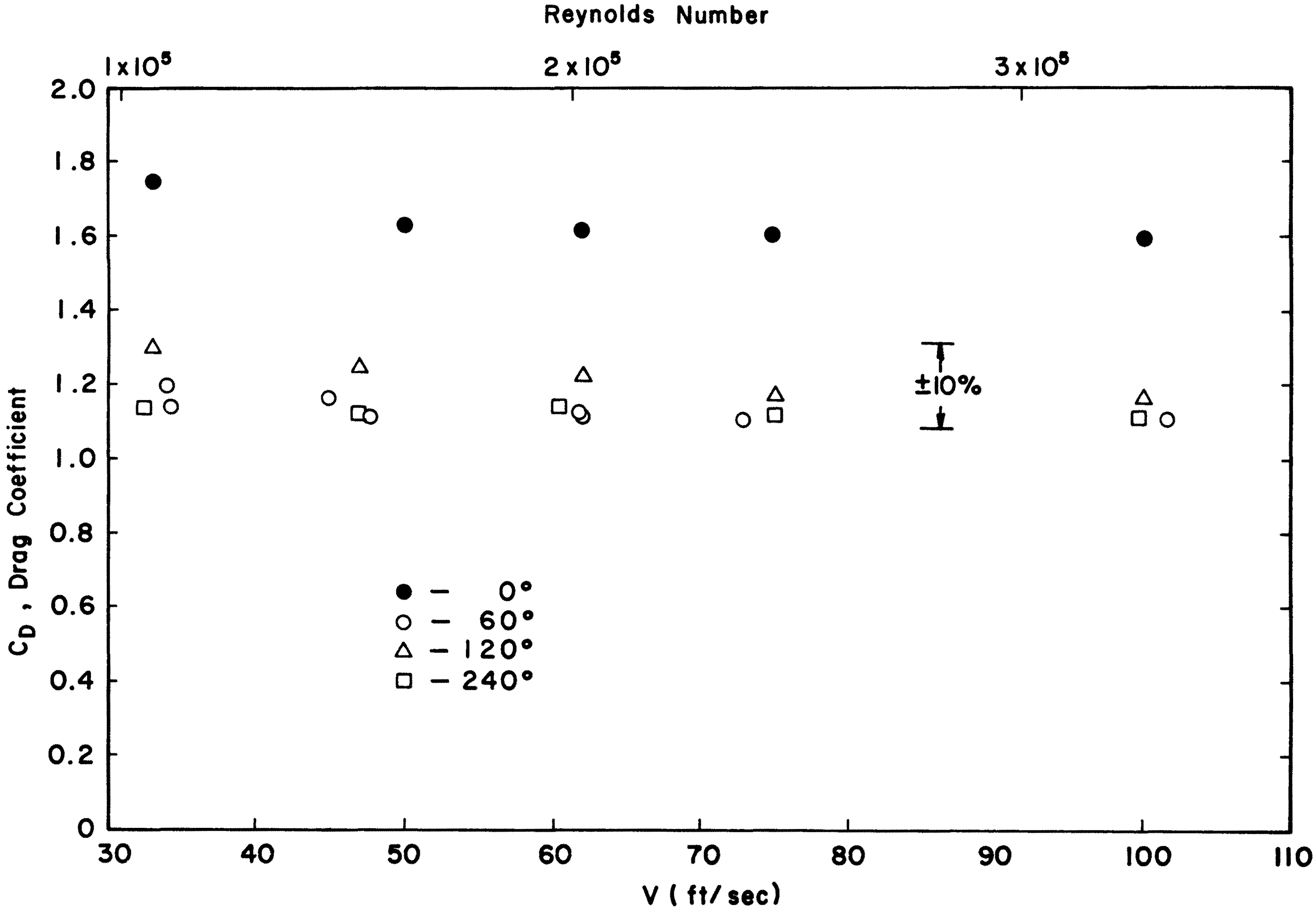

Fig. 9 Effect of Reynolds number on the drag coefficient (condition 1)

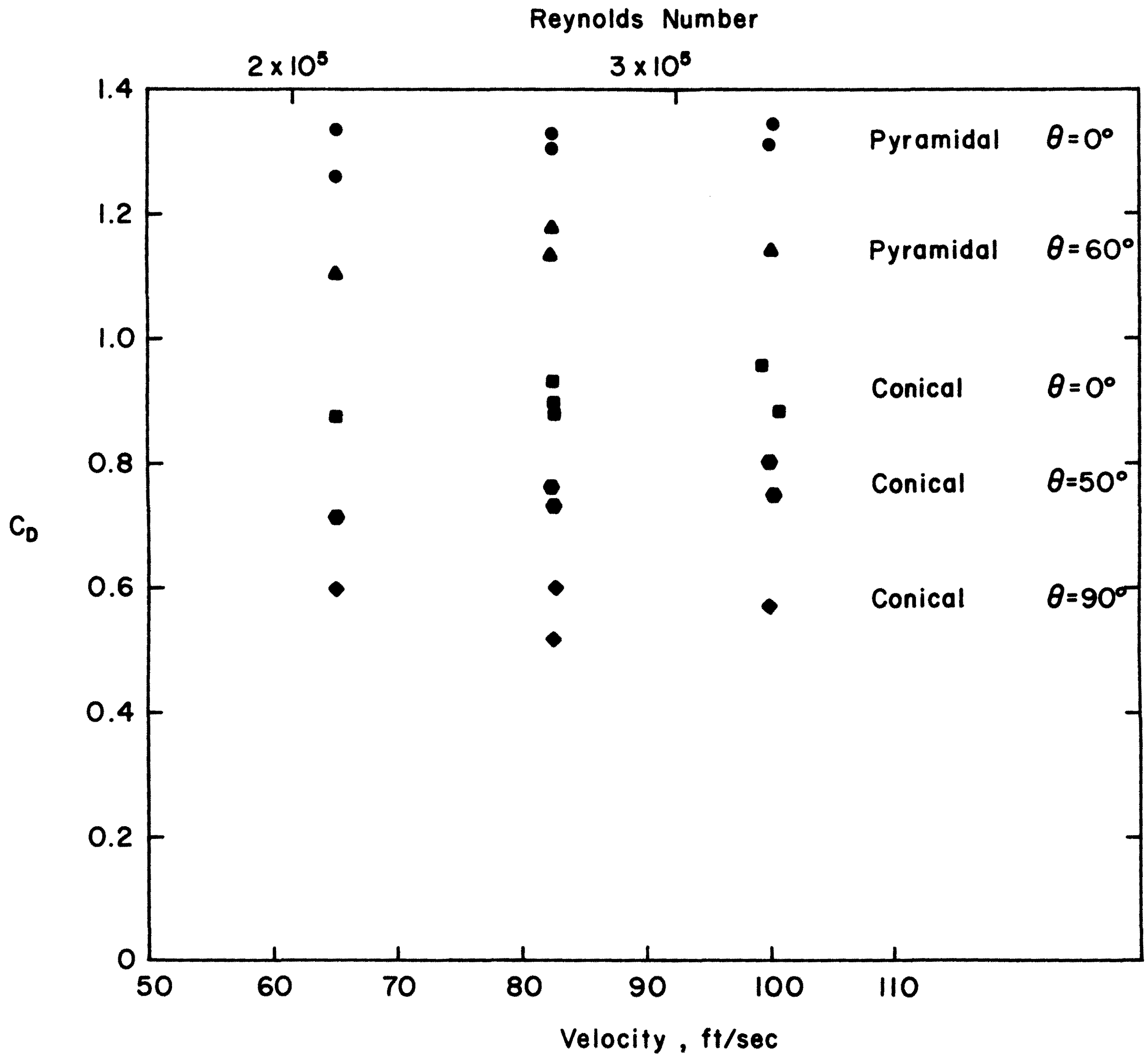

Fig. 10 Effect of Reynolds number on the drag coefficient of single horns

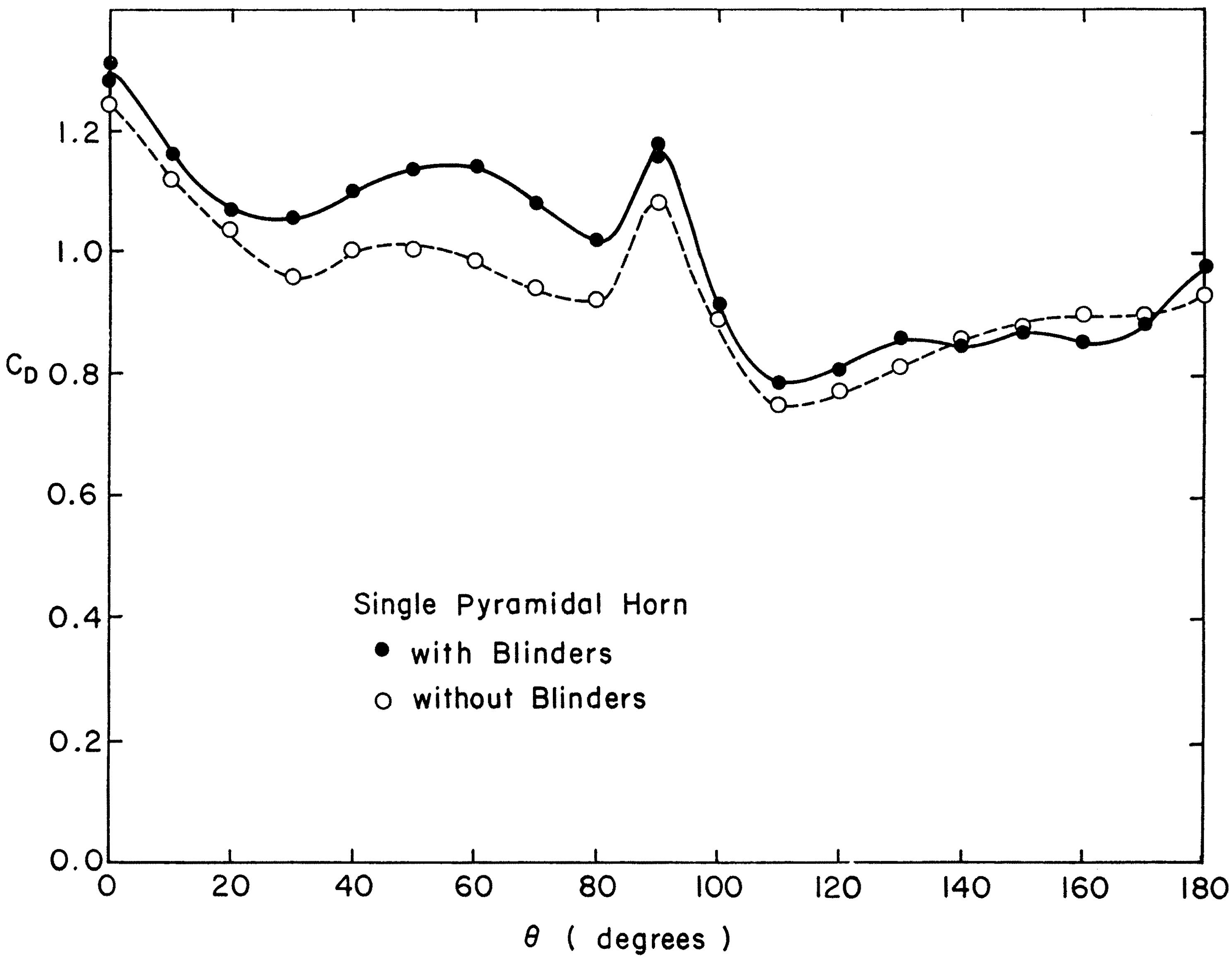

Fig. 11 Drag coefficients of single pyramidal horns

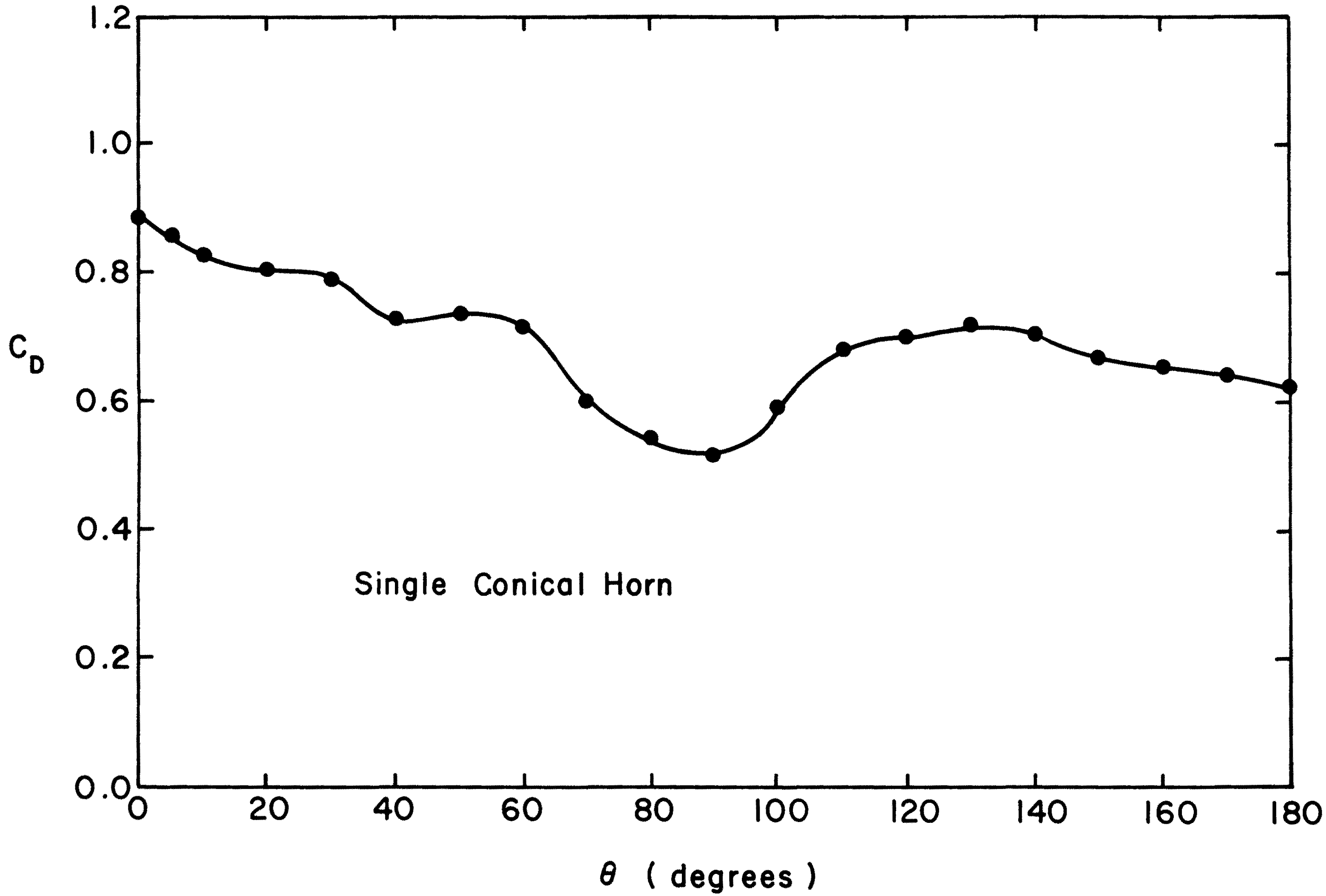

Fig. 12 Drag coefficients of a single conical horn

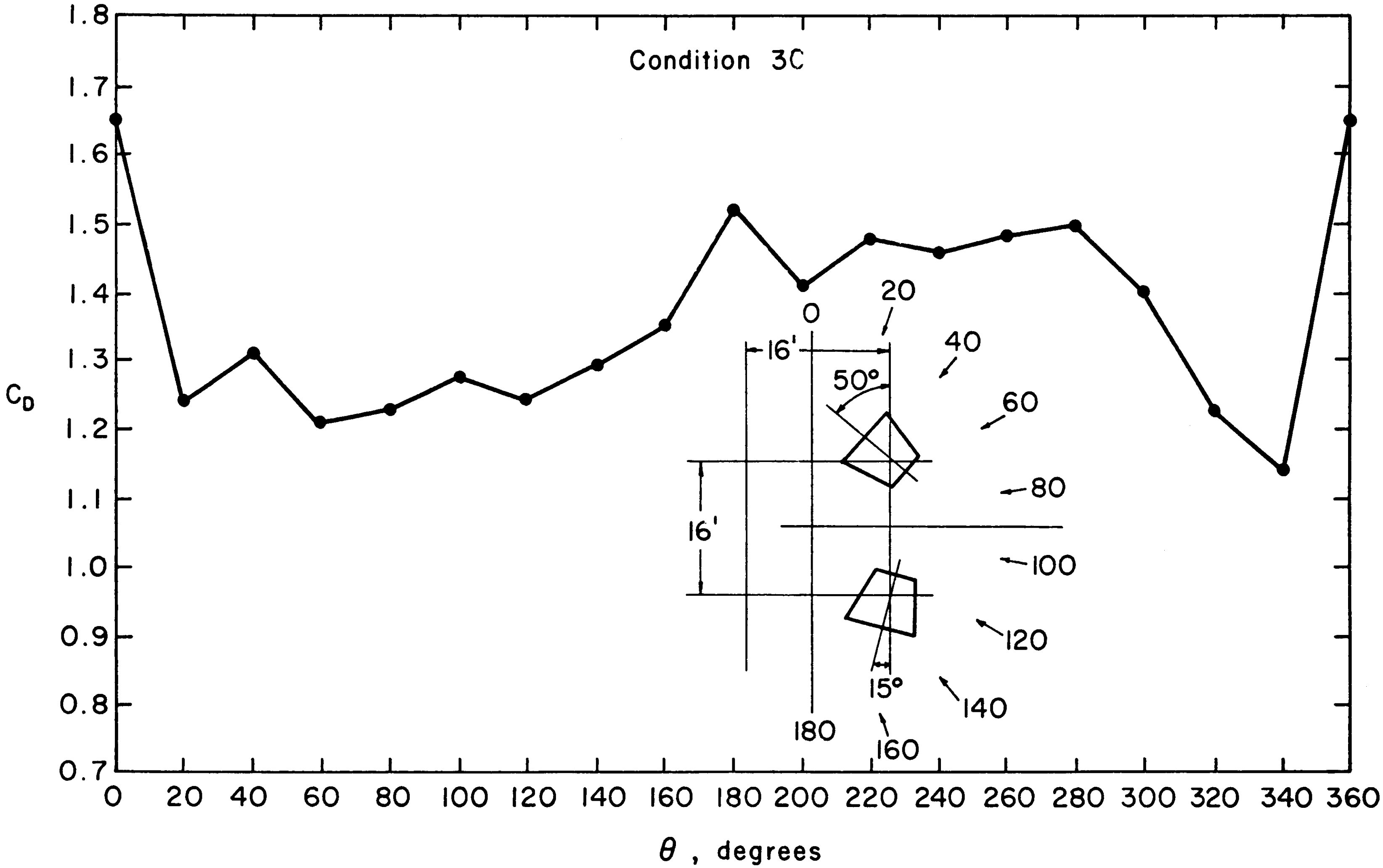

Fig. 13 Drag coefficients of a two-horn cluster (condition 3C)

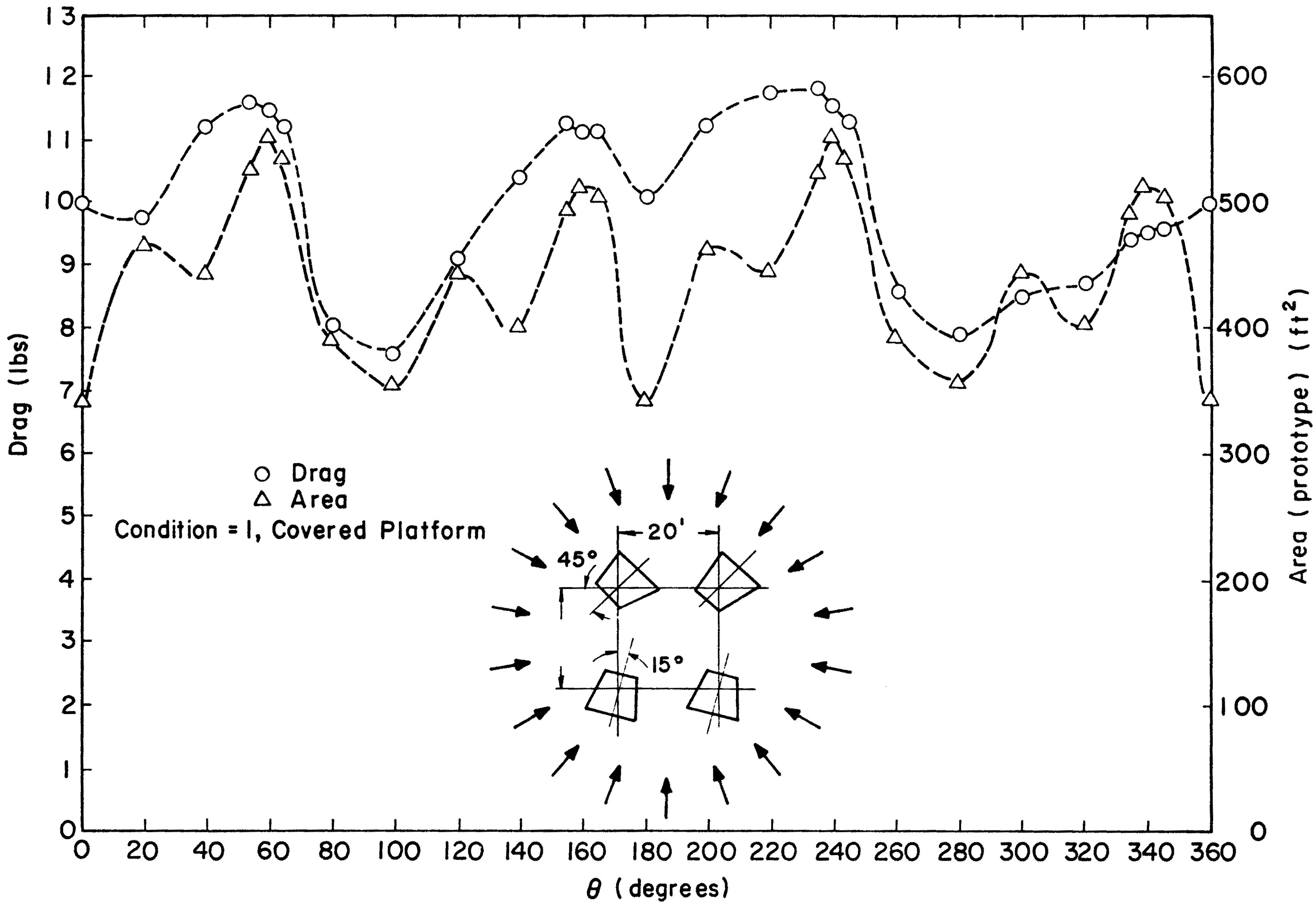

Fig. 14 Measured drag on a four horn cluster (condition 1 covered platform)

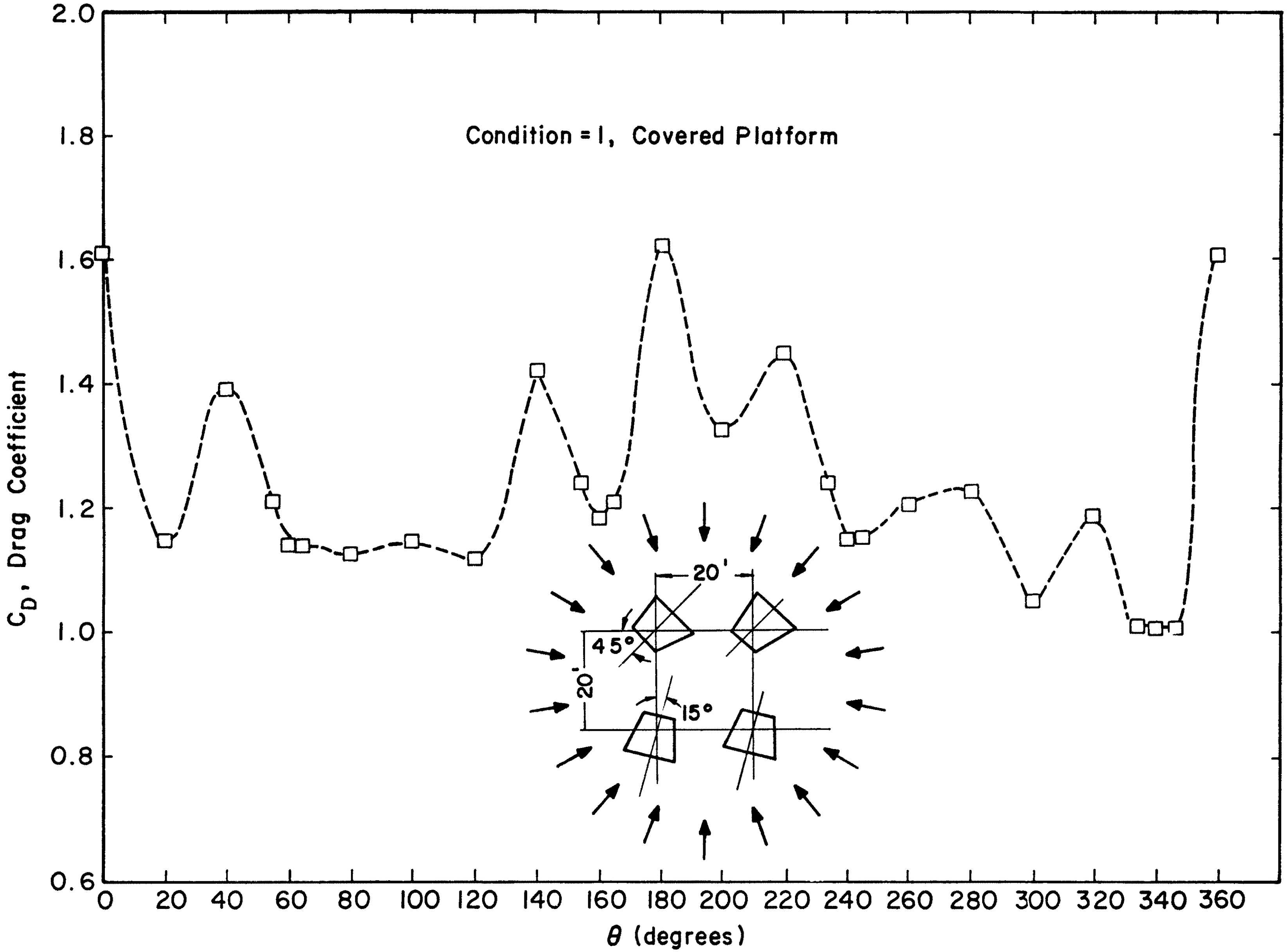

Fig. 15 Drag coefficients of a four-horn cluster (condition 1 covered platform)

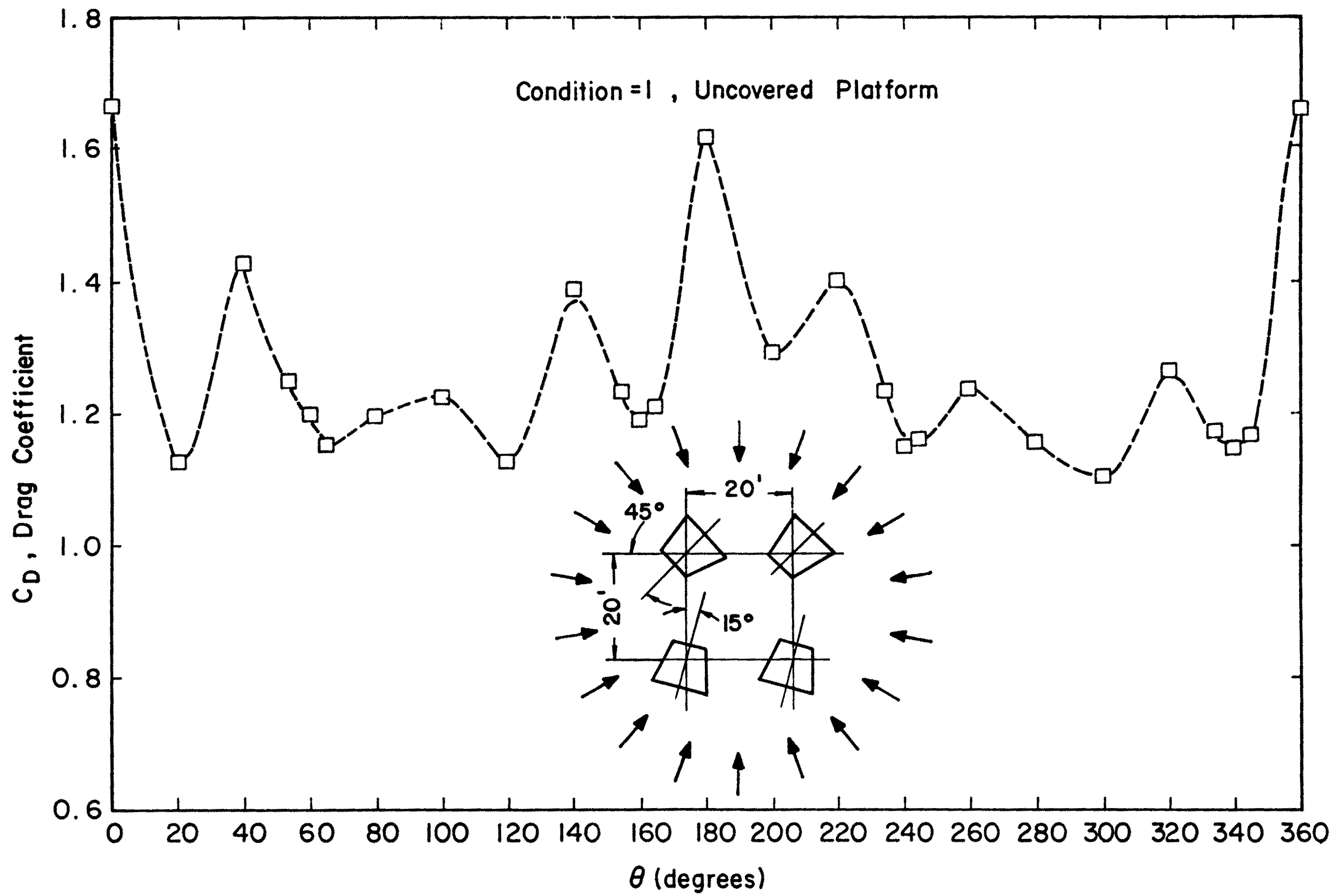

Fig. 16 Drag coefficient of a four horn cluster, condition 1

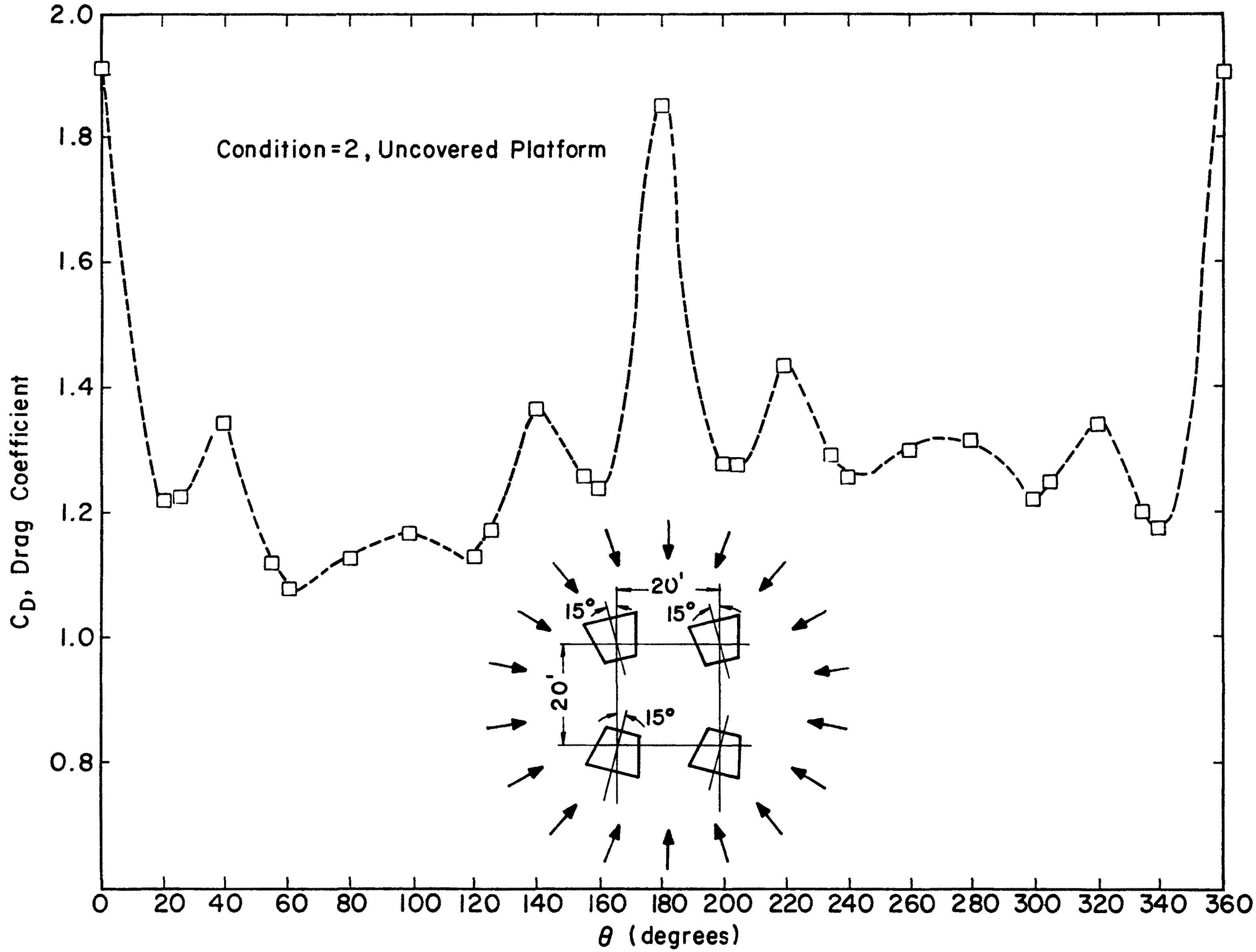

Fig. 17 Drag coefficients of a four-horn cluster (condition 3)

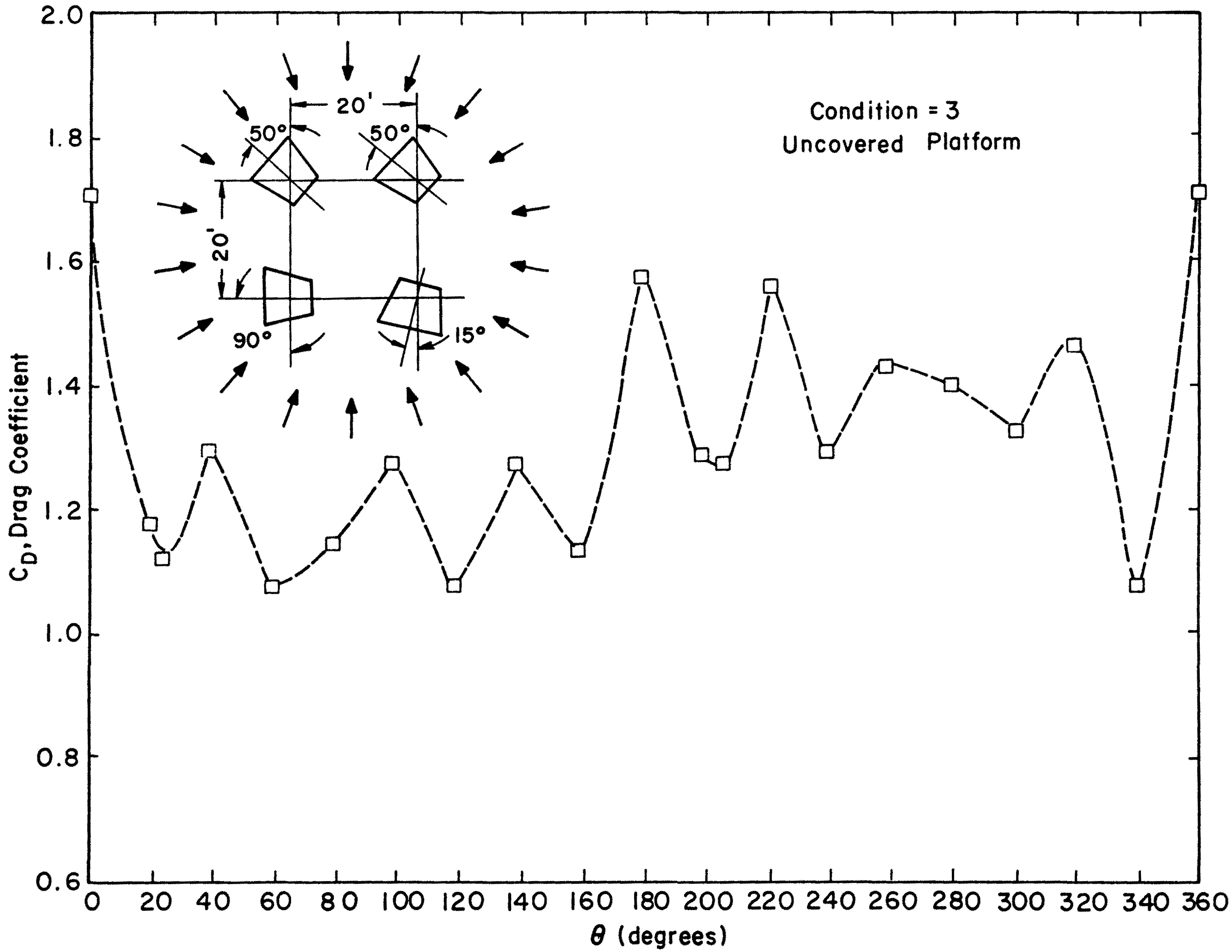

Fig. 18 Drag coefficients of a four-horn cluster (condition 3)

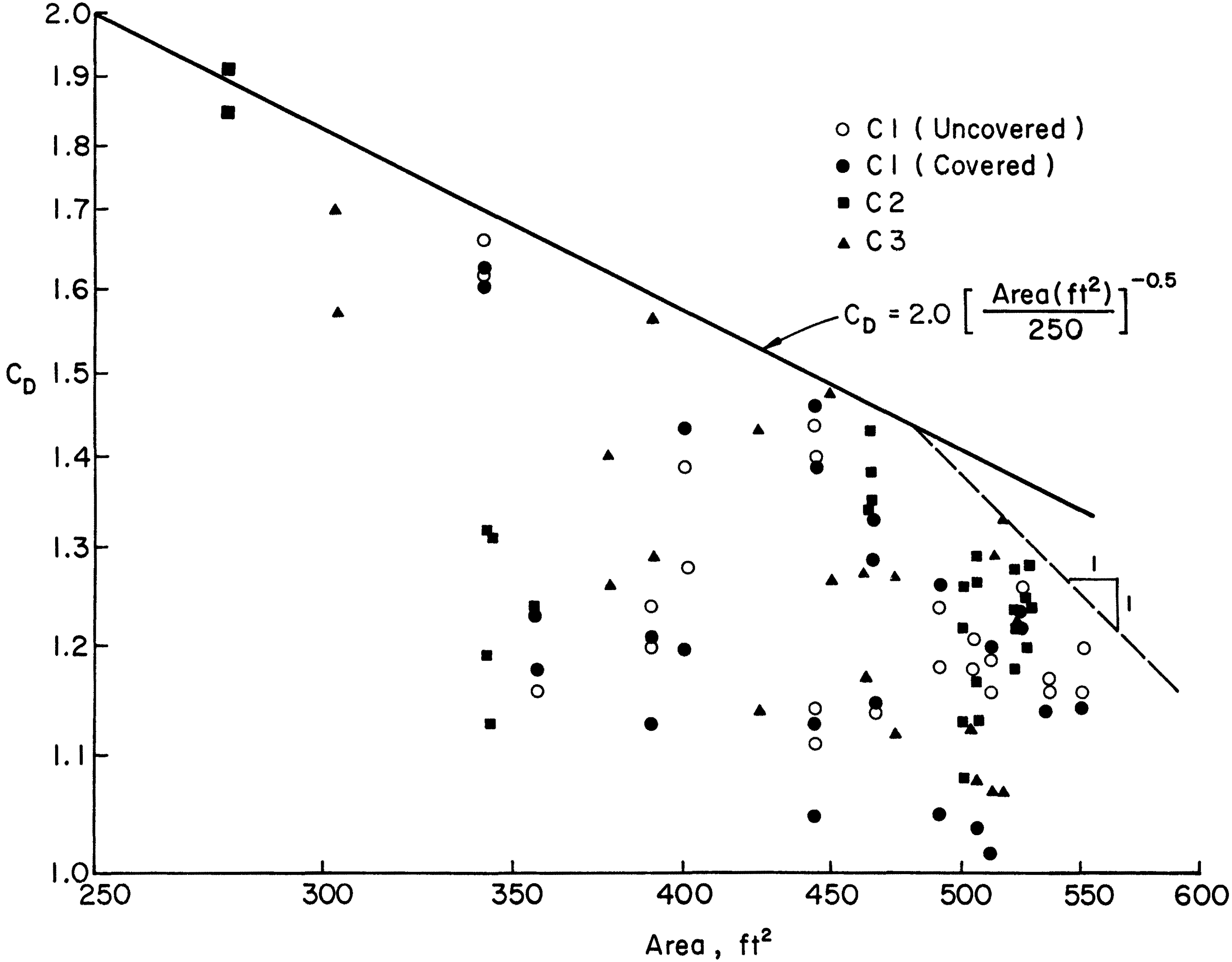

Fig. 19 Dependence of the drag coefficient of four-horn clusters on the projected area

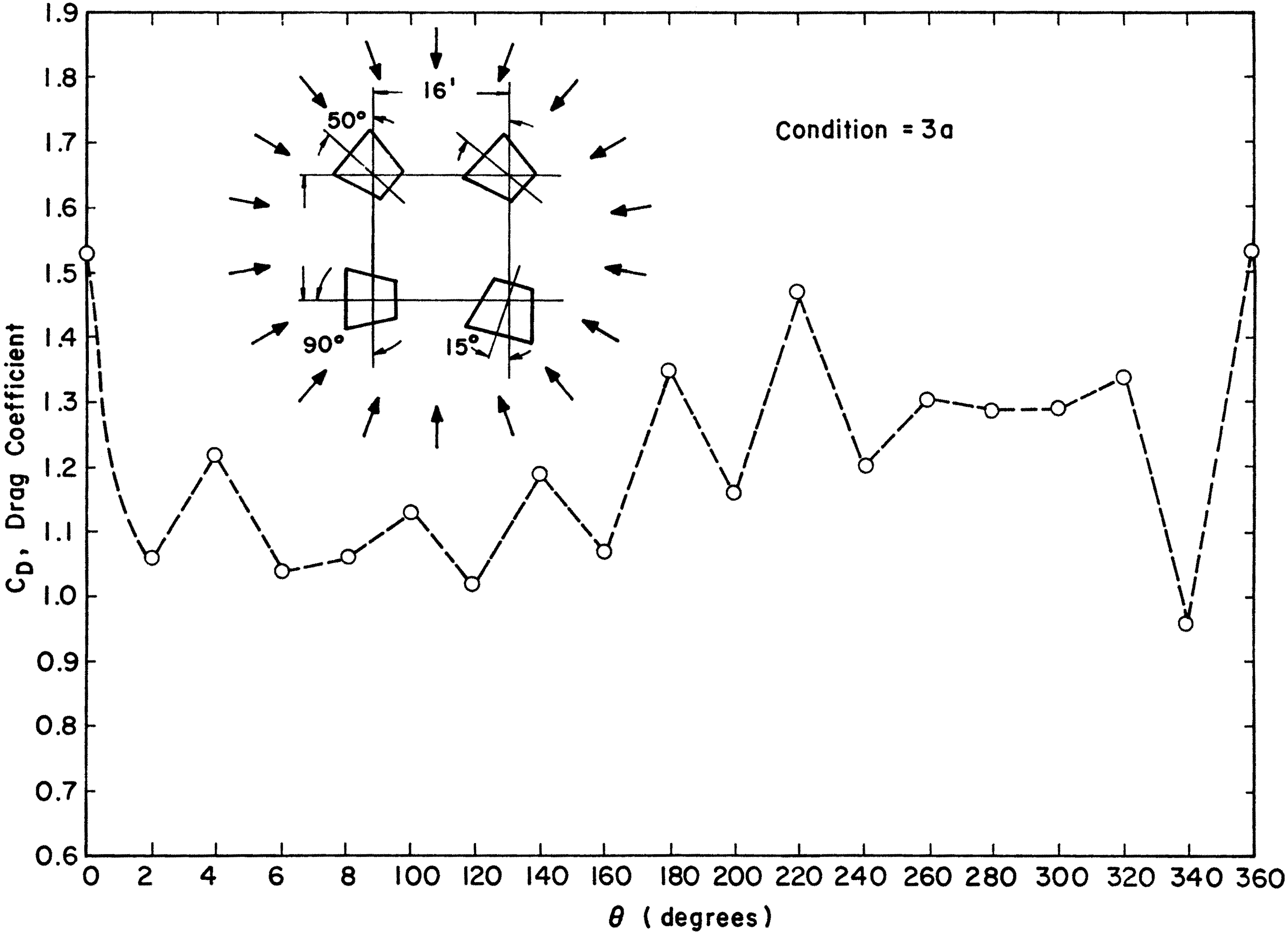

Fig. 20 Drag coefficients of a four-horn cluster (condition 3a)

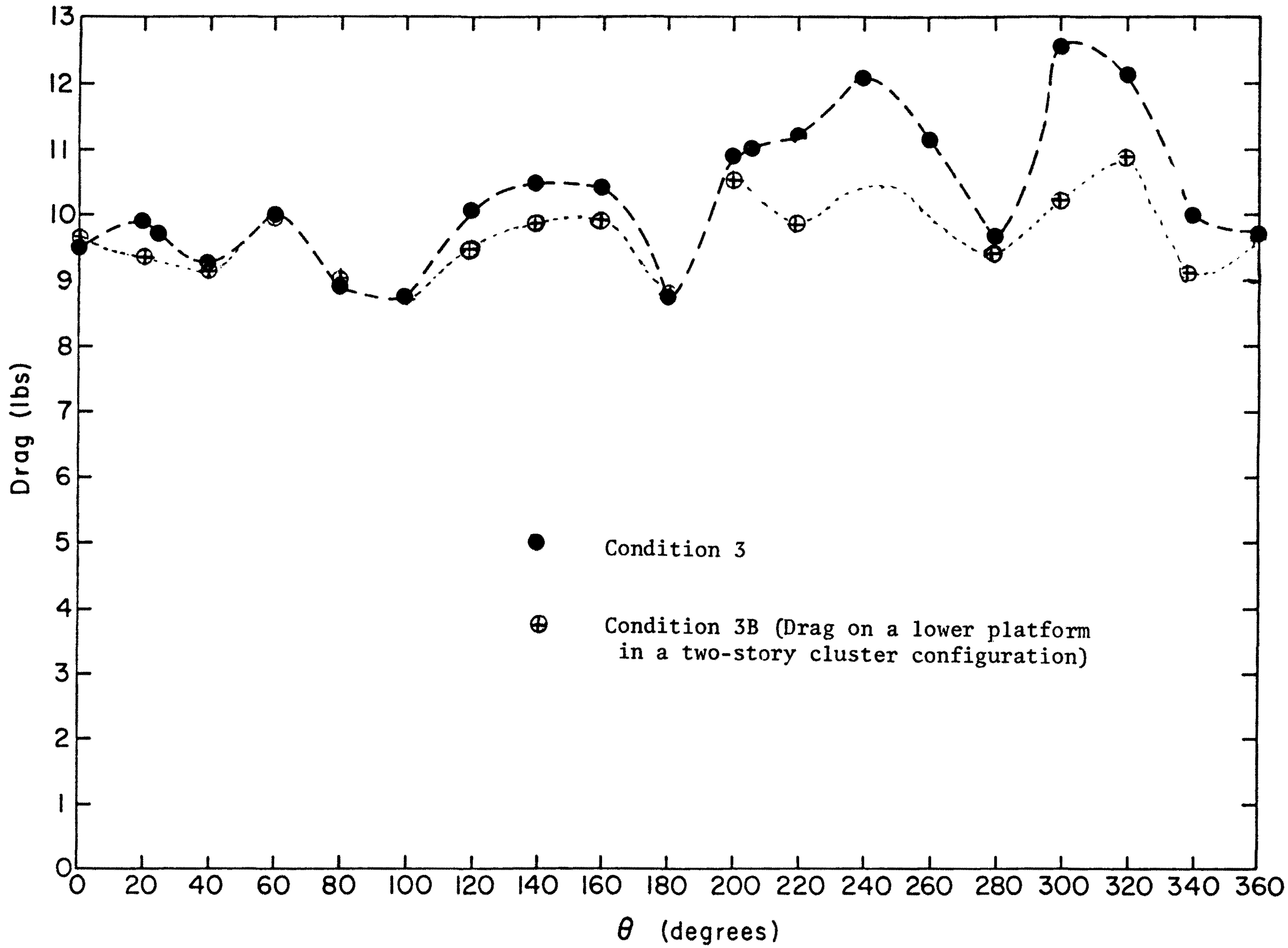

Fig. 21 Measured drag on a four-horn cluster with and without an upper platform

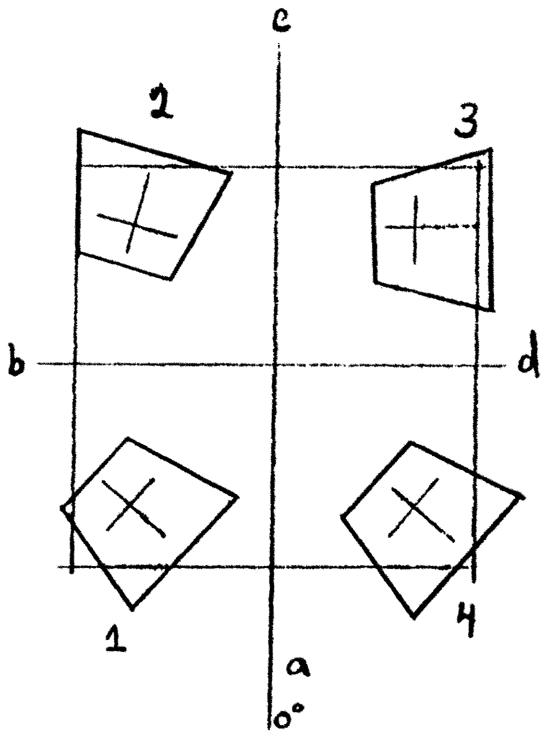

Condition 3
Wind Direction 0^{o}
C_D = 1.71
(uncovered platform).

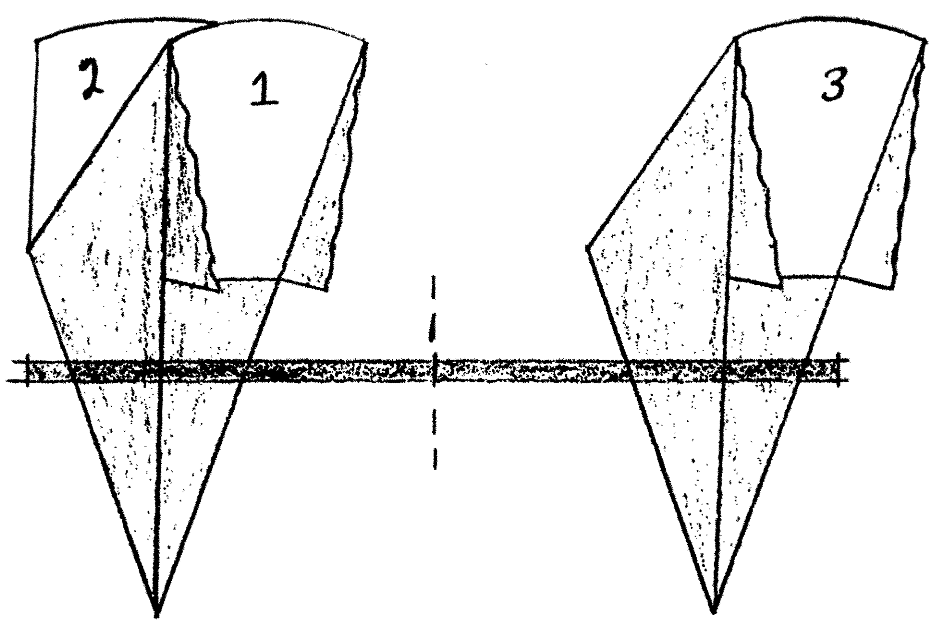

Fig. 22 Schematic view of cluster configuration facing downwind-Condition 3. Wind Direction 0^{o}.

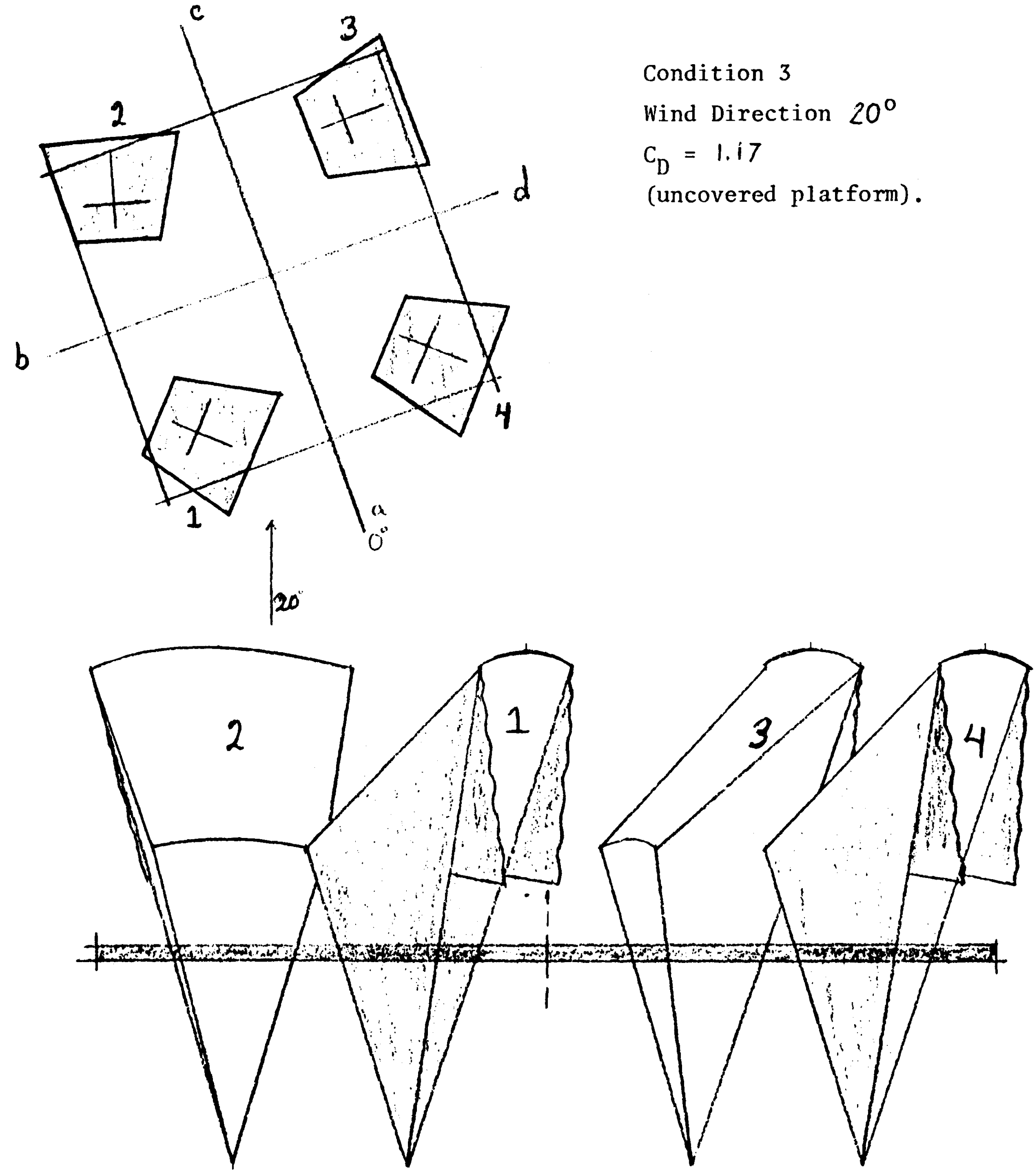

Fig. 23 Schematic view of cluster configuration facing downwind-
Condition 3. Wind Direction 20°.

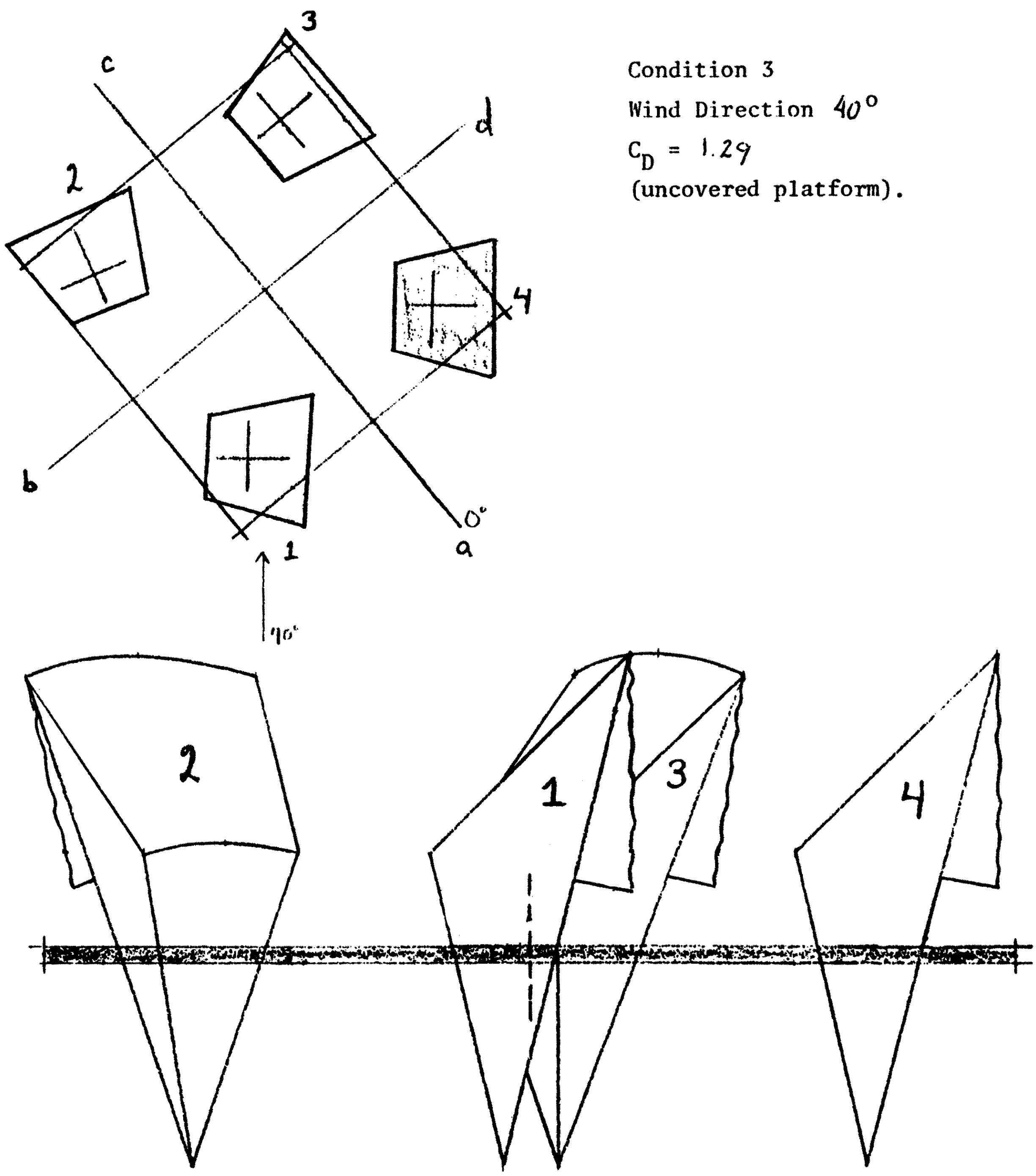

Condition 3

Wind Direction 40°

C_D = 1.29

(uncovered platform).

Fig. 24 Schematic view of cluster configuration facing downwind-Condition 3. Wind Direction 40°.

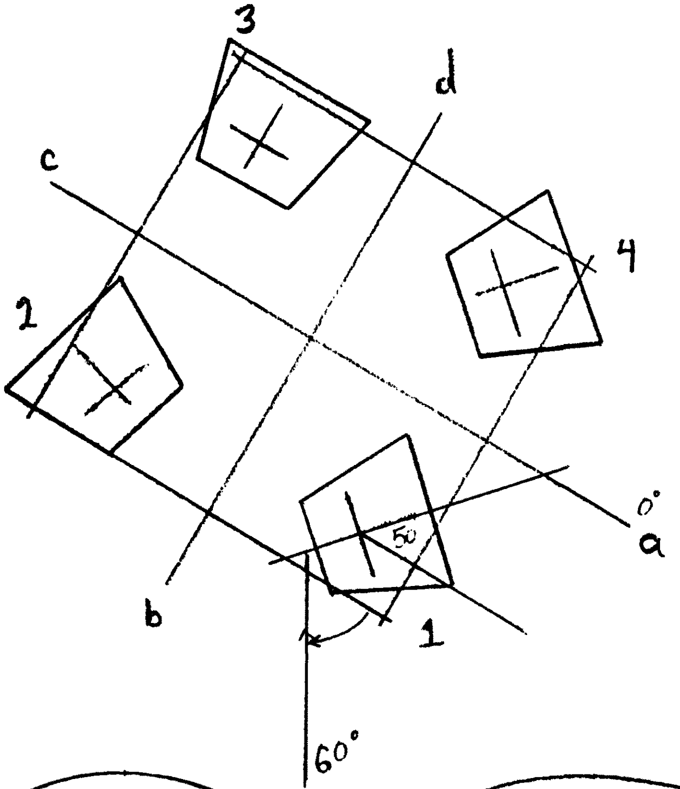

Condition 3
Wind Direction 60°
C_D = 1.07
(uncovered platform).

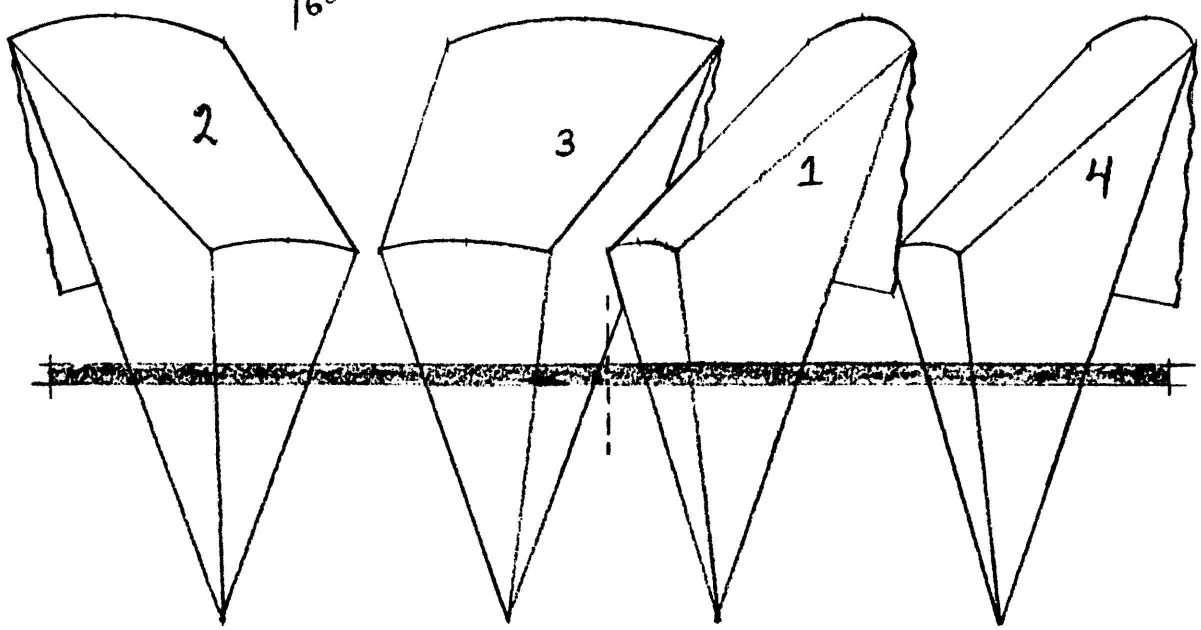

Fig. 25 Schematic view of cluster configuration facing downwind-
Condition 3. Wind Direction 60°.

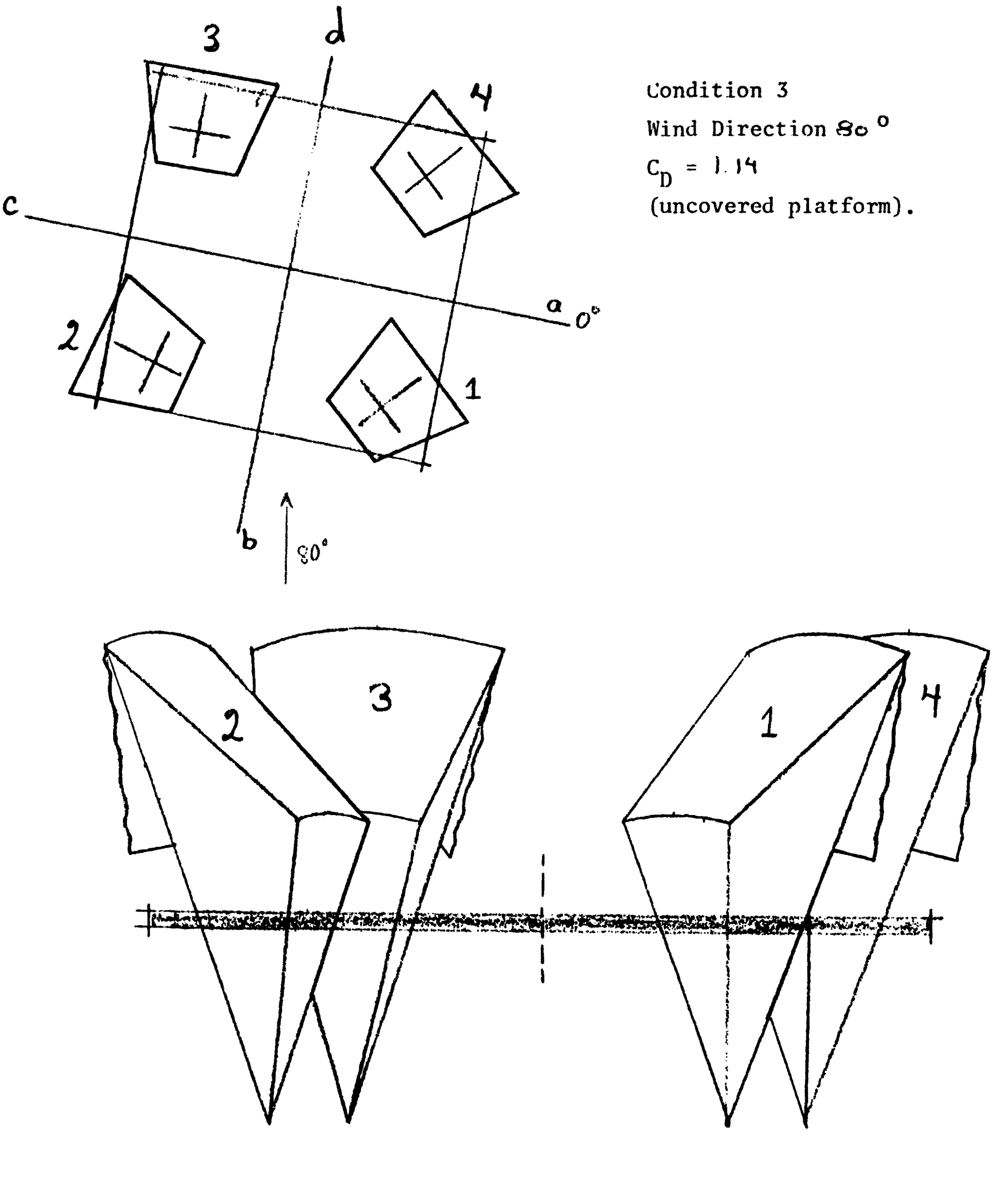

Condition 3
Wind Direction 80 °
C_D = 1.14
(uncovered platform).

Fig. 26 Schematic view of cluster configuration facing downwind-Condition 3. Wind Direction 80°.

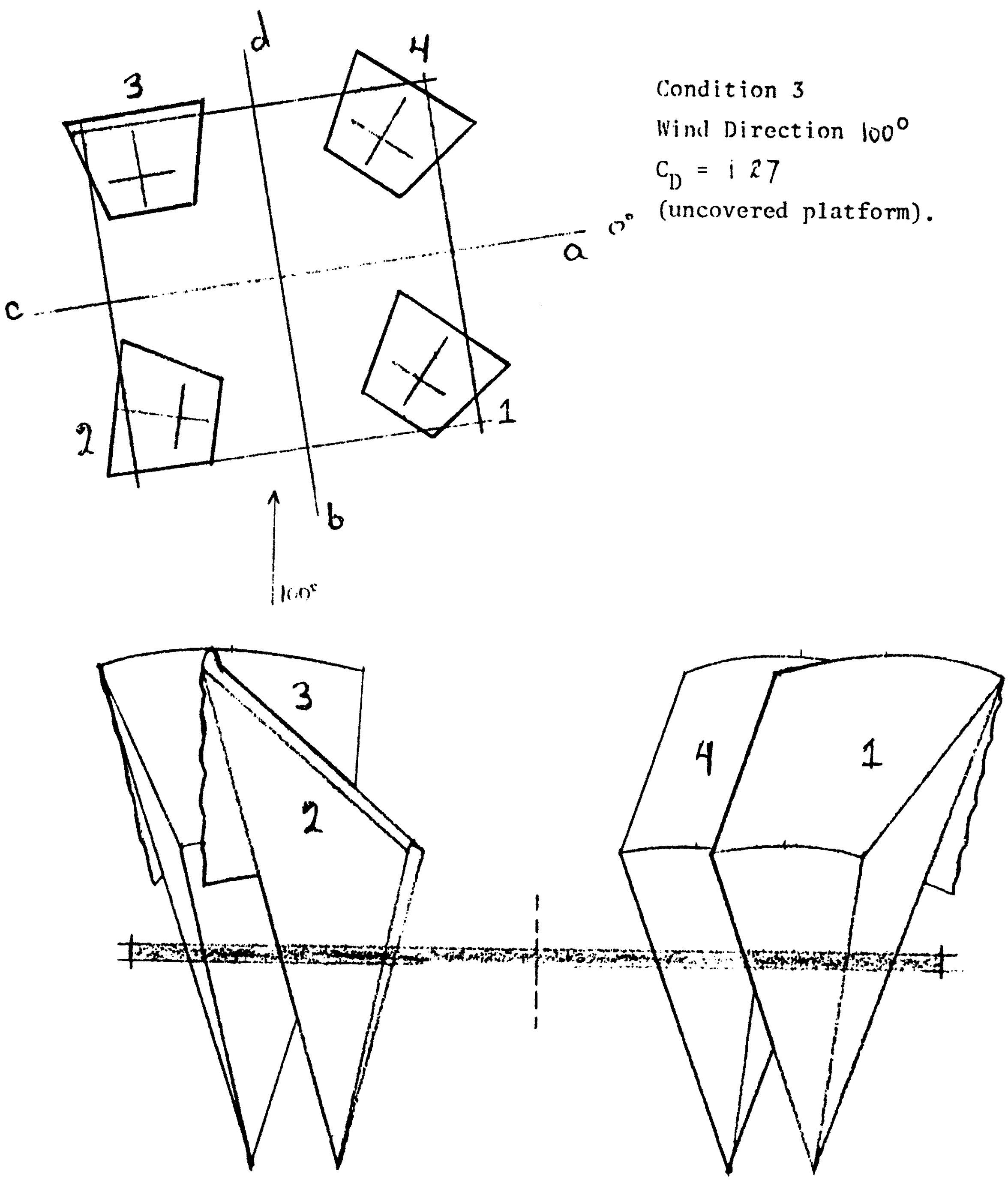

Fig. 27 Schematic view of cluster configuration facing downwind-Condition 3. Wind Direction 100°.

Condition 3
Wind Direction 120°
C_D = 1.07
(uncovered platform).

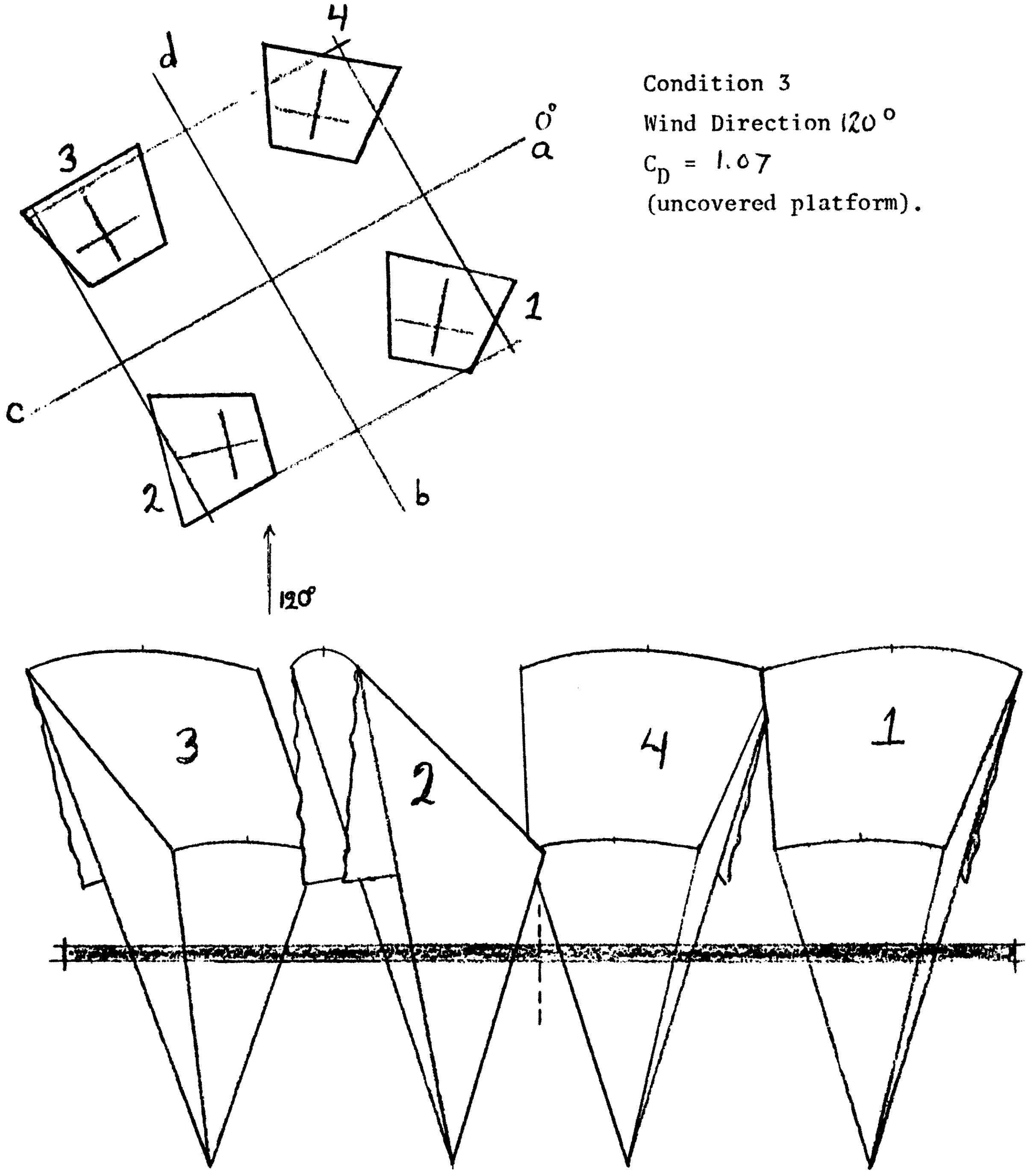

Fig. 28 Schematic view of cluster configuration facing downwind-Condition 3. Wind Direction 120°.

Condition 3
Wind Direction 140°
C_D = 1.27
(uncovered platform).

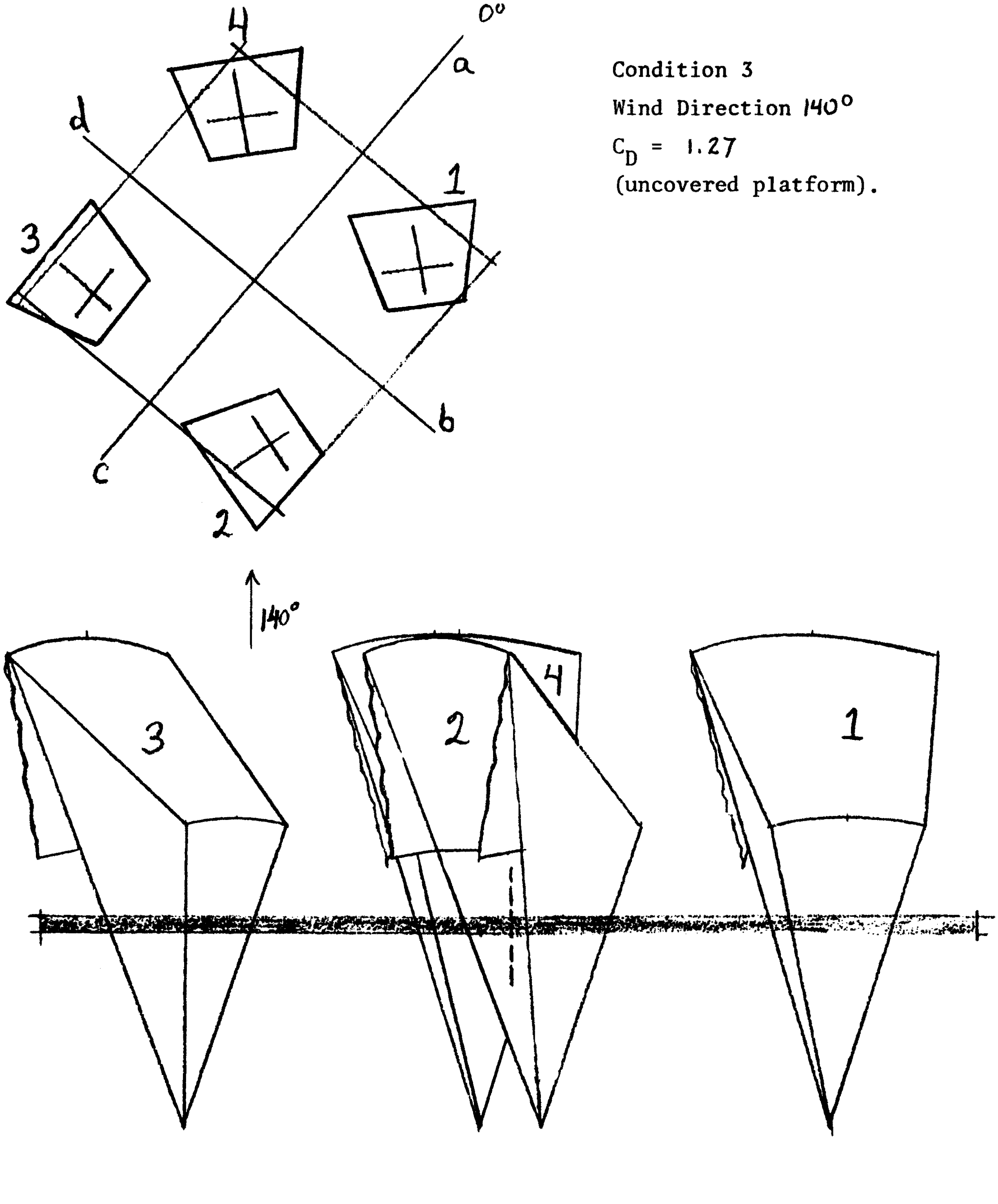

Fig. 29 Schematic view of cluster configuration facing downwind-Condition 3. Wind Direction 140°.

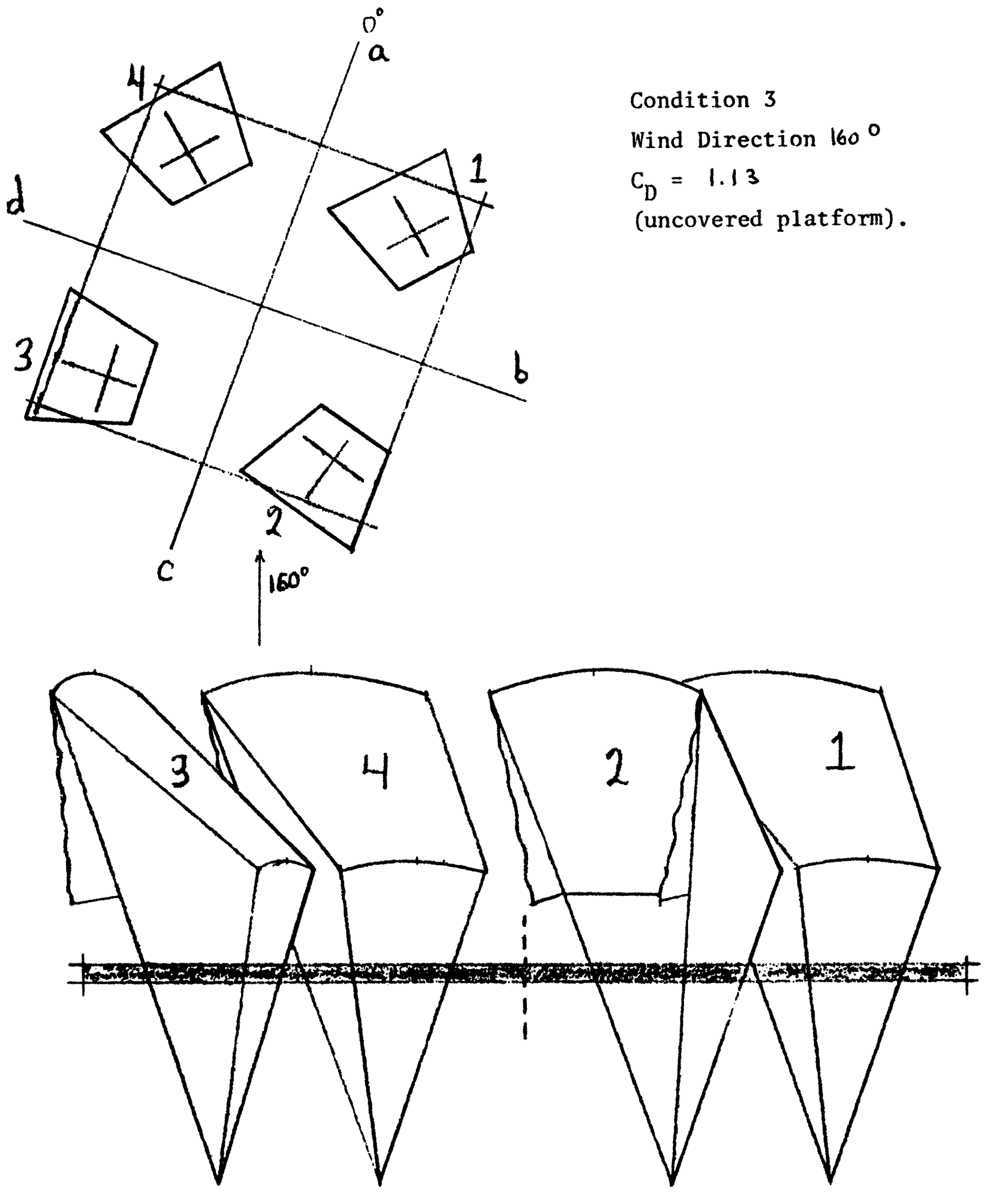

Condition 3

Wind Direction 160 °

C_D = 1.13

(uncovered platform).

Fig. 30 Schematic view of cluster configuration facing downwind-Condition 3. Wind Direction 160°.

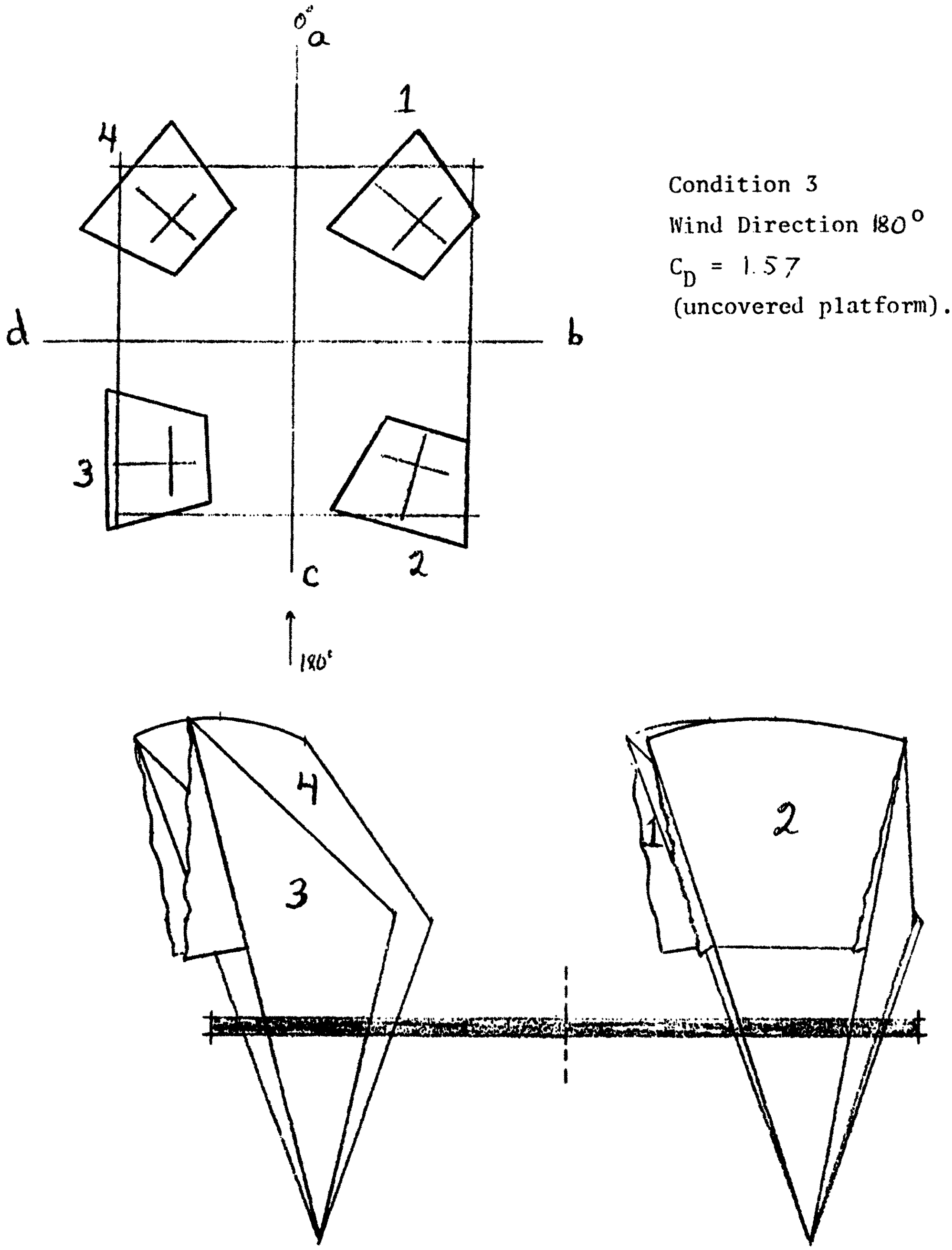

Fig. 31 Schematic view of cluster configuration facing downwind-Condition 3. Wind Direction 180°.

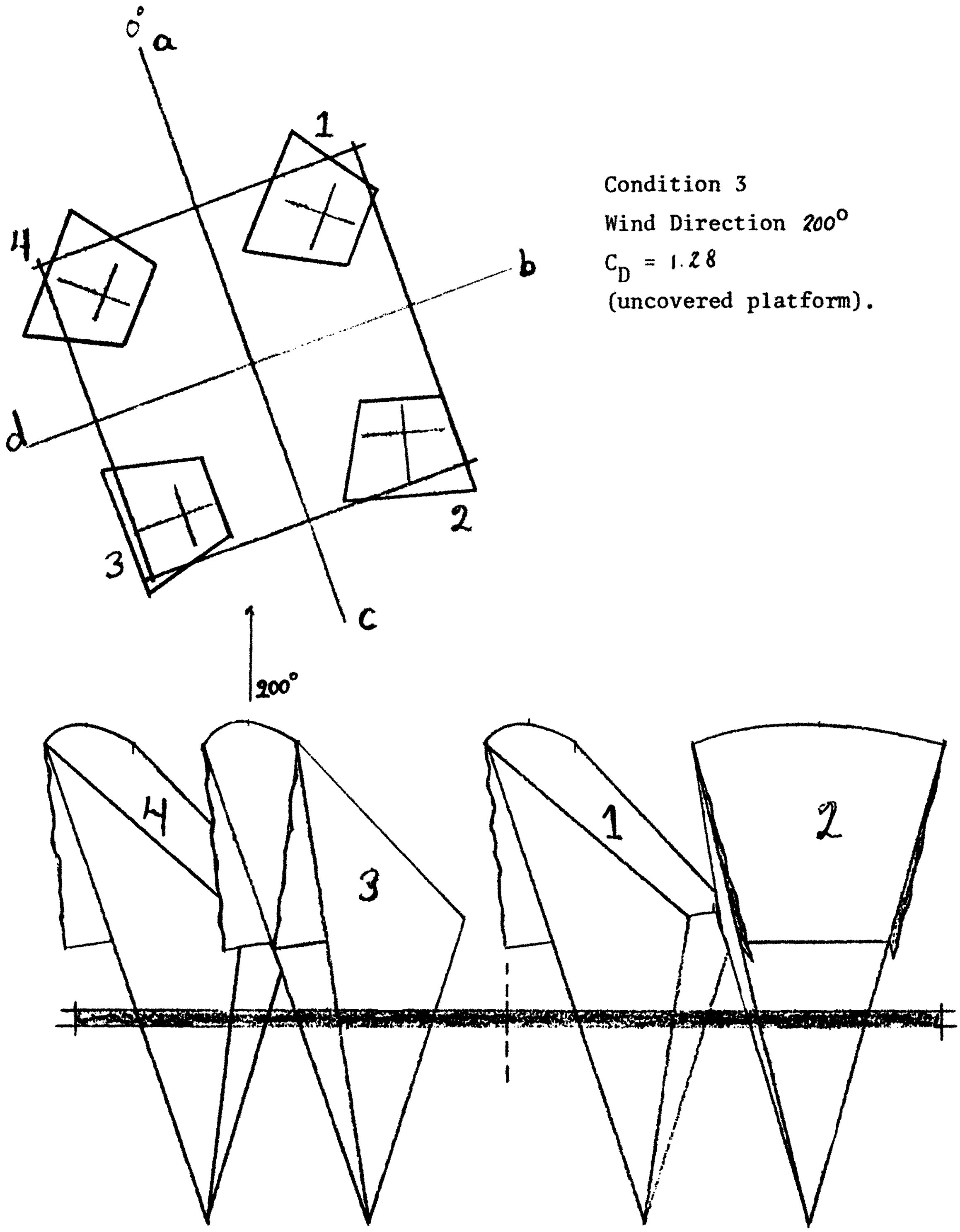

Condition 3
Wind Direction 200°
C_D = 1.28
(uncovered platform).

Fig. 32 Schematic view of cluster configuration facing downwind-Condition 3. Wind Direction 200°.

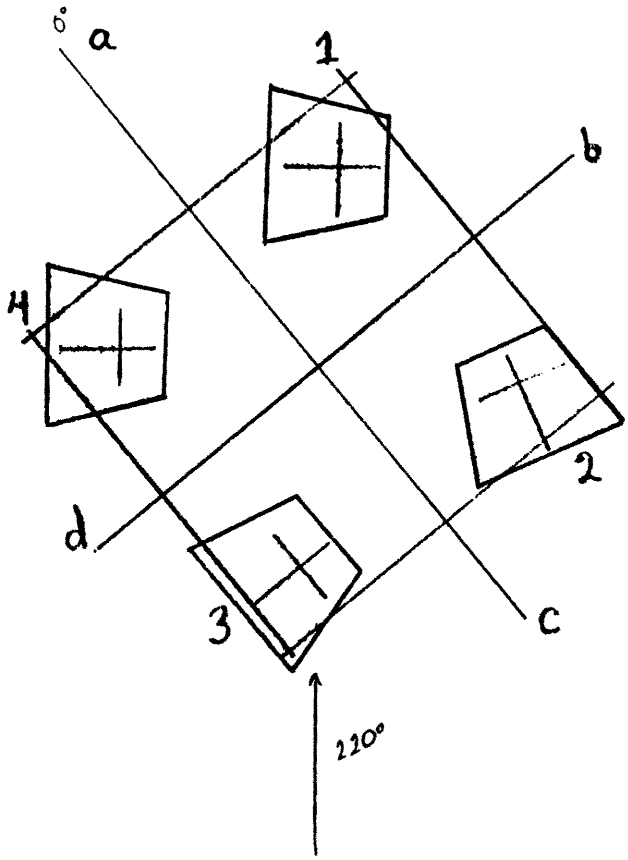

Condition 3
Wind Direction 220°
C_D = 1.56
(uncovered platform).

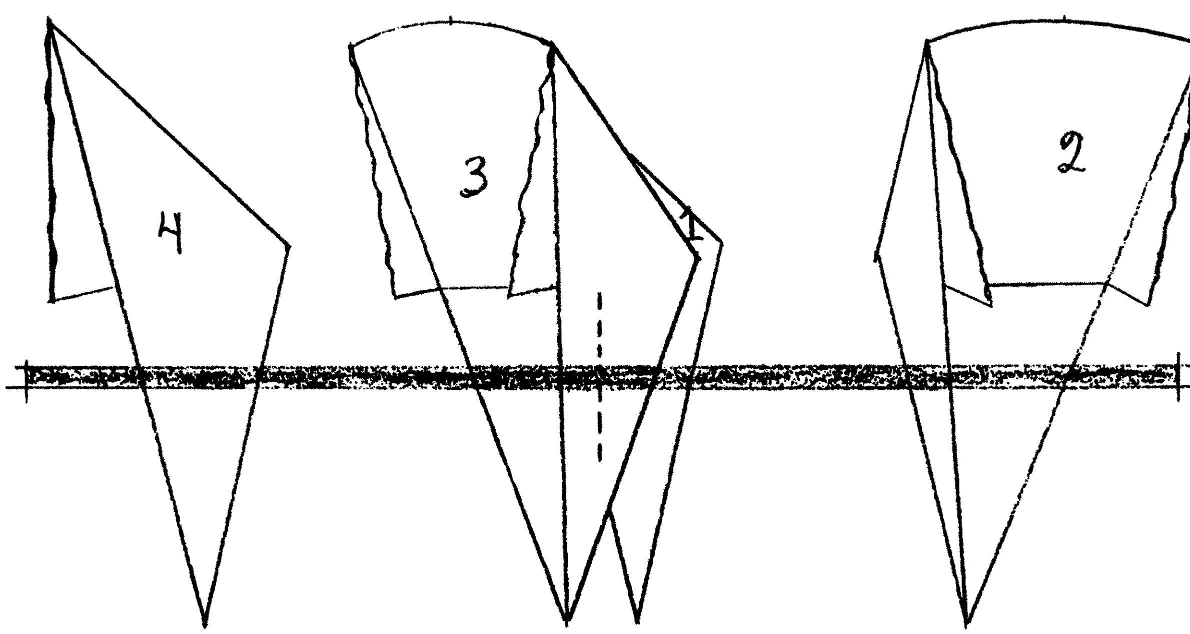

Fig. 33 Schematic view of cluster configuration facing downwind-Condition 3. Wind Direction 220°.

Condition 3

Wind Direction 240°

C_D = 1.29

(uncovered platform).

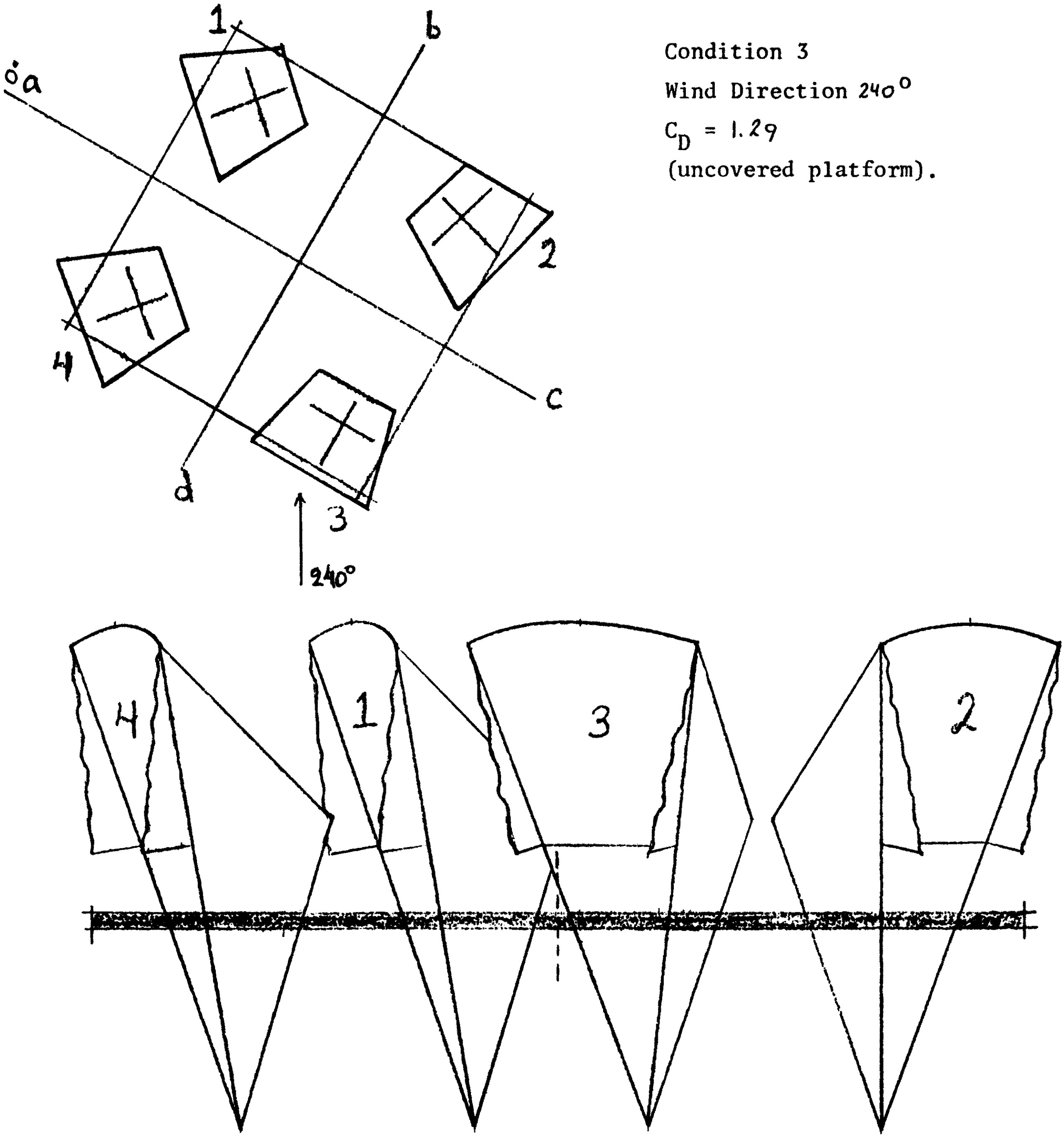

Fig. 34 Schematic view of cluster configuration facing downwind-Condition 3. Wind Direction 240°.

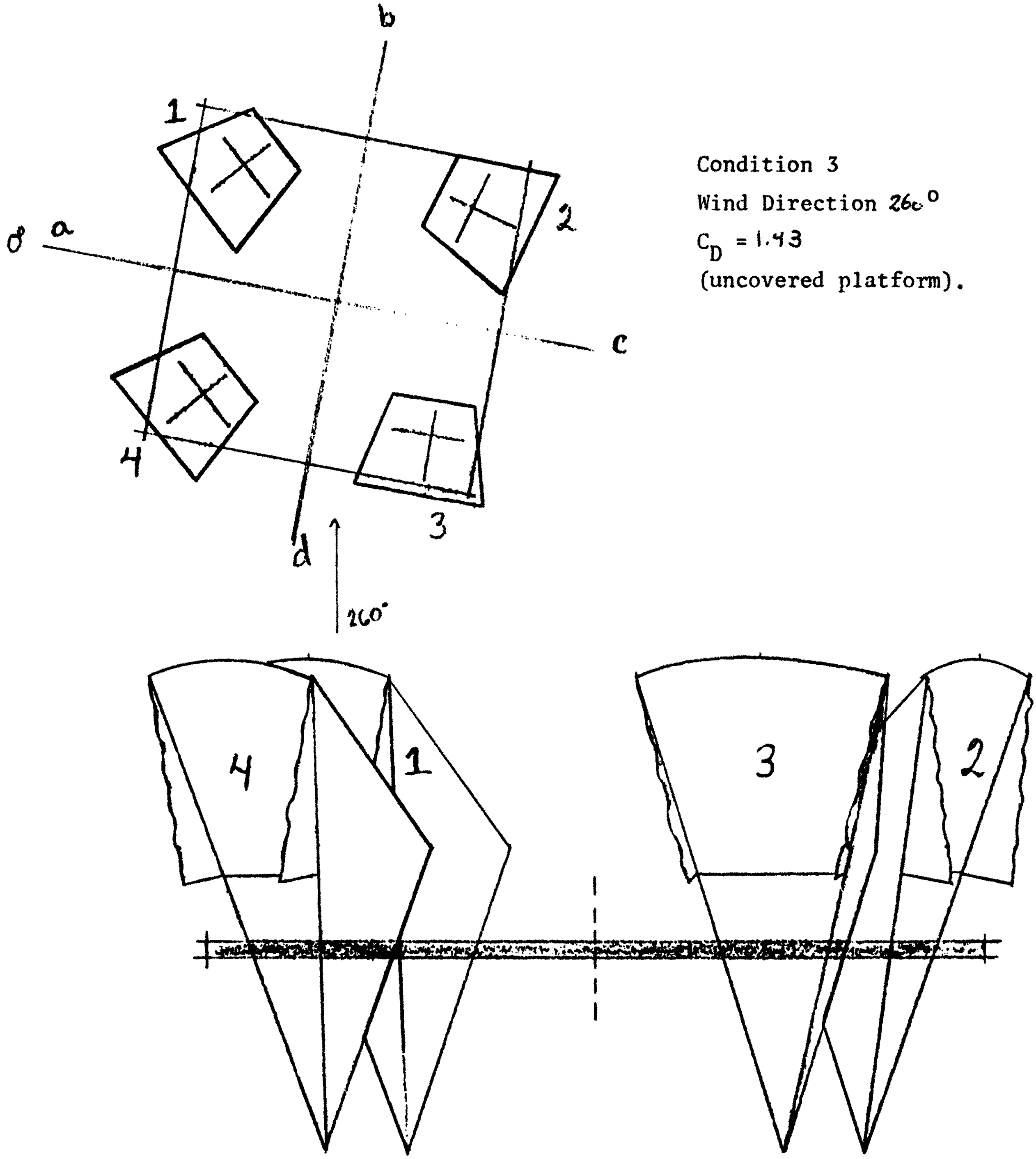

Condition 3
Wind Direction 260°
C_D = 1.43
(uncovered platform).

Fig. 35 Schematic view of cluster configuration facing downwind-Condition 3. Wind Direction 260°.

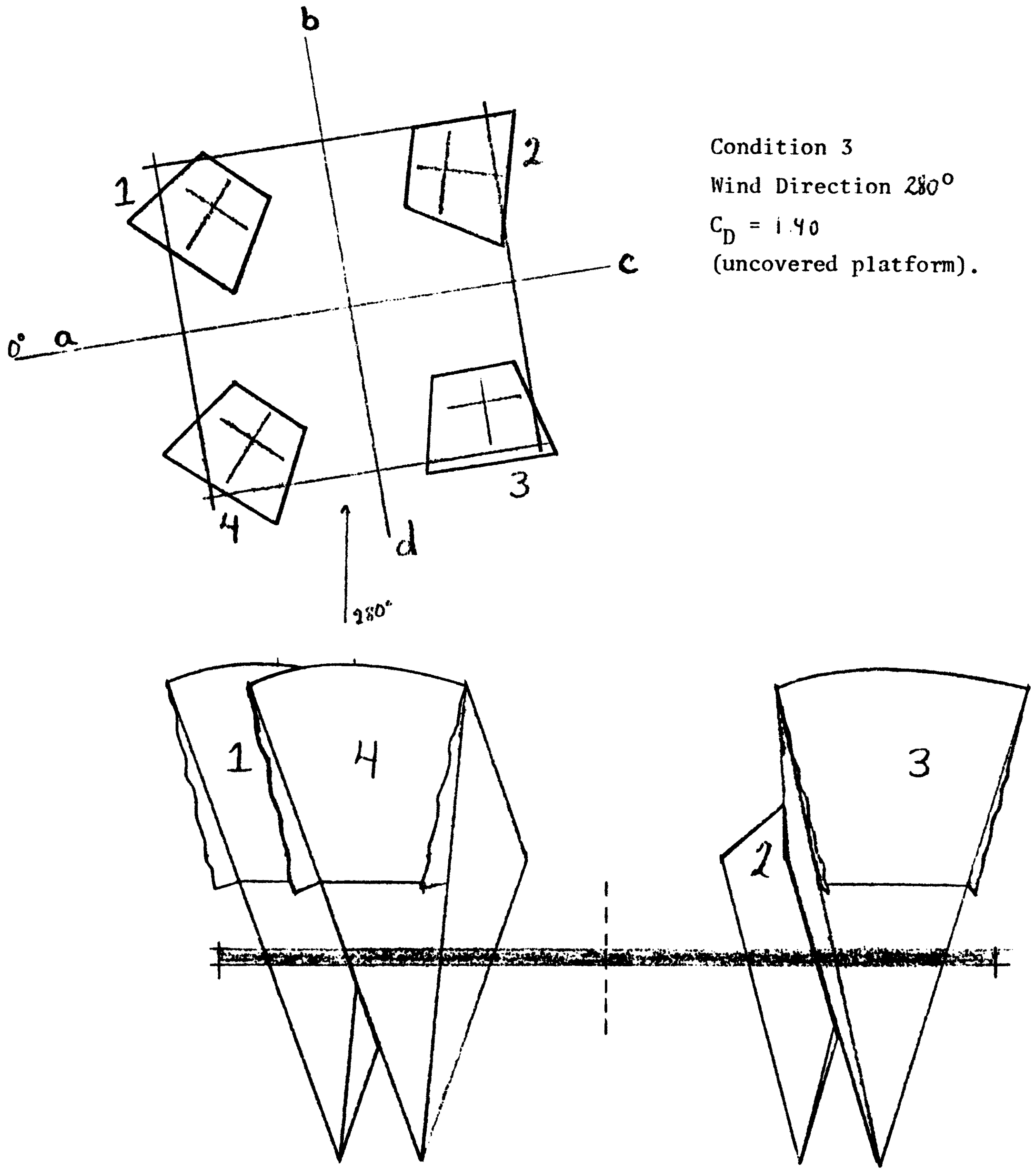

Fig. 36 Schematic view of cluster configuration facing downwind-
Condition 3. Wind Direction 280°.

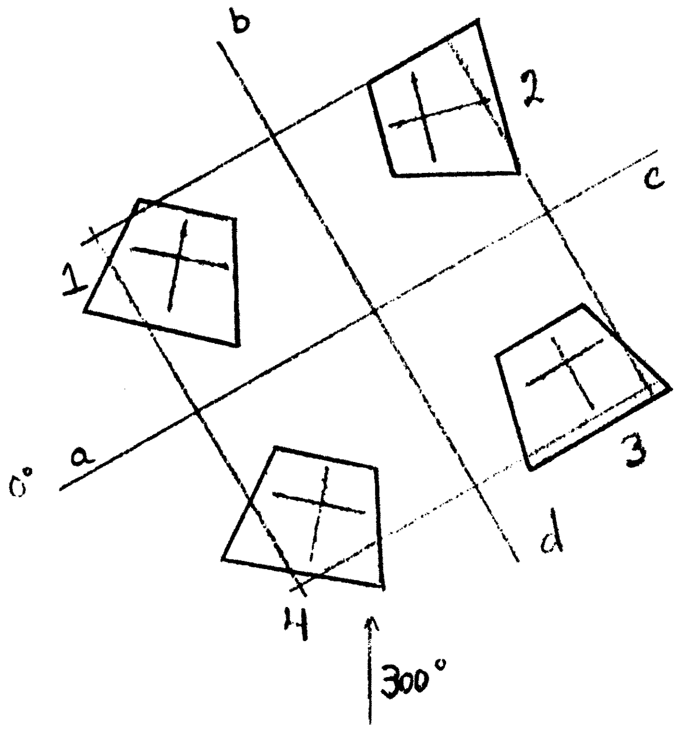

Condition 3

Wind Direction 300°

C_D = 1.33

(uncovered platform).

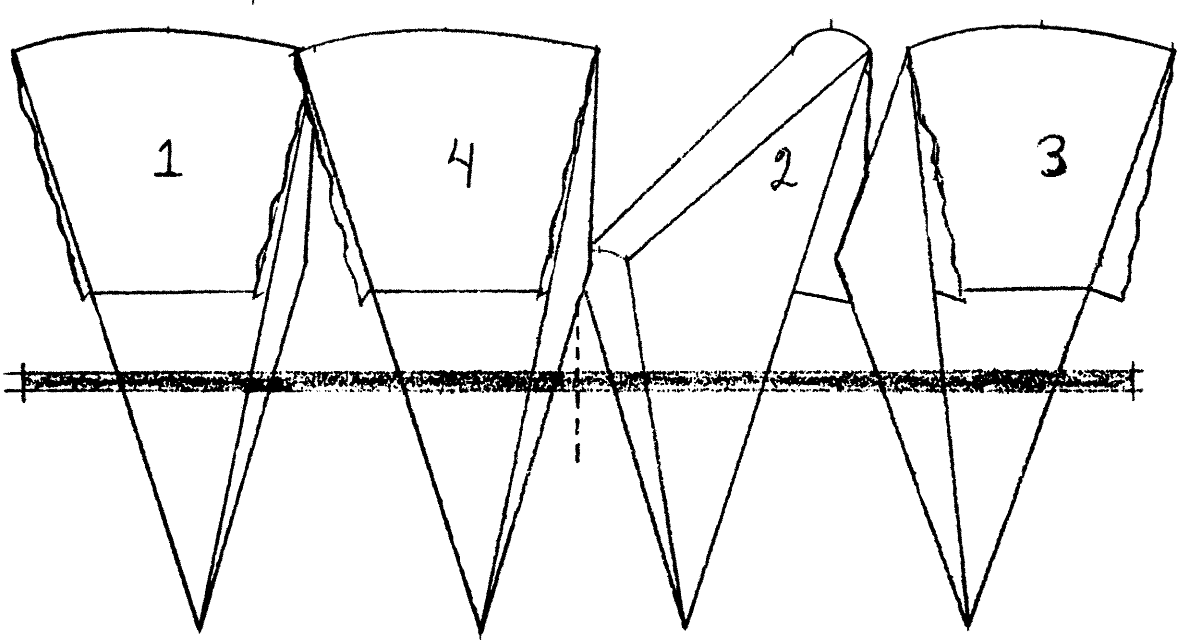

Fig. 37 Schematic view of cluster configuration facing downwind- Condition 3. Wind Direction 300°.

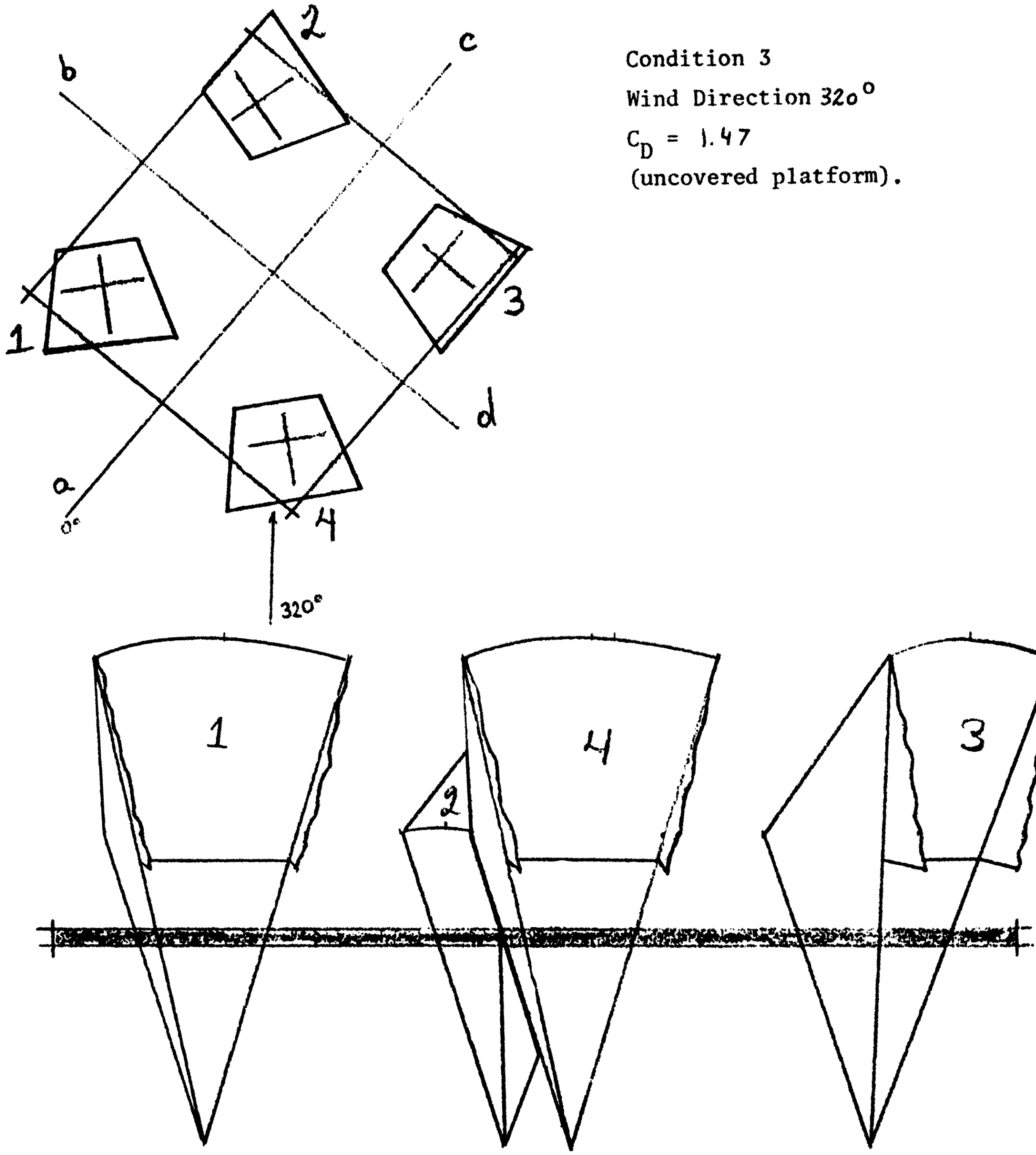

Condition 3

Wind Direction 320°

C_D = 1.47

(uncovered platform).

Fig. 38 Schematic view of cluster configuration facing downwind-Condition 3. Wind Direction 320°.

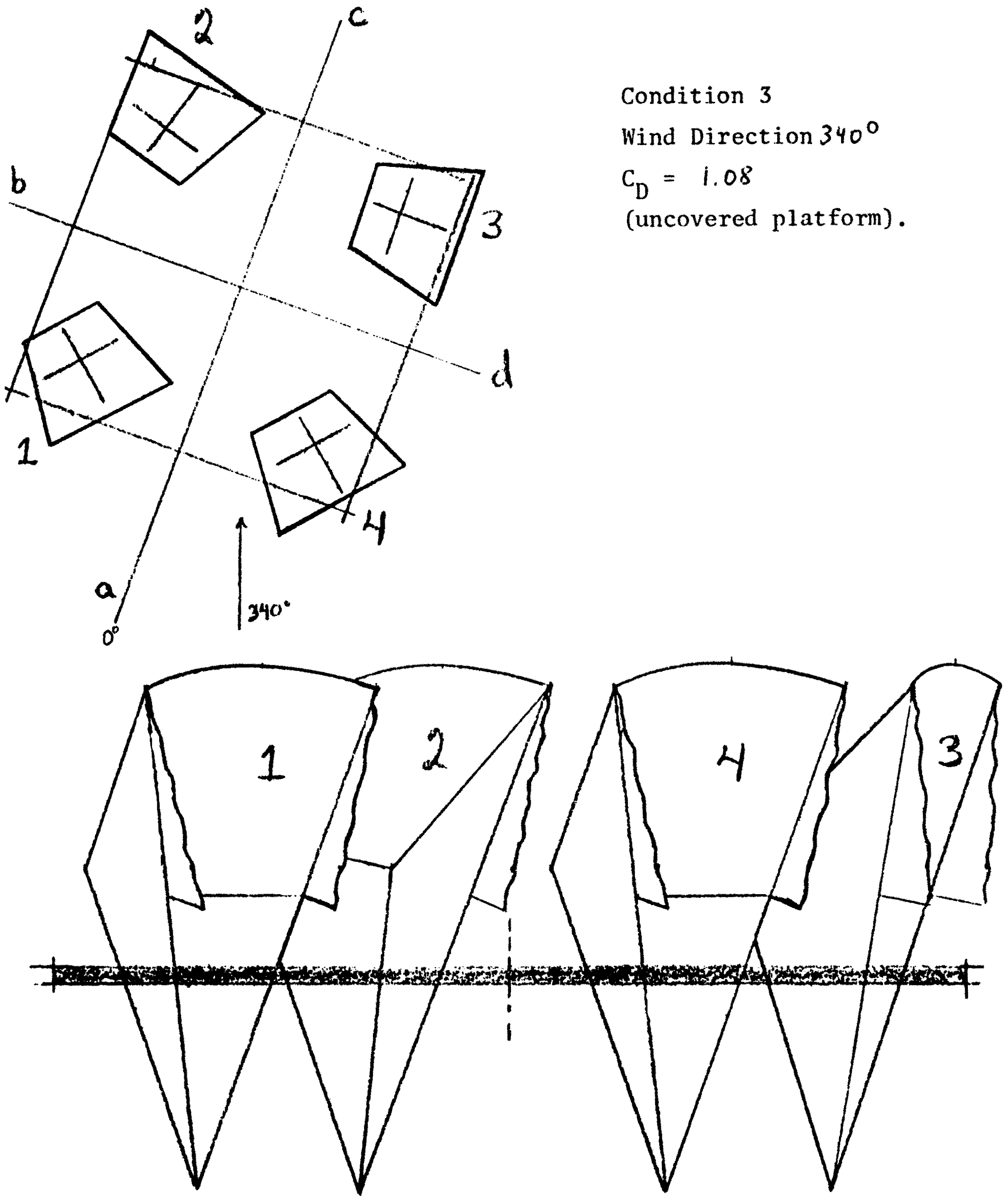

Fig. 39 Schematic view of cluster configuration facing downwind-Condition 3. Wind Direction 340°.

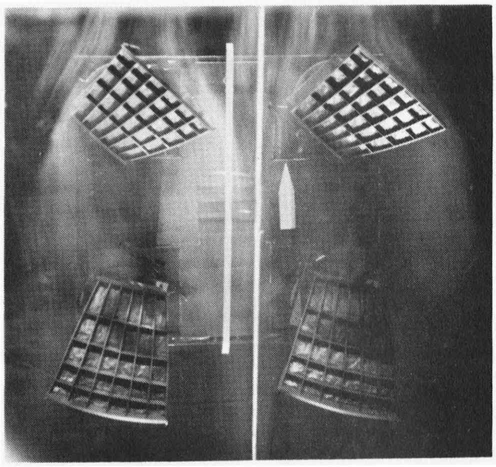

a. Smoke filaments exhibit the structure of the flow.

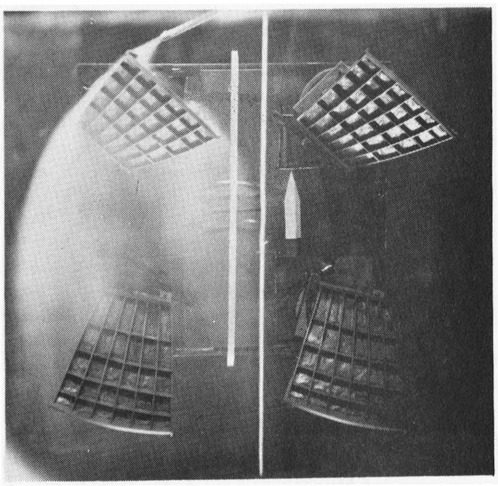

b. Smoke released from a point source shows that the downstream horn is submerged in the wake of the front horn.

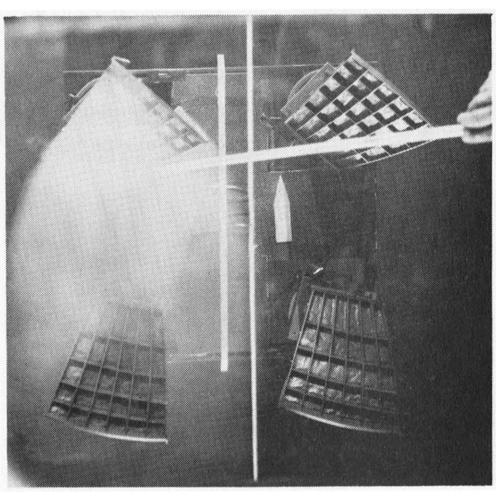

c. Smoke from a point source is trapped in the cavity behind the front horn.

Fig. 40 Structure of the flow around a four horn cluster "Condition 1", θ = 180. Direction of wind from top to bottom of page.

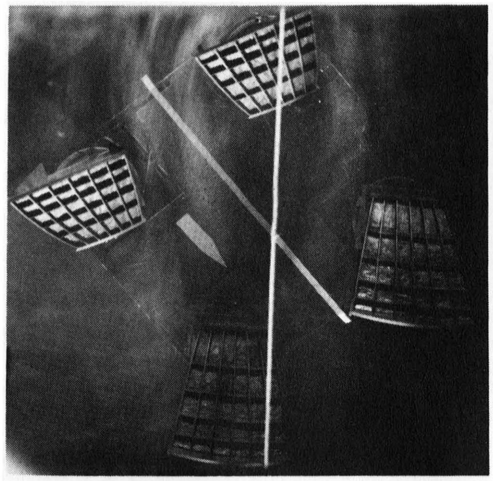

$\theta = 220^{\circ}$

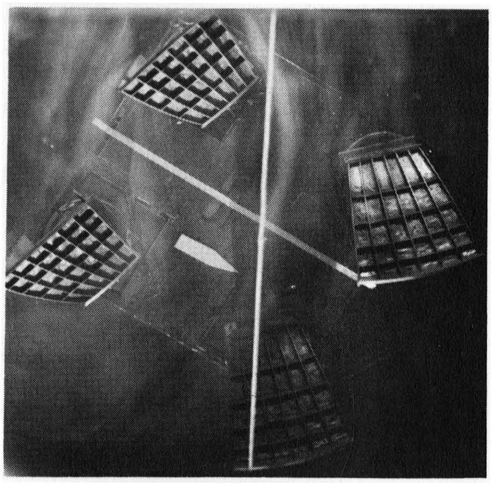

$\theta = 240^{\circ}$

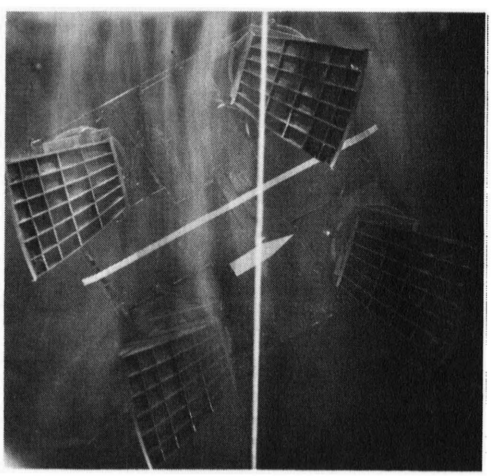

$\theta = 300^{\circ}$

Fig. 41 Structure of flow around a four-horn cluster, "Condition 1". (Wind direction from top to bottom of page)

TABLES

PLATFORM	ANGLE OF INCLINATION β (deg)	WIND DIRECTION θ (deg)	PROJECTED AREA OF PLATFORM A (ft^2)	Δp	DRAG (lbs)	C_D
uncovered	0	0	19.3	1.67	2.07	5.88
"	0	45	27.3	1.67	1.85	3.72
"	2	0	19.3	1.67	1.96	5.58
"	2	45	27.3	1.67	1.90	3.83
"	4	0	19.3	1.67	2.59	7.36
"	4	45	27.3	1.67	2.34	4.70
covered	0	0	19.3	1.67	1.71	4.86
"	0	45	27.3	1.67	1.19	2.40
"	2	0	19.3	1.67	1.49	4.25
"	2	45	27.3	1.67	1.58	3.19
"	4	0	19.3	1.67	2.45	6.97
"	4	45	27.3	1.67	2.12	4.26

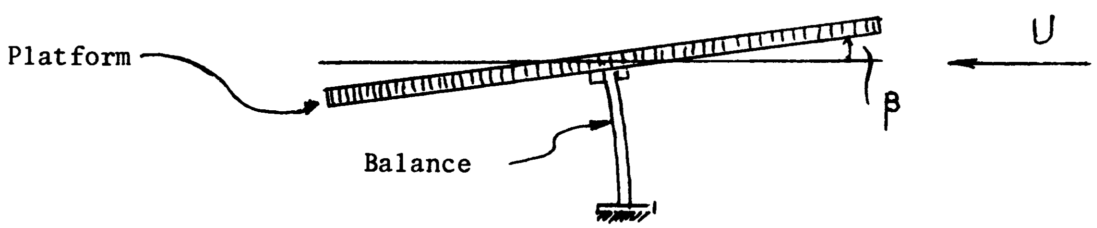

Table 1. Measured wind forces on model of the 29 x 29 ft platform

EFFECT OF REYNOLDS NUMBER CONDITION=1 COVERED

ANGLE	DP (MERC.MM)	DRAG (LB)	CD	RE $/10^5$	AREA (SQ.FT)	VEL. (FT/S)
0.0	.38	2.45	1.73	1.1	341.4	33.4
0.0	.78	4.71	1.63	1.5	341.4	47.8
0.0	1.31	7.85	1.61	2.0	341.4	61.9
0.0	1.93	11.51	1.61	2.4	341.4	75.1
0.0	3.50	20.74	1.60	3.2	341.4	101.0
60.0	.40	2.83	1.19	1.1	552.0	34.0
60.0	.71	4.98	1.16	1.4	552.0	45.6
60.0	1.31	8.67	1.11	2.0	552.0	61.7
60.0	1.80	11.92	1.11	2.3	552.0	72.4
60.0	3.56	23.58	1.11	3.2	552.0	101.8
60.0	1.32	8.91	1.13	2.0	552.0	61.9
60.0	.78	5.29	1.13	1.5	552.0	47.7
60.0	.40	2.76	1.14	1.1	552.0	34.3
160.0	.38	2.78	1.30	1.1	512.9	33.4
160.0	.78	5.41	1.24	1.5	512.9	47.8
160.0	1.31	8.90	1.22	2.0	512.9	61.9
160.0	1.93	12.62	1.17	2.4	512.9	75.1
160.0	3.50	22.89	1.17	3.2	512.9	101.0
240.0	.38	2.60	1.13	1.1	552.0	33.4
240.0	.78	5.24	1.12	1.5	552.0	47.8
240.0	1.31	8.85	1.13	2.0	552.0	61.9
240.0	1.93	12.97	1.12	2.4	552.0	75.1
240.0	3.42	22.98	1.12	3.2	552.0	99.8

Table 2. Effect of Reynolds number on the drag of a four-horn cluster (condition 1 covered platform)

NUMBER OF HORNS	CONDITION	PLATFORM	SEPARATION FT.	DATA APPEARS IN TABLE	FIGURE
1	-	-	-	4	11
1	-	-	-	5	11
1	-	-	-	6	12
2	3C	uncovered	16	7	13
4	1	covered	20	8	14,15
4	1	uncovered	20	9	16
4	2	uncovered	20	10	17
4	3	uncovered	20	11	18
4	3A	uncovered	16	12	20
4	3B	two story lower platform	20	13	21

Table 3. Summary of tests

PYRAMIDAL(WITH EARS)

ANGLE	DYNAMIC PRESSURE (MERC.MM)	DRAG FORCE (LB)	LATERAL FORCE (LB)	ROLL MOMENT (LB.FT)	CD	CL	C_{MR}	AREA (SQ.FT)
-5.0	2.49	4.04	-.28	.07	1.21	-.08	.03	123.8
0.0	2.49	4.15	-.13	-.05	1.31	-.04	-.02	117.4
10.0	2.49	4.07	.67	-.53	1.16	.19	-.24	129.4
20.0	2.49	3.99	1.13	-.74	1.07	.31	-.32	137.4
30.0	2.49	4.07	.92	-.44	1.06	.24	-.18	141.4
40.0	2.49	4.20	.95	-.48	1.10	.25	-.20	141.2
50.0	2.49	4.20	1.01	-.37	1.14	.27	-.16	135.8
60.0	2.49	3.94	.96	-.19	1.14	.28	-.09	128.4
70.0	2.49	3.40	.58	.06	1.08	.19	.03	116.3
80.0	2.49	2.79	.02	.30	1.02	.01	.18	100.8
90.0	2.49	2.61	-.09	.27	1.18	-.04	.19	82.2
100.0	2.49	2.51	.39	-.07	.92	.14	-.04	100.8
110.0	2.49	2.49	.52	-.23	.79	.17	-.11	116.3
120.0	2.49	2.82	.37	-.12	.81	.11	-.06	128.4
130.0	2.49	3.19	.38	-.10	.86	.10	-.04	135.8
140.0	2.49	3.22	.41	-.01	.85	.11	-.00	141.2
150.0	2.49	3.31	.48	-.10	.87	.13	-.04	141.4
160.0	2.49	3.18	.21	.02	.86	.06	.01	137.4
170.0	2.49	3.07	.06	.09	.88	.02	.04	129.4
180.0	2.49	3.10	-.18	.05	.98	-.06	.03	117.4
0.0	2.49	4.04	-.12	.00	1.28	-.04	.00	117.4
90.0	2.49	2.58	-.12	.27	1.16	-.05	.19	82.2

REYNOLDS NUMBER= 350000

Table 4. Forces and moments on a single pyramidal horn (with blinders)

PYRAMIDAL(WITHOUT EARS)

ANGLE	DYNAMIC PRESSURE (MERC.MM)	DRAG FORCE (LB)	LATERAL FORCE (LB)	ROLL MOMENT (LB.FT)	CD	CL	C_{MR}	AREA (SQ.FT)
-5.0	2.49	3.67	-.51	.27	1.19	-.17	.14	114.8
0.0	2.49	3.93	.00	.06	1.24	.00	.03	117.4
10.0	2.49	3.87	.54	-.34	1.12	.16	-.16	127.8
20.0	2.49	3.76	.71	-.58	1.04	.19	-.25	134.3
30.0	2.49	3.55	1.14	-.78	.96	.31	-.34	136.9
40.0	2.49	3.67	.89	-.59	1.00	.24	-.26	135.4
50.0	2.49	3.55	.91	-.44	1.01	.26	-.20	129.9
60.0	2.49	3.23	.67	-.34	.99	.20	-.17	120.6
70.0	2.49	2.73	.52	-.14	.94	.18	-.08	107.8
80.0	2.49	2.29	.10	.10	.92	.04	.07	91.9
90.0	2.49	2.15	.05	.08	1.09	.02	.06	73.2
100.0	2.49	2.21	.35	-.16	.89	.14	-.10	91.9
110.0	2.49	2.18	.55	-.27	.75	.19	-.15	107.8
120.0	2.49	2.54	.26	-.11	.78	.08	-.05	120.6
130.0	2.49	2.87	.17	-.03	.82	.05	-.01	129.9
140.0	2.49	3.14	.18	.01	.86	.05	.00	135.4
150.0	2.49	3.25	.24	.01	.88	.07	.00	136.9
160.0	2.49	3.28	.17	.01	.90	.05	.00	134.3
170.0	2.49	3.10	-.05	.10	.90	-.01	.05	127.8
180.0	2.49	2.96	-.20	.06	.93	-.06	.03	117.4
0.0	2.49	3.83	-.23	.08	1.21	-.07	.04	117.4
90.0	2.49	2.22	.04	.06	1.12	.02	.05	73.2

REYNOLDS NUMBER= 350000

Table 5. Forces and moments on a single pyramidal horn (without blinders)

CONE TYPE

ANGLE	DYNAMIC PRESSURE (MERC.MM)	DRAG FORCE (LB)	LATERAL FORCE (LB)	ROLL MOMENT (LB.FT)	CD	CL	C_{MR}	AREA SQ.FT)
-5.0	2.49	3.07	-.22	.05	.84	-.06	.02	135.6
0.0	2.49	3.16	-.13	-.09	.88	-.04	-.04	133.0
5.0	2.49	3.14	.21	-.23	.86	.06	-.10	135.6
10.0	2.49	3.08	.41	-.33	.83	.11	-.14	137.5
20.0	2.49	3.09	.61	-.43	.81	.16	-.18	140.4
30.0	2.49	3.01	.48	-.35	.79	.13	-.15	141.8
40.0	2.49	2.75	.22	-.09	.73	.06	-.04	140.3
50.0	2.49	2.67	.13	.03	.73	.04	.01	135.8
60.0	2.49	2.50	.22	.05	.72	.06	.02	128.6
70.0	2.49	1.94	.60	-.17	.60	.19	-.09	119.2
80.0	2.49	1.58	.29	-.03	.54	.10	-.01	107.6
90.0	2.49	1.43	.08	.08	.51	.03	.05	102.9
100.0	2.49	1.72	-.17	.25	.59	-.06	.14	107.6
110.0	2.49	2.20	-.03	.16	.68	-.01	.08	119.2
120.0	2.49	2.44	.39	-.03	.70	.11	-.01	128.6
130.0	2.49	2.64	.57	-.05	.72	.15	-.02	135.8
140.0	2.49	2.67	.63	-.06	.71	.17	-.03	140.3
150.0	2.49	2.58	.73	-.13	.67	.19	-.05	141.8
160.0	2.49	2.47	.64	-.14	.65	.17	-.06	140.4
170.0	2.49	2.36	.22	-.06	.64	.06	-.03	137.5
180.0	2.49	2.21	-.10	-.01	.62	-.03	-.00	133.0
0.0	2.49	3.18	-.20	-.05	.89	-.05	-.02	133.0
90.0	2.49	1.43	.15	.04	.52	.05	.02	102.9

REYNOLDS NUMBER= 350000

Table 6. Forces and moments on a single conical horn

UNCOVERED CONDITION=3 C (16FT.SEP.,2-HORNS)

ANGLE	DYNAMIC PRESSURE (MERC.MM)	DRAG FORCE (LB)	LATERAL FORCE (LB)	ROLL MOMENT (LB.FT)	PITCH MOMENT (LB.FT)	CD	CL	C_{MR}	C_{MP}	AREA (SQ.FT)	y_D
0.0	1.76	5.37	.65	-1.80	1.88	1.65	.20	-.89	.92	170.6	5.6
20.0	1.76	5.83	-.06	-1.65	1.51	1.24	-.01	-.56	.51	245.6	4.1
40.0	1.76	6.04	-.45	-1.82	1.31	1.31	-.10	-.63	.45	242.1	3.5
60.0	1.76	6.36	-.65	-1.18	.88	1.21	-.12	-.36	.27	275.6	2.2
80.0	1.76	6.48	-.30	-.23	.66	1.23	-.06	-.07	.20	275.5	1.6
100.0	1.76	6.07	.11	.58	.78	1.28	.02	.19	.26	248.8	2.1
120.0	1.76	6.11	-.25	.98	1.08	1.24	-.05	.32	.35	257.7	2.8
140.0	1.76	6.94	-.23	1.85	1.94	1.29	-.04	.55	.57	282.9	4.5
160.0	1.76	6.60	.21	2.50	1.93	1.36	.04	.82	.64	254.8	4.7
180.0	1.76	4.94	-.95	2.02	.91	1.52	-.29	.99	.45	170.6	2.9
200.0	1.76	6.63	-.86	1.46	1.18	1.41	-.18	.50	.40	245.6	2.8
220.0	1.76	6.83	.82	2.19	1.49	1.48	.18	.76	.51	242.1	3.5
240.0	1.76	7.68	.46	1.68	1.59	1.46	.09	.51	.48	275.6	3.3
260.0	1.76	7.76	-.19	.37	1.40	1.48	-.04	.11	.43	275.5	2.9
280.0	1.76	7.11	-.84	-1.12	1.24	1.50	-.18	-.38	.42	248.8	2.8
300.0	1.76	6.87	.37	-1.17	1.23	1.40	.08	-.38	.40	257.7	2.9
320.0	1.76	6.60	1.43	-1.54	1.40	1.22	.26	-.46	.41	282.9	3.4
340.0	1.76	5.62	1.50	-1.60	1.30	1.15	.31	-.53	.43	254.8	3.7

REYNOLDS NUMBER= 226000

Table 7. Experimental data for a two-horn cluster (condition 3c)

COVERED CONDITION=1 (20FT.SEP.)

ANGLE	DYNAMIC PRESSURE (MERC.MM)	DRAG FORCE (LB)	LATERAL FORCE (LB)	ROLL MOMENT (LB.FT)	PITCH MOMENT (LB.FT)	CD	CL	C_{MR}	C_{MP}	AREA (SQ.FT)	y_D FT
0.0	1.67	9.99	-1.21	1.06	4.72	1.61	-.19	.27	1.22	341.4	7.6
20.0	1.67	9.79	-2.15	.81	3.99	1.15	-.25	.15	.75	467.1	6.5
40.0	1.67	11.27	-.96	.32	4.36	1.39	-.12	.06	.86	446.0	6.2
55.0	1.67	11.61	.67	-.27	4.11	1.22	.07	-.05	.69	525.2	5.7
60.0	1.67	11.47	1.05	.29	3.85	1.14	.10	.05	.61	552.0	5.4
65.0	1.67	11.17	1.28	.77	3.56	1.14	.13	.13	.58	537.4	5.1
80.0	1.67	8.06	.44	.39	2.66	1.13	.06	.09	.60	391.3	5.3
100.0	1.67	7.62	.11	.90	1.88	1.18	.02	.22	.47	356.1	3.9
120.0	1.67	9.14	-1.49	-.43	2.19	1.13	-.18	-.09	.43	445.8	3.8
140.0	1.67	10.41	-1.51	.03	3.19	1.43	-.21	.01	.70	401.4	4.9
155.0	1.67	11.28	-.35	1.19	3.22	1.26	-.04	.21	.58	493.6	4.6
160.0	1.67	11.17	-.18	1.55	3.13	1.20	-.02	.27	.54	512.9	4.5
165.0	1.67	11.13	-.06	1.97	3.14	1.21	-.01	.34	.55	505.5	4.5
180.0	1.67	10.11	-.98	1.40	3.39	1.63	-.16	.36	.88	341.4	5.4
200.0	1.67	11.26	-1.21	-.91	4.49	1.33	-.14	-.17	.85	467.1	6.4
220.0	1.67	11.81	1.14	-.39	4.98	1.46	.14	-.08	.98	446.0	6.7
235.0	1.67	11.83	2.45	-.51	4.45	1.24	.26	-.09	.75	525.2	6.0
240.0	1.67	11.57	3.07	.79	4.38	1.15	.31	.13	.70	552.0	6.1
245.0	1.67	11.31	3.58	1.05	4.08	1.16	.37	.17	.67	537.4	5.8
260.0	1.67	8.60	1.99	.90	2.41	1.21	.28	.20	.54	391.3	4.5
280.0	1.67	7.95	.37	-.17	1.50	1.23	.06	-.04	.37	356.1	3.0
300.0	1.67	8.49	.77	.26	2.43	1.05	.09	.05	.48	445.8	4.6
320.0	1.67	8.72	.82	.41	3.17	1.20	.11	.09	.69	401.4	5.8
335.0	1.67	9.42	1.16	1.24	3.52	1.05	.13	.22	.63	493.6	6.0
345.0	1.67	9.59	.23	1.71	4.48	1.04	.02	.30	.78	505.5	7.5
340.0	1.67	9.52	.84	1.52	3.88	1.02	.09	.26	.67	512.9	6.5

REYNOLDS NUMBER= 221000

Table 8. Experimental data for a four-horn cluster (condition 1 covered platform)

UNCOVERED CONDITION=1 (20FT.SEP.)

ANGLE	DYNAMIC PRESSURE (MERC.MM)	DRAG FORCE (LB)	LATERAL FORCE (LB)	ROLL MOMENT (LB.FT)	PITCH MOMENT (LB.FT)	CD	CL	C_{MR}	C_{MP}	AREA (SQ.FT)	y_D FT.
0.0	1.67	10.34	-1.30	.89	4.40	1.67	-.21	.23	1.14	341.4	6.8
20.0	1.67	9.64	-2.01	1.02	3.22	1.14	-.24	.19	.61	467.1	5.3
40.0	1.67	11.64	-.71	.41	4.05	1.44	-.09	.08	.80	446.0	5.6
55.0	1.67	11.98	.68	-.43	3.81	1.26	.07	-.07	.64	525.2	5.1
60.0	1.67	12.06	1.01	.01	3.63	1.20	.10	.00	.58	552.0	4.8
65.0	1.67	11.40	1.41	.55	3.22	1.17	.14	.09	.53	537.4	4.5
80.0	1.67	8.56	.49	.19	2.18	1.20	.07	.04	.49	391.3	4.1
100.0	1.67	8.02	.60	1.33	1.94	1.24	.09	.33	.48	356.1	3.9
120.0	1.67	9.23	-.91	-.54	2.05	1.14	-.11	-.11	.41	445.8	3.6
140.0	1.67	10.14	-1.22	-.24	3.03	1.39	-.17	-.05	.66	401.4	4.8
155.0	1.67	11.09	-.10	1.02	3.11	1.24	-.01	.18	.55	493.6	4.5
160.0	1.67	11.13	.01	1.51	3.07	1.19	.00	.26	.53	512.9	4.4
165.0	1.67	11.15	.10	1.95	3.04	1.21	.01	.34	.53	505.5	4.4
180.0	1.67	10.06	-.25	1.64	2.85	1.62	-.04	.42	.73	341.4	4.5
200.0	1.67	10.98	-1.21	-.97	4.23	1.29	-.14	-.18	.80	467.1	6.2
220.0	1.67	11.35	1.00	-.21	4.52	1.40	.12	-.04	.89	446.0	6.4
235.0	1.67	11.77	1.90	.38	4.40	1.23	.20	.06	.74	525.2	6.0
240.0	1.67	11.60	2.47	.54	4.18	1.16	.25	.09	.67	552.0	5.8
245.0	1.67	11.31	2.72	.74	3.87	1.16	.28	.12	.63	537.4	5.5
260.0	1.67	8.82	1.17	.53	2.17	1.24	.16	.12	.49	391.3	3.9
280.0	1.67	7.50	.14	.24	1.16	1.16	.02	.06	.29	356.1	2.5
300.0	1.67	8.93	.11	.34	1.95	1.10	.01	.07	.39	445.8	3.5
320.0	1.67	9.32	.26	.29	2.58	1.28	.04	.06	.57	401.4	4.4
335.0	1.67	10.55	.13	1.14	3.34	1.18	.01	.20	.60	493.6	5.1
340.0	1.67	10.76	-.02	1.49	3.66	1.16	-.00	.26	.63	512.9	5.4
345.0	1.67	10.80	-.21	1.61	4.09	1.18	-.02	.28	.71	505.5	6.1

REYNOLDS NUMBER= 221000

Table 9. Experimental data for a four-horn cluster (condition 1 uncovered platform)

UNCOVERED CONDITION=2 (20FT.SEP.)

ANGLE	DYNAMIC PRESSURE (MERC.MM)	DRAG FORCE (LB)	LATERAL FORCE (LB)	ROLL MOMENT (LB.FT)	PITCH MOMENT (LB.FT)	CD	CL	C_{MR}	C_{MP}	AREA (SQ.FT)	y_o FT
0.0	1.69	9.77	1.13	-.98	3.45	1.91	.22	-.31	1.08	279.8	5.7
20.0	1.69	11.72	1.03	-1.02	4.81	1.22	.11	-.17	.80	524.2	6.6
25.0	1.69	11.96	1.06	-.76	4.68	1.24	.11	-.13	.77	529.6	6.3
40.0	1.69	11.46	.85	-.43	4.32	1.35	.10	-.08	.81	465.1	6.0
55.0	1.69	10.45	-.38	-.20	2.98	1.13	-.04	-.04	.51	507.7	4.6
60.0	1.69	9.98	-.80	.06	2.49	1.08	-.09	.01	.43	503.7	4.0
80.0	1.69	7.13	-.30	-.59	1.65	1.13	-.05	-.15	.47	344.7	4.2
100.0	1.69	7.44	-1.05	.49	1.79	1.19	-.17	.12	.46	343.5	3.9
120.0	1.69	10.41	-.53	-.17	2.53	1.13	-.06	-.03	.44	503.7	3.9
125.0	1.69	10.87	-.75	.05	2.92	1.17	-.08	.01	.50	507.7	4.3
140.0	1.69	11.76	-1.73	.22	4.06	1.38	-.20	.04	.76	465.2	5.5
155.0	1.69	12.19	-1.60	.82	4.31	1.26	-.17	.14	.71	529.1	5.7
160.0	1.69	11.87	-1.42	1.07	4.41	1.24	-.15	.18	.74	523.6	5.9
180.0	1.69	9.48	-1.71	.88	2.92	1.85	-.33	.27	.91	279.8	4.9
200.0	1.69	12.26	-1.22	-1.46	3.63	1.28	-.13	-.24	.61	524.2	4.7
205.0	1.69	12.35	-.03	-1.52	3.53	1.28	-.00	-.25	.58	529.6	4.6
220.0	1.69	12.17	.66	-.67	3.53	1.43	.08	-.13	.66	465.1	4.6
235.0	1.69	12.01	1.06	.27	3.24	1.29	.11	.05	.56	507.7	4.3
240.0	1.69	11.69	1.15	.44	3.14	1.27	.12	.08	.55	503.7	4.3
260.0	1.69	8.23	1.12	.24	1.88	1.31	.18	.06	.48	344.7	3.6
280.0	1.69	8.27	-.26	-.45	1.92	1.32	-.04	-.12	.49	343.5	3.7
300.0	1.69	11.25	-.63	-.50	3.28	1.22	-.07	-.09	.57	503.7	4.7
305.0	1.69	11.61	-.48	-.27	3.47	1.25	-.05	-.05	.60	507.7	4.8
320.0	1.69	11.42	-.52	.68	4.01	1.34	-.06	.13	.75	465.2	5.6
335.0	1.69	11.61	.27	1.43	4.21	1.20	.03	.24	.70	529.1	5.8
340.0	1.69	11.30	1.34	1.32	4.28	1.18	.14	.22	.72	523.6	6.1

REYNOLDS NUMBER= 221000

Table 10. Experimental data for a four-horn cluster (condition 2)

UNCOVERED CONDITION=3 (20FT.SEP.)

ANGLE	DYNAMIC PRESSURE (MERC.MM)	DRAG FORCE (LB)	LATERAL FORCE (LB)	ROLL MOMENT (LB.FT)	PITCH MOMENT (LB.FT)	CD	CL	C_{MR}	C_{MP}	AREA (SQ.FT)	y_b ft.
0.0	1.69	9.55	1.14	-1.27	4.20	1.71	.20	-.37	1.21	304.9	7.0
20.0	1.69	9.93	.21	-.88	3.46	1.17	.02	-.17	.65	464.7	5.6
25.0	1.69	9.72	-.16	-.59	3.16	1.12	-.02	-.11	.58	476.0	5.2
40.0	1.69	9.24	-.16	-.54	2.90	1.29	-.02	-.12	.65	392.8	5.0
60.0	1.69	10.06	.10	-.54	2.84	1.07	.01	-.09	.48	514.5	4.5
80.0	1.69	8.91	-.23	-.15	2.05	1.14	-.03	-.03	.42	425.9	3.7
100.0	1.69	8.78	-1.25	.31	2.95	1.27	-.18	.07	.68	378.3	5.4
120.0	1.69	10.10	-1.41	-.86	3.34	1.07	-.15	-.15	.56	518.5	5.3
140.0	1.69	10.49	-1.40	.16	4.07	1.27	-.17	.03	.79	451.5	6.2
160.0	1.69	10.40	-.41	1.72	3.60	1.13	-.04	.30	.62	505.4	5.5
180.0	1.69	8.76	-.91	1.26	2.69	1.57	-.16	.36	.77	304.9	4.9
200.0	1.69	10.89	-1.84	-.86	2.45	1.28	-.22	-.16	.46	464.7	3.6
205.0	1.69	11.01	-1.58	-.56	2.62	1.27	-.18	-.10	.48	476.0	3.8
220.0	1.69	11.21	-.70	.87	3.23	1.56	-.10	.19	.72	392.8	4.6
240.0	1.69	12.13	.46	1.73	3.17	1.29	.05	.29	.54	514.5	4.2
260.0	1.69	11.15	.66	1.79	2.95	1.43	.09	.37	.61	425.9	4.2
280.0	1.69	9.65	.69	.39	2.75	1.40	.10	.09	.64	378.3	4.6
300.0	1.69	12.56	.01	.28	4.19	1.33	.00	.05	.71	518.5	5.3
320.0	1.69	12.15	2.82	.19	4.22	1.47	.34	.04	.82	451.5	5.6
340.0	1.69	9.96	3.40	.03	3.38	1.08	.37	.00	.59	505.4	5.4

REYNOLDS NUMBER= 221000

Table 11. Experimental data for a four-horn cluster (condition 3)

UNCOVERED CONDITION=3A (16FT.SEP.)

ANGLE	DYNAMIC PRESSURE (MERC.MM)	DRAG FORCE (LB)	LATERAL FORCE (LB)	ROLL MOMENT (LB.FT)	PITCH MOMENT (LB.FT)	CD	CL	C_{MR}	C_{MP}	AREA (SQ.FT)	y_D ft
0.0	1.76	8.93	1.25	-.67	3.50	1.53	.21	-.18	.96	305.3	6.3
20.0	1.76	8.93	.22	-.54	2.98	1.06	.03	-.10	.56	441.8	5.3
40.0	1.76	9.13	-.29	-.61	2.59	1.22	-.04	-.13	.55	392.8	4.5
60.0	1.76	9.75	-.14	-.23	2.19	1.04	-.02	-.04	.37	493.0	3.6
80.0	1.76	8.25	-.14	-.34	1.52	1.06	-.02	-.07	.31	408.6	3.0
100.0	1.76	7.85	-.63	-.07	1.90	1.13	-.10	-.02	.44	364.8	3.9
120.0	1.76	9.36	-1.15	-.86	2.68	1.02	-.13	-.15	.47	482.5	4.6
140.0	1.76	10.11	-1.10	.28	3.87	1.19	-.13	.05	.73	445.7	6.1
160.0	1.76	9.59	.14	1.12	3.01	1.07	.02	.20	.54	467.6	5.0
180.0	1.76	7.85	-.79	.92	2.25	1.35	-.14	.25	.62	305.3	4.6
200.0	1.76	9.78	-1.23	-.55	2.34	1.16	-.15	-.10	.44	441.8	3.8
220.0	1.76	11.00	-.54	.68	3.32	1.47	-.07	.14	.71	392.8	4.8
240.0	1.76	11.29	.71	1.30	3.30	1.20	.08	.22	.56	493.0	4.7
260.0	1.76	10.12	.83	1.58	2.99	1.30	.11	.32	.61	408.6	4.7
280.0	1.76	9.01	.62	.34	2.67	1.29	.09	.08	.61	364.8	4.7
300.0	1.76	11.91	.69	.10	3.95	1.29	.07	.02	.69	482.5	5.3
320.0	1.76	11.39	3.01	.24	4.03	1.34	.35	.04	.76	445.7	5.7
340.0	1.76	8.56	2.70	-.42	2.83	.96	.30	-.07	.51	467.6	5.3

REYNOLDS NUMBER= 226000

Table 12. Experimental data for a four-horn cluster (condition 3A)

UNCOVERED CONDITION=3B (20FT.SEP.) TWO STORY

ANGLE	DYNAMIC PRESSURE (MERC.MM)	DRAG FORCE (LB)	LATERAL FORCE (LB)	ROLL MOMENT (LB.FT)	PITCH MOMENT (LB.FT)	CD	CL	C_{MR}	C_{MP}	AREA (SQ.FT)	y_D ft.
0.0	1.70	9.61	1.33	-.65	3.91	1.72	.24	-.19	1.12	304.9	6.5
20.0	1.70	9.29	.71	-.47	3.11	1.09	.08	-.09	.58	464.7	5.4
40.0	1.70	9.10	.49	-.92	2.70	1.26	.07	-.20	.60	392.8	4.7
60.0	1.70	9.94	.17	-.06	2.15	1.05	.02	-.01	.36	514.5	3.5
80.0	1.70	9.00	-.33	-.29	1.47	1.15	-.04	-.06	.30	425.9	2.6
100.0	1.70	8.66	-.86	.26	2.06	1.25	-.12	.06	.47	378.3	3.8
120.0	1.70	9.49	-1.84	-.71	2.79	1.00	-.19	-.12	.47	518.5	4.7
140.0	1.70	9.87	-1.15	.13	3.35	1.19	-.14	.03	.65	451.5	5.4
160.0	1.70	9.92	-.67	1.09	3.31	1.07	-.07	.19	.57	505.4	5.3
180.0	1.70	8.79	-1.00	.59	2.86	1.57	-.18	.17	.82	304.9	5.2
200.0	1.70	10.55	-1.42	-.83	2.71	1.24	-.17	-.16	.51	464.7	4.1
220.0	1.70	9.80	.35	.54	3.28	1.36	.05	.12	.73	392.8	5.3
280.0	1.70	9.44	.34	-.34	3.92	1.36	.05	-.08	.90	378.3	6.6
300.0	1.70	10.19	-1.00	.08	4.55	1.07	-.11	.01	.76	518.5	7.1
320.0	1.70	10.87	2.30	-.16	4.57	1.31	.28	-.03	.88	451.5	6.7
340.0	1.70	9.07	3.27	-.53	3.98	.98	.35	-.09	.69	505.4	7.0

REYNOLDS NUMBER= 240000

Table 13. Experimental data for a four-horn cluster with an upper platform (two story cluster, Condition 3B)

APPENDIX

DESCRIPTION OF THE HORNS, ANTENNA AND CONFIGURATIONS SUPPLIED BY THE SPONSOR

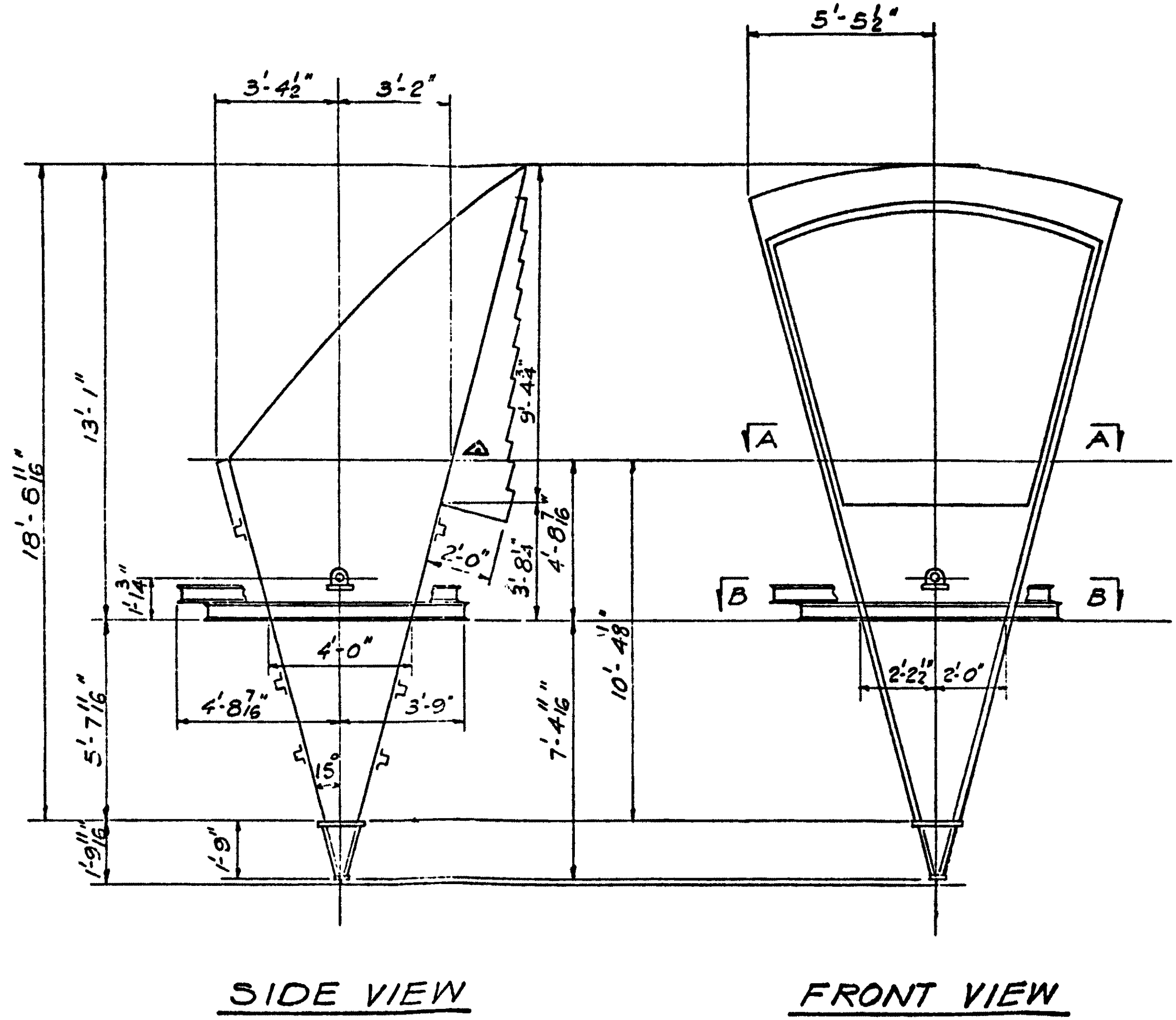

Fig. A1 Dimensions of the pyramidal horn

Rose, Chulkoff & Rose
Structural Engineers
RC&R
6 Corporate Park Drive, White Plains, New York 10604

Sheet No. 1 of 4
Date 7/22/76
By

Project: PROJECTED AREAS IN SQ. FT. (20'-0" SEPARATION)

ANGLE OF YAW	SINGLE HORN			CONDITION 1.			CONDITION 2.			CONDITION 3.		
	HORN	MTG.	TOTAL	HORNS	MTG.	TOTAL	HORNS	MTG.	TOTAL	HORNS	MTG.	TOTAL
0	115.0	2.4	117.4	325.0	16.4	341.4	263.4	16.4	279.8	287.0	17.9	304.9
5	121.5	2.3	123.8		16.1			16.1			16.5	
10	127.1	2.3	129.4		14.6			14.6			14.6	
15	131.7	2.1	133.8		13.6		455.8	13.6	469.4		13.6	
20	135.3	2.1	137.4	450.8	16.3	467.1	507.9	16.3	524.2	448.4	16.3	464.7
25	137.9	2.0	139.9	492.2	20.5	512.7	509.1	20.5	529.6	455.9	20.1	476.0
30	139.4	2.0	141.4	503.5	20.2	523.7	489.7	20.7	509.9	445.4	20.3	465.7
35	139.9	2.0	141.9	471.3	19.9	491.2		19.9			20.0	
40	139.3	1.9	141.2	423.8	22.2	446.0	442.9	22.2	465.1	370.4	22.4	392.8
45	137.6	1.9	139.5	405.4	24.2	429.6	423.2	24.2	447.4	366.6	24.5	391.1
50	134.9	1.9	136.8		22.1			22.1			22.3	
55	131.2	2.0	133.2	505.2	20.0	525.2	487.7	20.0	507.7	460.5	20.2	480.7
60	126.4	2.0	128.4	531.6	20.4	552.0	483.3	20.4	503.7	494.0	20.5	514.5
65	120.7	2.1	122.8	516.7	20.7	537.4	454.8	20.7	475.5	506.4	20.7	527.1
70	114.1	2.2	116.3	486.2	16.3	502.5	418.8	16.3	435.1	493.3	16.3	509.6
75	106.7	2.3	109.0		13.6			13.6			13.6	
80	98.4	2.4	100.8	377.5	13.8	391.3	330.9	13.8	344.7	412.1	13.8	425.9
85	89.3	2.5	91.8		20.7			20.7			20.3	
90	79.6	2.6	82.2	244.3	21.9	266.2	213.4	21.9	235.3	280.2	21.3	301.5
95					20.7			20.7			20.3	
100				342.3	13.8	356.1	329.7	13.8	343.5	364.5	13.8	378.3
105					13.6			13.6			13.6	
110				398.8	16.3	415.1	418.8	16.3	435.1		16.3	
115				418.8	20.7	439.5	454.8	20.7	475.5	476.8	20.7	497.5
120				435.4	20.4	445.8	483.3	20.4	503.7	498.0	20.5	518.5
125				413.1	20.0	433.1	487.7	20.0	507.7	479.9	20.2	500.1
130					22.1			22.1			22.3	
135				332.7	24.2	356.9	423.2	24.2	447.4	410.2	24.5	434.7
140				379.2	22.2	401.4	443.0	22.2	465.2	429.1	22.4	451.5
145					19.9			19.9			20.0	
150					20.2		489.4	20.2	509.6	502.5	20.3	522.8
155				473.1	20.5	493.6	508.6	20.5	529.1	514.1	20.1	534.2
160				496.6	16.3	512.9	507.3	16.3	523.6	489.1	16.3	505.4
165				491.9	13.6	505.5	455.6	13.6	469.2		13.6	
170				457.8	14.6	472.4		14.6		384.5	14.6	399.1

Rose, Chulkoff & Rose
Structural Engineers
6 Corporate Park Drive, White Plains, New York 10604

RC&R

Sheet No. ______
Date 8/11/76
By ______

Project: PROJECTED AREA OF AFC, CH-10 CONICAL ANTENNA INCLUDING MOUNTING RING

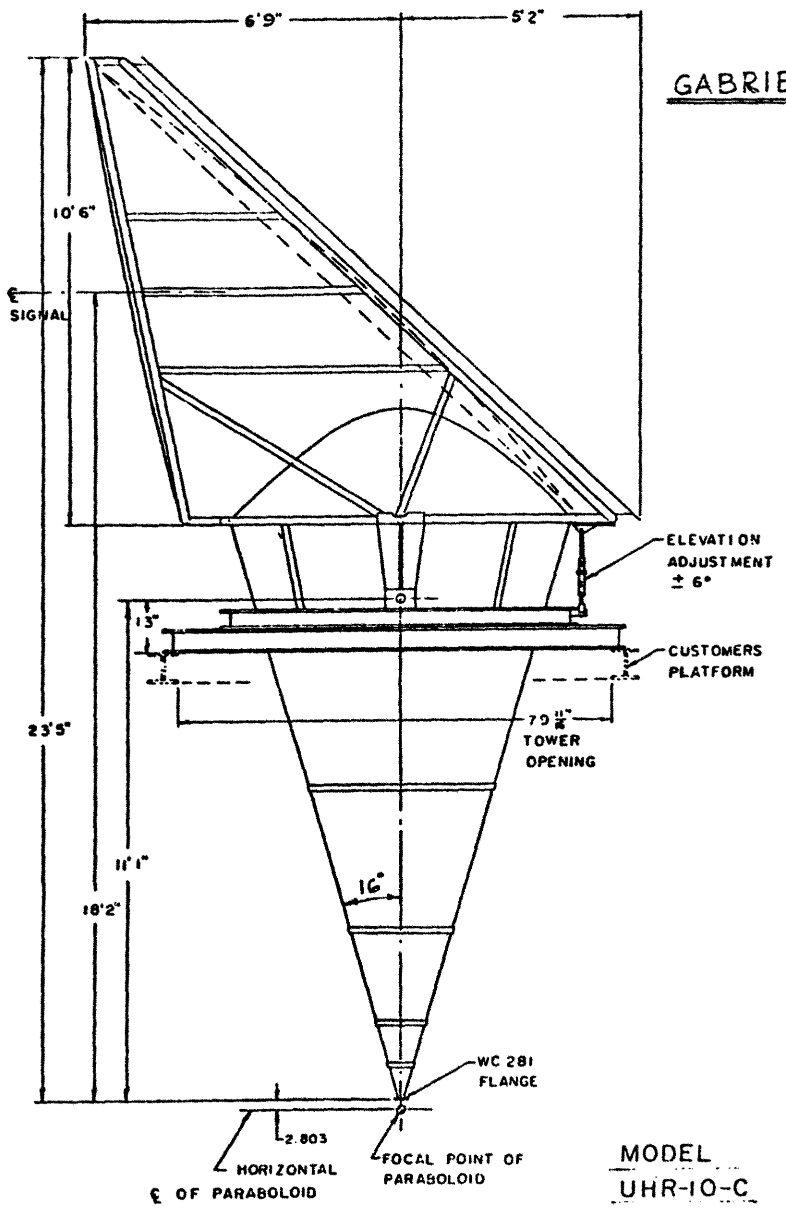

ANGLE OF YAW	AREA IN SQ. FT.
0	102.86
5	103.99
10	107.56
15	113.65
20	119.22
25	124.21
30	128.60
35	132.54
40	135.82
45	138.40
50	140.26
55	141.41
60	141.82
65	141.50
70	140.44
75	138.67
80	137.54
85	135.62
90	133.04

Fig. A2 Dimensions of the conical horn

Rose, Chulkoff & Rose
Structural Engineers
6 Corporate Park Drive, White Plains, New York 10604

RC&R

Sheet No. 1 Of 3
Date 7/30/76
By

Project: PROJECTED AREAS in SQ. FT. (16'-0" SEPARATION)

ANGLE OF YAW	CONDITION 3A (4-HORNS)			CONDITION 3B (7-HORNS)			CONDITION 3C (2-HORNS)		
	HORNS	MTG.	TOTAL	HORNS	MTG.	TOTAL	HORNS	MTG.	TOTAL
0	287.0	18.3	305.3				151.8	18.8	170.6
5		18.5						20.1	
10		18.1						20.6	
15		17.1						20.7	
20	426.8	15.0	441.8	SAME AS CONDITION 3, BUT WITH AN UPPER PLATFORM.			224.8	20.8	245.6
25	437.4	16.5	453.9				231.0	22.0	253.0
30	428.3	17.9	446.2				230.1	23.3	253.4
35		20.1					224.6	23.9	248.5
40		22.5					217.5	24.6	242.1
45	366.6	23.6	390.2				228.7	24.8	253.5
50		23.1					238.3	25.2	263.5
55	448.2	21.1	469.3				246.0	24.5	270.5
60	473.0	20.0	493.0				251.7	23.9	275.6
65	481.1	19.3	500.4				255.6	23.0	278.6
70	467.0	16.1	483.1				257.6	22.1	279.7
75		16.4					257.6	21.0	278.6
80	392.1	16.5	408.6				255.6	19.9	275.5
85		16.7					251.7	18.5	270.2
90	280.2	16.6	296.8				246.0	17.2	263.2
95		16.7					238.3	18.5	256.8
100	348.3	16.5	364.8				228.7	19.9	248.8
105		16.4					217.5	21.0	238.5
110		16.1					224.6	22.1	246.1
115	445.7	19.3	465.0				230.1	23.0	253.1
120	462.5	20.0	482.5				233.8	23.9	257.7
125	463.1	21.1	484.2				235.6	24.5	260.1
130		23.1					235.7	25.2	260.9
135	410.2	23.6	433.8				247.9	24.8	272.7
140	423.2	22.5	445.7				258.3	24.6	282.9
145		20.1					266.6	23.9	290.5
150	470.6	17.9	488.5				264.0	23.3	287.3
155	469.3	16.5	485.8				251.0	22.0	273.0
160	452.6	15.0	467.6				234.0	20.8	254.8
165		17.1						20.7	
170	363.5	18.1	381.6				185.6	20.6	206.2
175		18.5						20.1	
180	287.0	18.3	305.3				151.8	18.8	170.6

CONDITION 1

PROJECTED AREAS OF HORNS, MOUNTING FRAMES & PLATFORM

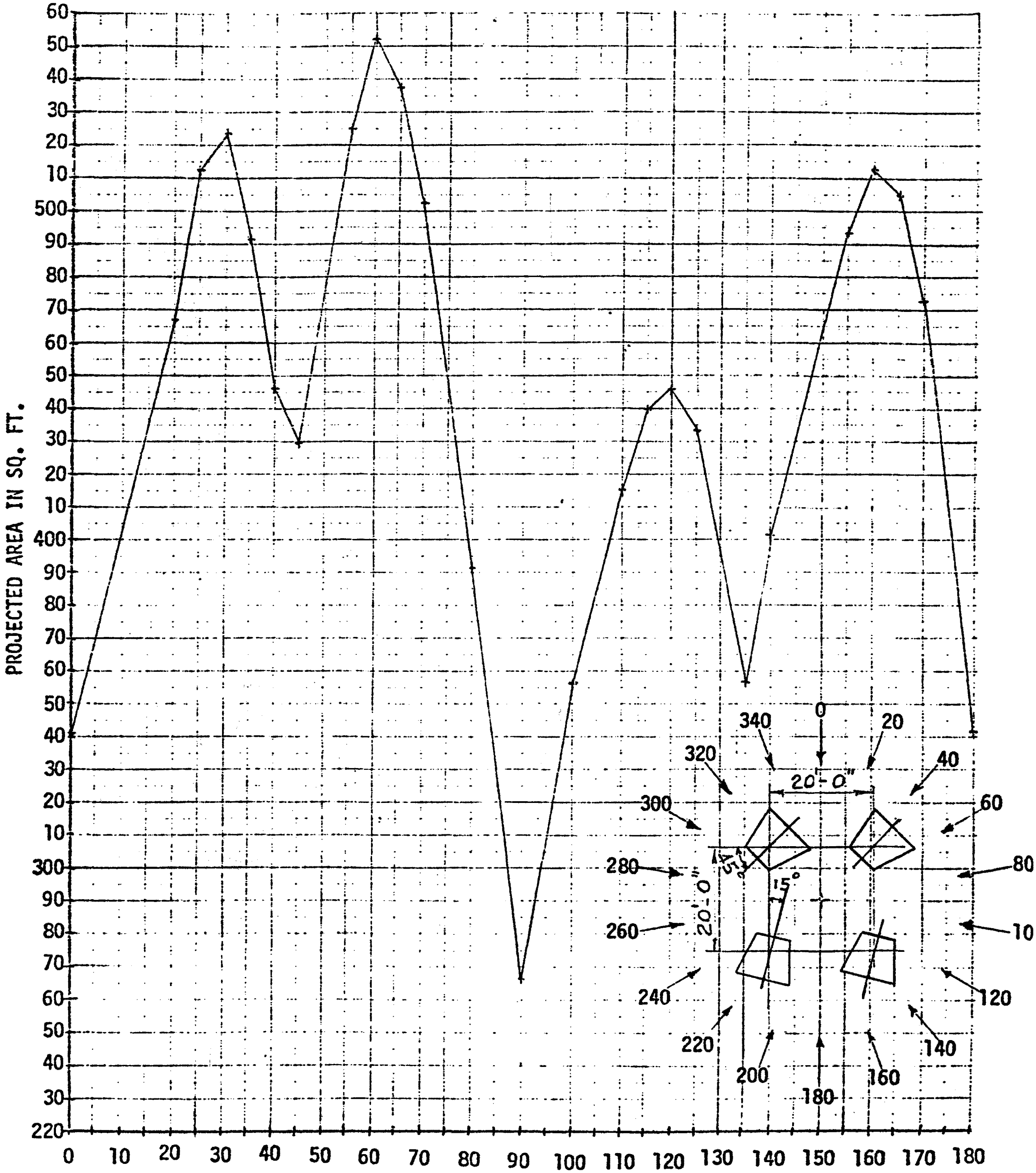

ANGLE OF YAW IN DEGREES

CONDITION 2

PROJECTED AREAS OF HORNS, MOUNTING FRAMES & PLATFORM

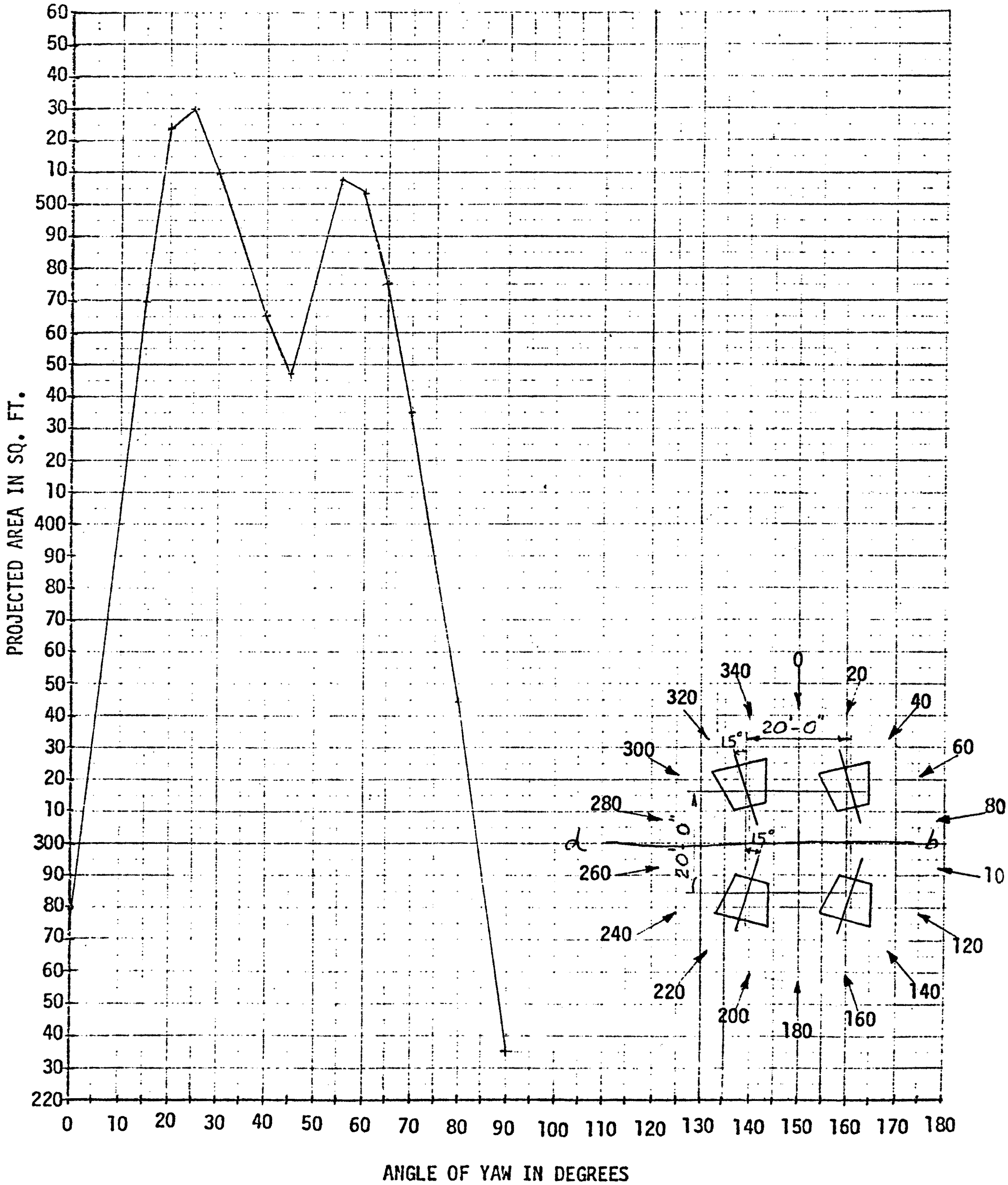

CONDITION 3

PROJECTED AREAS OF HORNS, MOUNTING FRAMES & PLATFORM

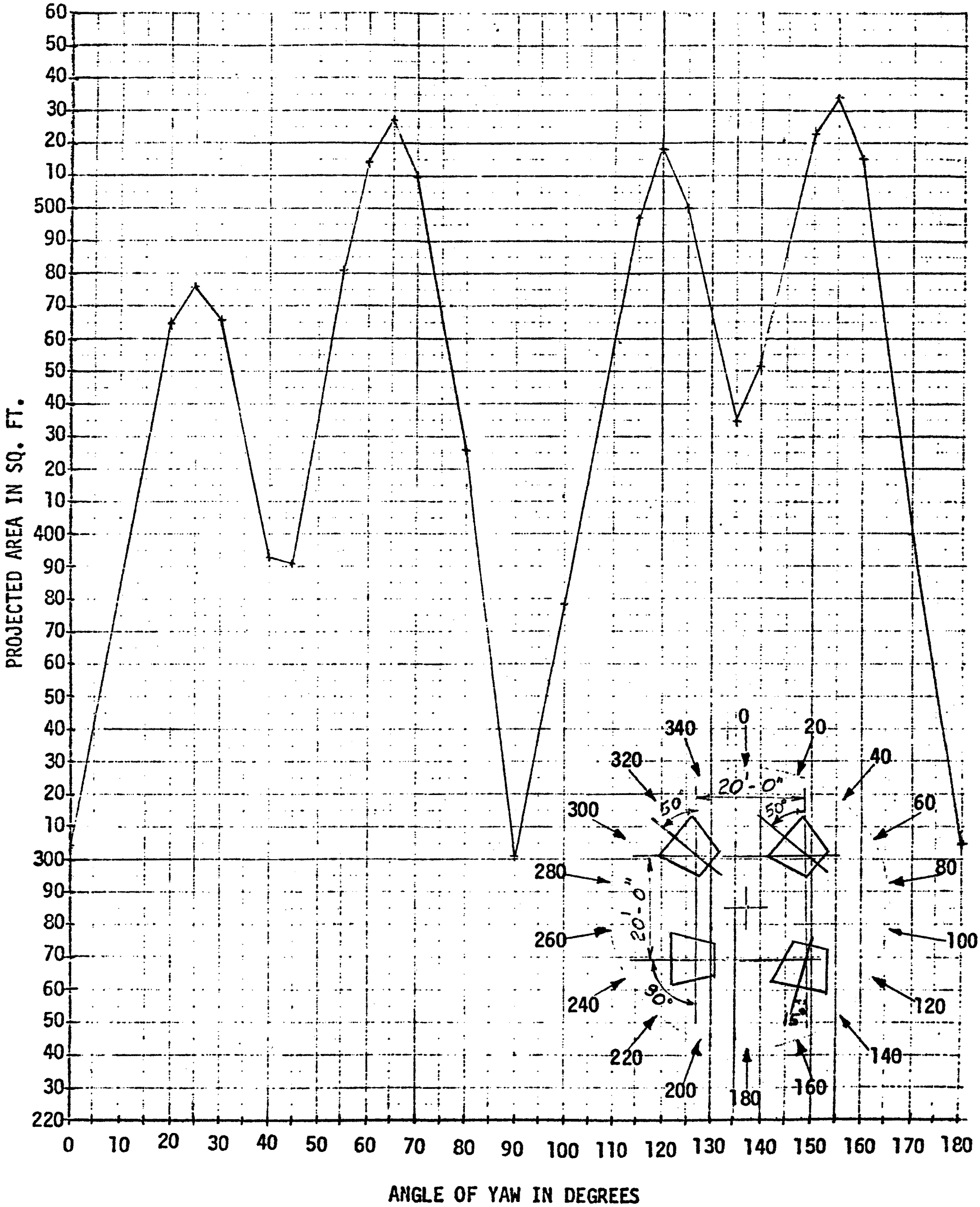

CONDITION 3A
(16'-0" Seperation)

PROJECTED AREAS OF HORNS, MOUNTING FRAMES & PLATFORM

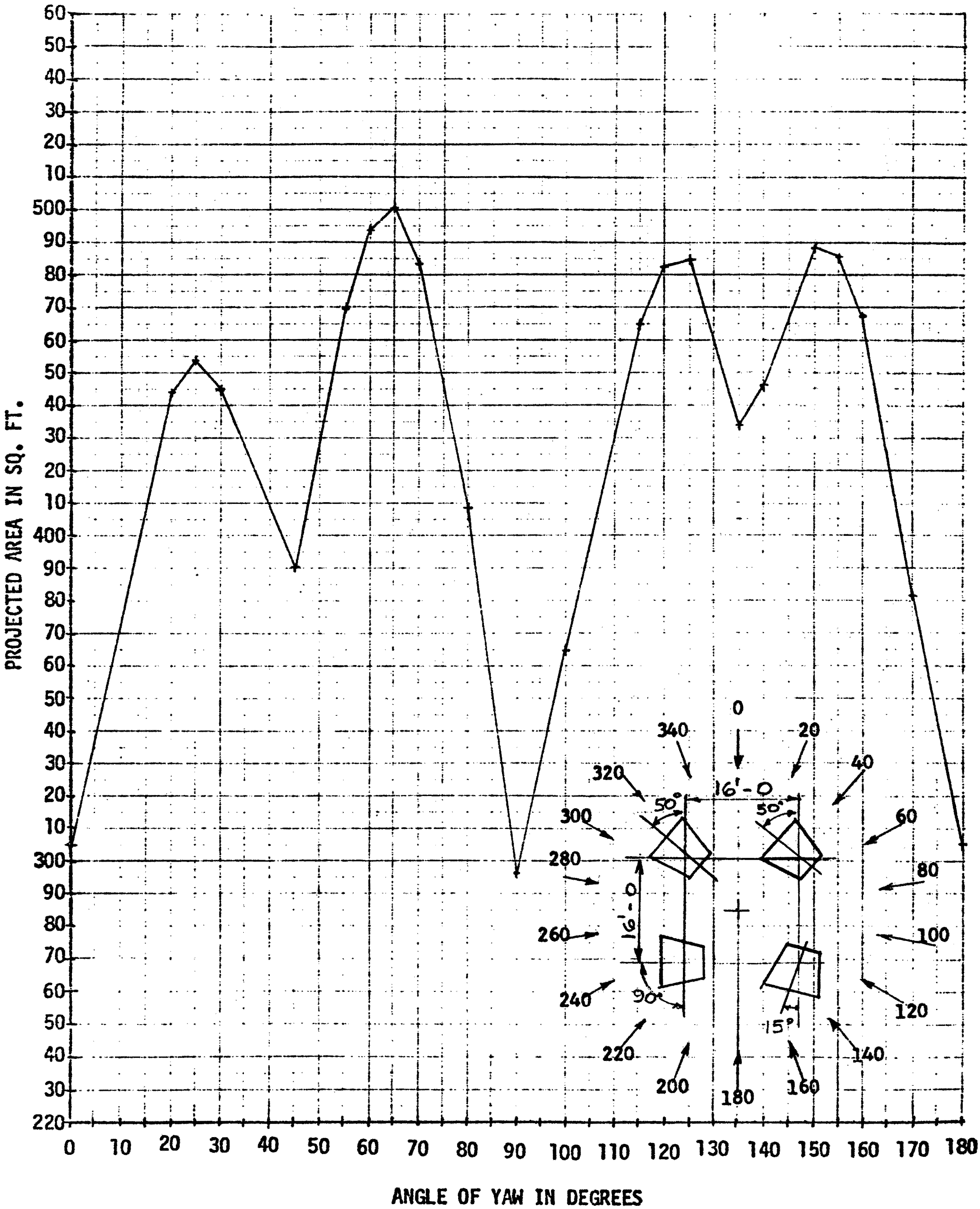

CONDITION 3C
(16'-0" Separation)
PROJECTED AREAS OF HORNS, MOUNTING FRAMES & PLATFORM

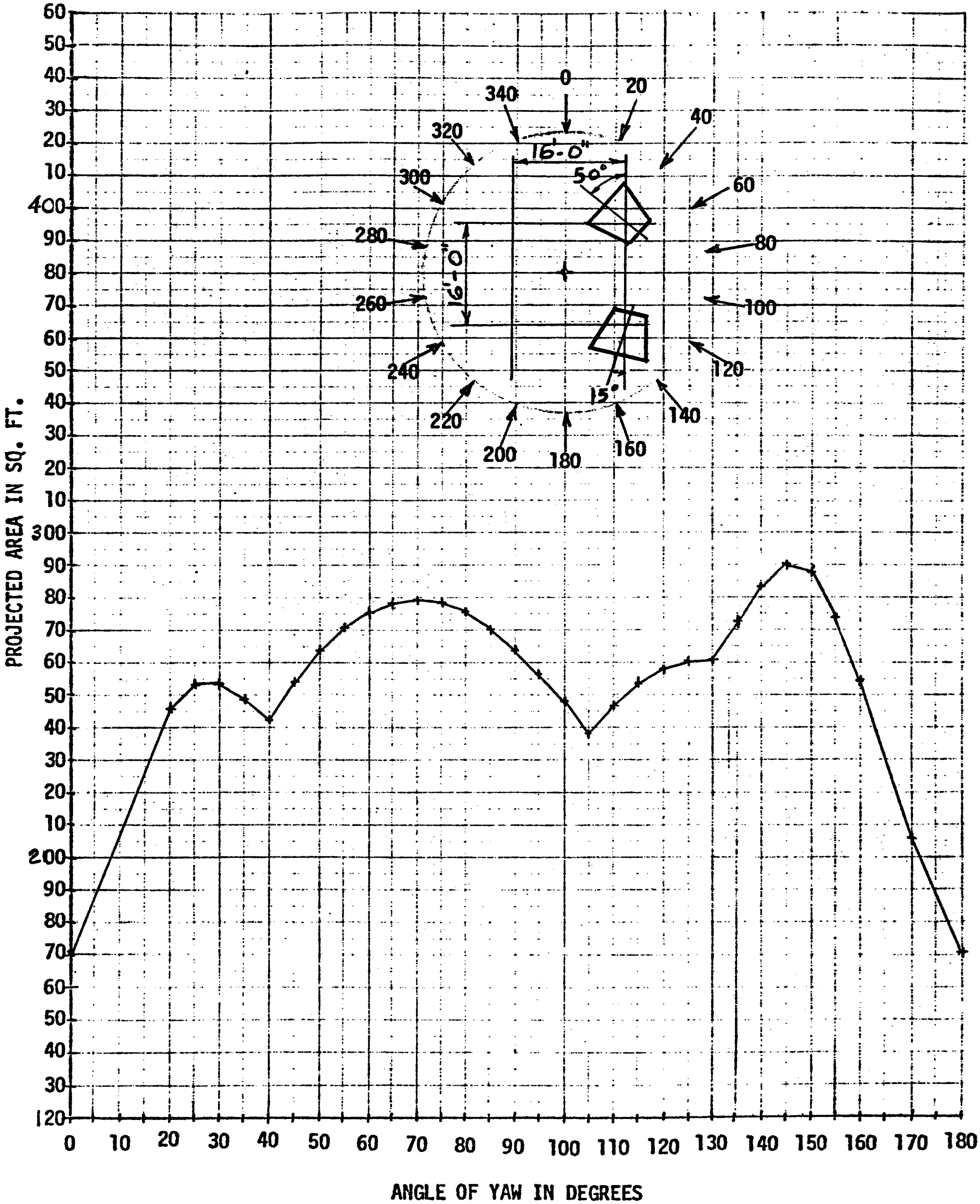

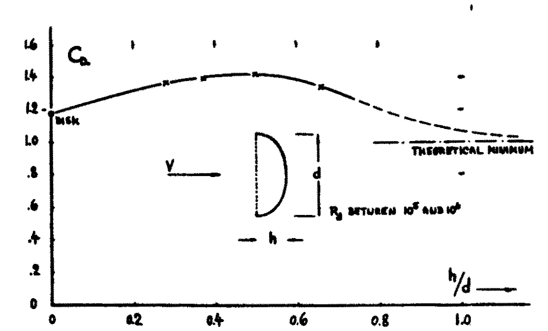

Fig. 31. Drag coefficient of sheet-metal "caps" (40,a) as a function of their height ratio.

Caps and Cups. As large as the drag coefficients of plates may be, there are other shapes exhibiting still higher values. Figure 31 shows the drag coefficient of open cup- or cap-like bodies (similar to parachute canopies). The maximum drag coefficient (on projected area) is obtained for h/d in the order of 0.5, a shape which is ≈ hemispherical. Upon further increasing the height ratio, the rear side more and more changes into a wake "fairing". The drag coefficient is, therefore, expected to approach the theoretical minimum which corresponds to full stagnation pressure across the opening.

7. DRAG OF WEDGES AND CONES

Figures 32 and 33 present shape and drag coefficient of a number of three- and two-dimensional bodies. All of these shapes have a more or less separated flow pattern; most of them have negative pressure on their rear side; and their drag coefficients are comparatively high.

Angle of Flow. To establish some order in the drag coefficients of various shapes, the geometrical angle is very useful, at which the flow is guided by the body's surface upon separating from its rear side. The flat plate, for example, has such an angle "ε" = 90°. A "fold" with a vertex angle of two times 45°, has a separation angle of 90° plus or minus 45°, depending upon the direction of the oncoming flow. Figure 34 demonstrates how the drag coefficient increases as a function of the shape angle. Two branches are found, of course; one for two-dimensional bodies (between walls) and another one for three-dimensional conditions. At "ε" = 0, parallel-sided round-nosed shapes have been used in the graph; a hallow, scoop-like body is plotted at 180°.

Figure 32 (near). Drag coefficients of various 3-dimensional bodies (40) at R'numbers between 10^4 and 10^6. Note: (•) tested on wind-tunnel floor.

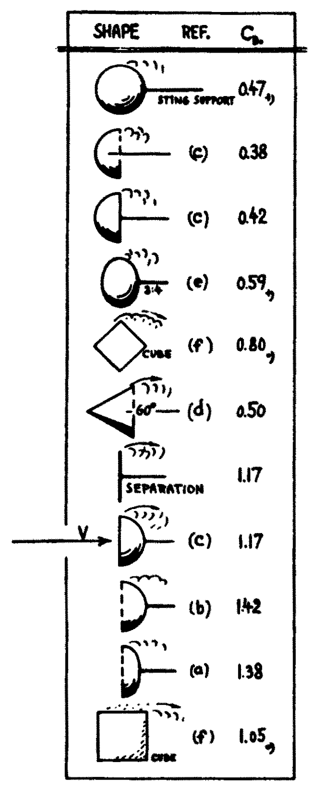

Figure 33 (right). Drag coefficients (41) of 2-dimensional shapes (between walls) at R between 10^4 and 10^6. Note: (+) in subcritical flow.

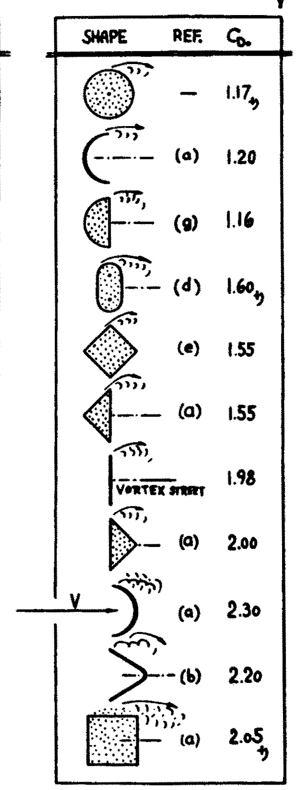

¶ (37) Information on rear-side pressure of plates:
a) On disks and small-aspect-ratio plates see: NACA (36, a); AVA Ergebnisse IV; reference (40,f).
b) On plates between walls see: (12), (35,a) and (40,f).
¶ (40) Experimental results on three-dimensional bodies:
a) Doetsch, Parachute Models, Lufo 1938 p.577.
b) NACA, Cup Anemometer, Tech Rpt 513 (1935).
c) AVA, Hemispherical Bodies, Ergebnisse IV (1932).
d) Eiffel, Recherches a Tour Eiffel, Paris 1907.
e) Hemispherical Cup at $R_d = 2\ 10^5$, ARC RM 712 (1919).
f) Irminger and Nokkentved, Elementary Bodies and Buildings, Kopenhagen 1930 and 1936; Transl'n by Jarvis.
¶ (41) Sections (tested between plates or walls):
a) Lindsey, Simple Shapes, NACA T. Rpt 619 (1940).
b) Junkers Wind-Tunnel, Report Ströte V.9609 (1940).
c) Interference Between Struts, NACA T. Rpt 468 (1933).
d) Delany-Sorensen, Various Shapes, NACA T.Note 3038.
e) AVA Göttingen, Ergebnisse II (1923) and III (1926).
f) Junkers Wind-Tunnel Result on Angle Profile.
g) Reported by Barth, Zt.Flugwissen 1954 p.309.
¶ (42) Free-streamline (cavitation) theory:
a) Kirchhoff, Free Jet Theory, Crelle 1869 (see Lamb).
b) Bobyleff, Russian Phys. Chem. Society 1881 (see Lamb).
c) Riabouchinsky-Plesset-Schafer, Journal Appl.Physics 1948 p.934, and Review Modern Physics 1948 p.228.
d) Reichardt, Laws of Cavities, German ZWB UM 6628.
¶ (43) Neef, Dive Brakes, Fieseler Tunnel Rpt 22 (1941).